


12-2015

High-Resolution Correlation of a Time-Bounded Unit of the Pisco Formation, Peru

Daniel J. O'Hare

Follow this and additional works at: <http://scholarsrepository.llu.edu/etd>

 Part of the [Geology Commons](#), and the [Sedimentology Commons](#)

Recommended Citation

O'Hare, Daniel J., "High-Resolution Correlation of a Time-Bounded Unit of the Pisco Formation, Peru" (2015). *Loma Linda University Electronic Theses, Dissertations & Projects*. 333.
<http://scholarsrepository.llu.edu/etd/333>

This Thesis is brought to you for free and open access by TheScholarsRepository@LLU: Digital Archive of Research, Scholarship & Creative Works. It has been accepted for inclusion in Loma Linda University Electronic Theses, Dissertations & Projects by an authorized administrator of TheScholarsRepository@LLU: Digital Archive of Research, Scholarship & Creative Works. For more information, please contact scholarsrepository@llu.edu.

Loma Linda University
School of Medicine
in conjunction with the
Faculty of Graduate Studies

High-Resolution Correlation of a Time-Bounded Unit of the Pisco Formation, Peru

by

Daniel J. O'Hare

A Thesis submitted in partial satisfaction of
the requirements for the degree
Master of Science in Geology

December 2015

©2015

Daniel O'Hare
All Rights Reserved

Each person whose signature appears below certifies that this dissertation in his/her opinion is adequate, in scope and quality, as a thesis for the degree of Master of Science.

_____, Chairperson

Kevin Nick, Associate Professor of Geology

Leonard Brand, Professor of Palentology

Paul Buchheim, Professor of Geology

Ronald Nalin, Adjunct Assistant Professor of Earth and Biological Sciences

ACKNOWLEDGEMENTS

The author is extremely grateful to several people and organizations for their support and contributions to the success of this project. The Department of Earth and Biological Sciences at Loma Linda University and the Geoscience Research Institute provided funds to support this research. Fellow graduate students Monte Fleming and Jankel Coronado and Orlando Poma, a researcher at the Universidad Peruana Unión, provided much assistance with the field work.

The committee members Dr. Kevin Nick, Dr. Ronald Nalin, Dr. Leonard Brand, and Dr. Paul Buchheim provided much guidance and input. Dr. Nick was very patient, helpful, and available for consultation throughout the project, and each of the other committee members provided valuable feedback and guidance with the research and thesis. I am also greatly appreciative of the endless support and encouragement of my parents, brothers and sister, friends, and relatives during the completion of this project.

CONTENTS

Acknowledgements.....	iv
Contents	v
Tables.....	viii
Figures.....	ix
Abbreviations.....	xiii
Abstract of the Thesis	xiv
Chapter	
1. Introduction.....	1
Goals and Significance.....	1
Geologic Setting and Background.....	3
2. Methods and Study Area	10
Field Methods.....	10
Laboratory Work	14
Synthesis Work	16
3. Results	18
Map of Time Surface.....	18
Facies Descriptions	18
Facies Sc: Coarse Sandstone.....	22
Facies Sldp: Planar-Laminated Diatomaceous Siltstone.....	24
Facies Sldm: Massive Diatomaceous Siltstone	26
Facies Sld: Diatomaceous Siltstone with Climbing Wave Ripples	27
Facies Sfsl: (Planar-Laminated) Fine Sand to Siltstone	29
Facies T: Tuff.....	30

Sections	32
Measured $^{40}\text{Ar}/^{39}\text{Ar}$ Dates of Tuffs	48
Magnetic Susceptibility.....	56
4. Discussion.....	58
Map.....	58
Structure Implications.....	59
Paleoenvironmental Interpretation of Facies.....	59
Interpretation of Facies Sc (Coarse Sandstone).....	59
Interpretation of Facies Sldp	61
Interpretation of Facies Sldm.....	61
Interpretation of Facies Sld	62
Interpretation of Facies Sfsl: Fine Sandy Siltstone.....	62
Interpretation of Facies T	63
Post-Depositional Processes	63
Provenance	64
Tuffs	64
Sandstones and Siltstones.....	64
Diatoms.....	66
Stratigraphic Sections and Correlation.....	66
Identification of Tuffs with Unique Characteristics and Dates	66
The Dark Gray Tuff and Correlation of the Top of the Section.....	67
The Dated White Tuff and Correlation of the Base of the Sections	69
Are the Tuffs Airfall?.....	71
Correlation of the Top vs. the Base.....	72
Correlating Units on Each Side of the Ica River	75
$^{40}\text{Ar}/^{39}\text{Ar}$ Dates of Tuffs	76
Magnetic Susceptibility.....	77
Paleoenvironmental Model	80
Chemistry	81

Temperature/Climate	82
Sedimentary Processes and Depositional Stages	83
5. Conclusions	94
References	96
Appendices	
Sample Descriptions and Data from Each Facies	101
Grain Size Data from Laser Diffraction.....	139

TABLES

Table	Page
1. Facies and their Characteristics	20
2. $^{40}\text{Ar}/^{39}\text{Ar}$ radiometric age results.....	49
3. Summary of $^{40}\text{Ar}/^{39}\text{Ar}$ Ages of Tuffs	55

FIGURES

Figure	Page
1. Map of Study Area	4
2. Pisco Basin Stratigraphy	5
3. Map of T ₂ dark gray tuff	19
4. Field photo of outcrop CB	21
5. Field photo of outcrop CBN	21
6. Field photo of Facies Sc in CBN	23
7. Thin section photo of sample P11-33B.....	23
8. Thin section photo of O11-31D	25
9. Thin section photo of O11-51C	26
10. Outcrop photo of CBN showing Sld units	27
11. Thin section photo of P11-15B (Sld).....	28
12. Thin section photo of P11-31D.....	28
13. Thin section photo of O11-53E.....	29
14. Photo of white T ₁ tuff with sedimentary structures	31
15. Thin section photo of Sample O11-53E (light-gray T _s).....	31
16. Legend for Stratigraphic Sections.....	33
17. Stratigraphic section of Cerro Ballena North.....	35
18. Stratigraphic section of Cerro Ballena.....	37
19. Stratigraphic section of Cerro Ballena South.....	39
20. Stratigraphic section of Cerro Blanco.....	41
21. Stratigraphic section of Cerro Hueco La Zorra.....	44

22. Stratigraphic section of Cerro La Yeseras	47
23. ⁴⁰ Ar/ ³⁹ Ar Plots for Sample A07-77A	50
24. ⁴⁰ Ar/ ³⁹ Ar Plots for Sample A07-27B	51
25. ⁴⁰ Ar/ ³⁹ Ar Plots for Sample A07-36A	52
26. ⁴⁰ Ar/ ³⁹ Ar Plots for Sample A07-35E	53
27. ⁴⁰ Ar/ ³⁹ Ar Plots for Sample A07-139C	54
28. Magnetic Susceptibility Plots of Cerros La Yesera and Cerro Ballena	57
29. Thin Section Photograph of Sc	65
30. Correlation Panel of Sections.....	68
31. Photographs of Upper Time Marker Tuffs T ₂ and T ₃	69
32. Photographs of Lower Time Marker Tuff T ₁	71
33. Photograph of Red-pink Coloration in T ₁	73
34. Thin Section photograph of T ₂ from Sample A11-16B.....	74
35. Field Photograph of T ₁ and Burrowing.....	81
36. Thin Section photograph of Sc from Sample P11-35A	82
37. Diagram of Paleoenvironments through time	86
38. Field Photo of Hummocky Cross-Strata above T ₂ in Cerro Ballena North.....	91
39. Field Photograph of Interval from T ₂ to T ₃ in Cerro Ballena North.....	92
A1. X-Ray Diffraction of Sample P11-33B.....	103
A2. Thin Section Photo of P11-33B	104
A3. X-Ray Diffraction of P11-35A	106
A4. X-Ray Diffraction of P11-31E.....	108
A5. Thin Section Photo of P11-31E	108

A6. Thin Section Photo of P11-31E with Feldspar	109
A7. X-Ray Diffraction of O11-51B	111
A8. Thin Section Photo of O11-51B with Barnicle	112
A9. Thin Section Photo of O11-51B with VRFs	112
A10. Thin Section Photo of Sandstone Fragments	113
A11. Magnetic Susceptibility Plot of CB	114
A12. X-Ray Diffraction of O11-31D	116
A13. Thin Section Photo of O11-31D	117
A14. X-Ray Diffraction of O11-29F	119
A15. Thin Section Photo of O11-29F	120
A16. X-Ray Diffraction of O11-51C	121
A17. Thin Section Photo of O11-29F	122
A18. Thin Section of O11-29F Opaque Minerals.....	122
A19. X-Ray Diffraction of P11-15B.....	124
A20. X-Ray Diffraction of P11-31D	126
A21. Thin Section of P11-31D	127
A22. X-Ray Diffraction of O11-53E	128
A23. Thin Section Photo of O11-53E with Burrowing	129
A24. Thin Section Photo of O11-53E with Phosphate	129
A25. Thin Section Photo of O11-53E General	130
A26. Thin Section Photo of O11-53E with Shells.....	130
A27. Thin Section Photo of O11-53E with Zircon.....	131
A28. Thin Section Photo of O11-53E with Glauconite	131

A29. Thin Section Photo of Facies T ₂ in CY	136
A30. Thin Section Photo 2 of T ₂	136
A31. Thin Section Photo of Facies T ₃	137
A32. Thin Section Photo of T ₃ with Pleochroism	139

ABBREVIATIONS

CBS	Cerro Ballena South (location)
CB	Cerro Ballena
CBN	Cerro Ballena North
CBL	Cerro Blanco
CZ	Cerro Hueco La Zorra
CY	Cerro La Yeseras South
VRF	Volcanic Rock Fragments
XRD	X-ray Diffraction
MS	Magnetic Susceptibility
SEM	Scanning Electron Microscope

ABSTRACT OF THE THESIS

High-Resolution Correlation of a Time-Bounded Unit of the Pisco Formation, Peru

by

Daniel J. O'Hare

Master of Science, Graduate Program in Geology
Loma Linda University, December 2015
Dr. Kevin Nick, Chairperson

Correlation of beds in the Pisco Basin across significant distances is problematic and has not yet been effectively achieved. I chose to examine an interval bounded by two time markers, an $^{40}\text{Ar}/^{39}\text{Ar}$ -dated white tuff at the base and an $^{40}\text{Ar}/^{39}\text{Ar}$ -dated tuff couplet at the top. This interval was chosen because of the continuity and excellent exposure of the tuff beds at six distinct locations in a linear transect 30 km long. Correlation of units was achieved through $^{40}\text{Ar}/^{39}\text{Ar}$ dating, lithology, sedimentary structures, and magnetic susceptibility. The vertical and lateral variability in lithology, fossil assemblages, structures, and sequences was examined in detail and used to develop a paleoenvironmental model of the time-bounded sequence. Six distinct facies from the Pisco Formation were defined and used toward developing the paleoenvironmental model. Sedimentary structures associated with the facies, such as hummocky cross-stratification and ripple laminations, suggest wave reworking in a nearshore environment. The presence of clastics and coarse-grained sediments decrease from the northern outcrops to the southern outcrops, suggesting a decrease in energy levels and an increase of water depth away from the shore. This study provides the first secure correlation across a significant distance and a more comprehensive stratigraphy and paleoenvironmental interpretation of the Upper Pisco Formation.

CHAPTER ONE

INTRODUCTION

Although a general stratigraphy of the Pisco Basin has been developed, correlation of beds in the Pisco Basin across significant distances has not yet been effectively achieved. This gap in knowledge has stymied progress in developing comprehensive paleoenvironmental models in the Pisco Formation. My project addresses this critical gap in sedimentological research in the Pisco Basin by correlating a 30m-thick, time-surface-bounded unit across the basin. I examine in detail both the vertical and lateral variability in lithology, fossil assemblage, structures, and sequences toward the development of a paleoenvironmental model, beyond what has been possible to this point.

Goals and Significance

The ultimate goals of this research are to produce a paleoenvironmental interpretation for a laterally extensive but temporally constrained unit in the upper Pisco Formation and to relate recorded details to the basinal, regional, and global geological conditions, including sea level, tectonism, and climate. In order to accomplish this, I adopted the following multi-step procedure.

First, I was part of a team that identified a unit of the Pisco Formation bounded by at least two laterally extensive, synchronous beds in the basin that can successfully be correlated across relatively large distances (tens of kilometers).

Second, I characterized and defined six facies within that time-bounded unit and examined the lateral and vertical scale of variability in lithology, fossil assemblage, and

structures. Third, I identified possible indicators of cyclical deposition, such as color change and magnetic susceptibility. Finally, I combined the data obtained from each task to produce a paleoenvironmental model for the studied interval.

This project contributes significantly to scientific progress in both theoretical and applied geology. My research provides the first high-resolution correlation of environments in the Upper Pisco Formation, laying the groundwork for future studies requiring knowledge of stratigraphic position in the basin or comparison between outcrops. The fossils, sedimentary processes, and measurements of magnetic susceptibility obtained in this project also add to our understanding of the paleoclimate. Information gleaned in this study provides further insight toward developing sequence stratigraphic models for Miocene restricted shelf environments.

Research advances in the Pisco Basin also have implications for the petroleum industry. The Pisco Basin is an analog for restricted shelf fore-arc basin reservoirs. Thus, a paleoenvironmental model of the basin will generate a better understanding of the scale of facies changes, typical bed thicknesses, and other aspects of reservoir architecture. Studying the Pisco Basin will also improve our understanding of reservoir quality in this geological setting. The low level of diagenesis in the Pisco provides a unique opportunity to see earliest diagenesis in this setting. Well-exposed outcrops of the Pisco Formation also make it an ideal study site for improving reservoir models of fine-grained volcanoclastic shelf deposits.

Geologic Setting and Background

The study area is located in the Pisco Basin along the western coast of southern Peru, approximately 310 kilometers (190 miles) south of Lima, Peru, near the town of Ica. The study area spans an approximately 30-kilometer NW-SE transect.

The East Pisco Basin infill constitutes a series of transgressive-regressive cycles developed in a shallow bay. It sits atop a block-faulted massif that received about 3km of sediment during the Mesozoic and Cenozoic (Kulm et. al, 1982). It is one of at least eight paired forearc basins along the central and northern Peruvian margin (Dunbar et. al, 1990). My project focused on one of the Basin's formations, the Pisco Formation, which is 200-1000 meters thick (Brand et al., 2004) and exhibits facies changes through a nearshore-offshore trend. The study area is located in the Ica River Valley south of the town of Ica (Fig. 1). Paleontological, biostratigraphic, and radiometric dating methods establish a Miocene and Pliocene age for sediments of the Pisco Formation (De Muizon and DeVries, 1985; Machare and Fourtanier, 1987; Mertz, 1966).

Three major transgressive/regressive cycles of sedimentation are reported for the Pisco Basin and are thought to have developed since the middle to late Eocene (Dunbar et al., 1990). In Dunbar et. al.'s model, each sequence exhibits a vertical facies succession of bioclastic coarse conglomerates in the central part of the basin to the south and sandstones that grade into sandy siltstone and mudstones overlain by diatomaceous and other biogenic sediments. Basin deposits have been divided into five formations: the Eocene Caballas Formation, upper Eocene Los Choros Formation, upper Eocene to lowermost Oligocene Yumaque Formation, uppermost Oligocene to Middle Miocene

Chilcatay Formation, and upper Miocene to Pliocene Pisco Formation (Fig. 2). The focus of my research is solely on the upper Miocene to Pliocene Pisco Formation.

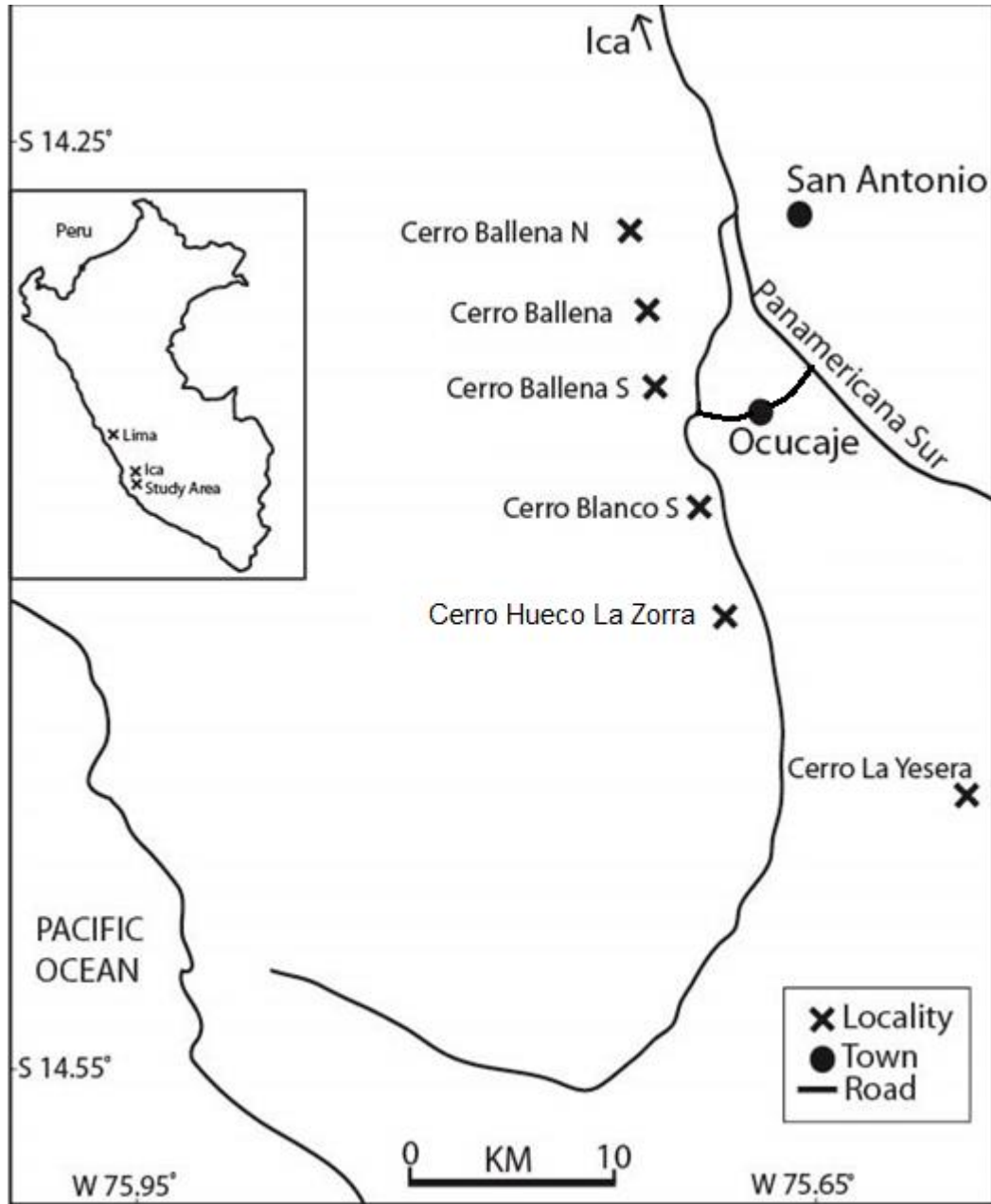


Figure 1. Map of study area. Measured sections are located near the town of Ica along the coast of Peru.

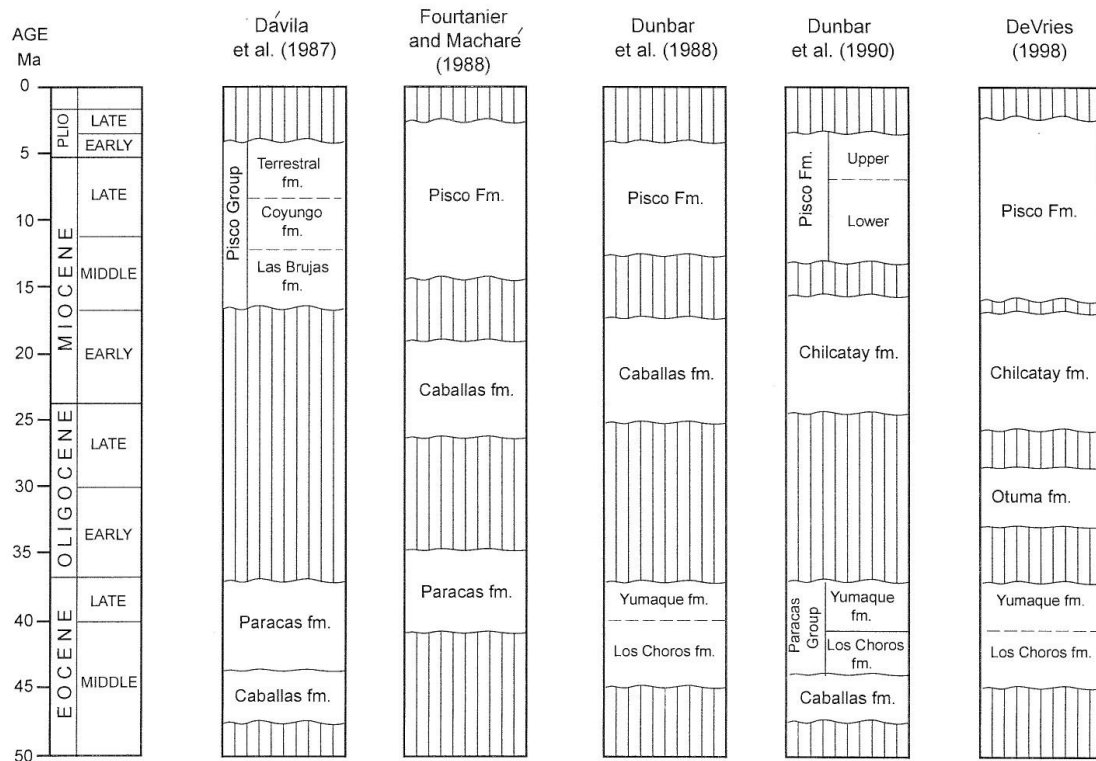


Figure 2. Pisco Basin Stratigraphy. Formations and chronostratigraphy of the Pisco Basin as suggested by previous researchers. Adapted from Figure 4 of Leon et al. (2008).

Other studies have attempted to develop a complete stratigraphy of the Pisco Formation in particular (Brand et al., 2006; Brand et al., 2011). Brand et al. (2006) published a stratigraphy of the Pisco Formation on the west side of the Ica River from Yesera de Amara to Cerro Blanco and Cerro Ballena. They accomplished the correlation by walking out marker beds. They also attempted a tentative correlation toward the west, from the modern dune field to Dos Quesos and Cerro Queso Grande. The interval I examined spans M16 to M20 stratigraphically, as defined in Brand et al.'s (2011) study of the Upper Pisco Formation.

De Muizon and DeVries (1985) note that the major sedimentary rock types of the Pisco Formation are tuffaceous sandstone, siltstone, and shelly sandstone. A major portion of these sedimentary rocks are diatomaceous or diatomite (Brand et. al, 2004). Its fine-grained sediments are thought to have been deposited in a large coastal lagoon environment, and its coarse-grained sediments are thought to have accumulated in semiprotected littoral and nearshore environments (DeMuizon and DeVries, 1985). The formation is more than 435 m thick (Brand, et al. 2011).

Other researchers have noted that considerable volcanism occurred in central and southern Peru during the time of deposition of the Pisco Formation, from Early to Middle Miocene (Noble et al., 1974). This is consistent with the occurrence of volcaniclastic and tuff deposits in the Pisco Formation.

According to DeVries (1998), sequence boundaries observed in the Pisco Basin are associated with either compressional events or eustatic low stands of sea level. DeVries (2007) has also noted that significant intervals of relatively high sea-surface temperatures as well as “warm costal upwelling” were active here during the Cenozoic. He cites evidence from sedimentology and paleontology that suggests coastal upwelling was significant along with high primary and secondary productivity since the late Middle Eocene.

Studies of faunal assemblages have enabled researchers to ascertain climatic conditions throughout the history of deposition within the Pisco Basin. DeVries (2007) notes that $\delta^{18}\text{O}$ values were lowest (since the Late Eocene) during the Late Oligocene to early middle Miocene. This also corresponds to the time when mollusks of tropical affinity inhabited the coasts of Chile. By the late Middle Miocene, global sea surface

temperatures fell, but warm-water equatorial taxa persisted into late Miocene and early Pliocene times.

A variety of paleontological studies conducted in the East Pisco Basin have been published. A diverse range of both vertebrate and invertebrate fossils have been preserved in the basin. Vertebrate fauna include cetaceans (Bianucci, et. al, 2010; Reumer, et al., 2010; Esperante 2008; Brand et. al, 2004), beaked whales (Bianucci, et. al, 2010), white sharks (Ehret et. al, 2009a; Ehret et. al, 2009b), penguins (Clark et. al, 2010), pinnipeds (Bianucci et. al, 2010), sea turtles (Parham and Pyenson, 2010), fish (Bianucci et. al, 2010), and other birds (Bianucci et. al, 2010) including Phalacrocoracidae (Urbina and Stucchi, 2005) and Sulidae (genus *Ramphastosula*) (Stucchi and Urbina, 2004). Also of note is the unique preservation of whale fossils and baleen in the Pisco Basin (Brand et. al, 2004; Esperante et. al, 2008), which has been used to aid interpretation of sedimentation processes and paleoenvironmental conditions. Invertebrate fauna preserved as fossils in the Pisco Formation include mollusks (DeVries, 2007), such as cypraeid gastropods (DeVries et. al, 2006) and muricid gastropods (DeVries and Vermeij, 1997). Microfossils such as diatoms and silicoflagellates (dictyochales) are abundant (Machare and Fourtanier, 1987), especially in the sections that I examined. Sixty-nine species, varieties, and forms of diatoms from 23 genera have been described in detail (Mertz 1966), and fossils of *Rhaphoneis ischaboensis* var., *Nitzschia pliocena*, and *Hercotheca peruviana* are thought to be diagnostic of the Pisco Formation.

Biostratigraphy has also been used extensively to constrain the age of the Pisco Formation. Previous studies have used diatoms to determine the ages of the Pisco

Formation (Machare and Fourtanier, 1987). Mertz (1966) identified sixty-nine species of diatom in the Pisco Formation, and determined that the formation is Miocene in age based on the similarity of its plankton with that of the Miocene coast of Chile. De Muizon and DeVries (1985) have used paleontological, stratigraphic, and K-Ar evidence to establish a Miocene and Pliocene age. Dunbar et. al (1990) cite evidence from the distribution of radiolarian and diatom species that deposition of organic rich sediments occurred during 40-36 Ma, 24-16 Ma, and 11-3 Ma in the Pisco Basin. Biostratigraphy of mollusks, foraminifera, nanofossils, and $^{87}\text{Sr}/^{86}\text{Sr}$ ratios also help constrain the ages of Pisco sediments. Three specimens from the Paracas Formation were dated as 37 Ma at minimum from Ar-Ar dates from a tuff layer above (Uhen et. al, 2011).

Nick (2015) also conducted an investigation of tephrochronology and its usefulness in correlation of beds in the Pisco Basin. Lateral correlation of beds has been attempted in nearby regions outside of the Pisco Basin (de Silva and Francis 1989, p. 133-149). Researchers studied ignimbrite units in the Central Andes of Chile, and correlated these units laterally using field mapping, geochemical analyses, and K-Ar dates. The researchers found that geochemical “fingerprinting” was the most successful means of correlating. The “fingerprints” were based on determinations of the Fe, Mg, Mn, and Ti composition of the biotite, the Fe, Mg, and Mn composition of the hornblende, and trace elements in the dominant pumice type of the ignimbrite. Although these tools were found to be most useful, the authors stress that multiple techniques must be used in addition to this method in order to provide successful correlations. They also used bulk-matrix analyses as well as trace-element compositions of glass and modal phenocryst abundances. Using these methods, the researchers found that one particular

unit, the 8.33 Ma dated Sifon ignimbrite was much more extensive than previously thought. I adopted a similar approach of correlation in this study.

The Pisco Basin represents a shallow-shelf forearc setting. This type of setting has been studied extensively in other parts of the world (Takahashi and Matsukawa, 2000; Walter et al., 2002), both ancient and modern. One example of a shallow marine succession with characteristics similar to the Pisco Basin is the Upper Cretaceous Kanguk Formation on the Devon Island of the Canadian High Arctic (Witkowski et. al., 2011), which is characterized by nearly a hundred fossil marine diatom species, very good preservation of fossils, and an abundance of volcanic material. Preservation of fossils was also aided by protection from downfaulted linear grabens.

Another stratigraphic unit with similar characteristics to those of the Pisco Basin deposits is the Devonian Clifty Formation of northern Arkansas (Boss and Blackstock, 2008). The authors of the study observed massive sandstone deposits with burrows and trails; crossbedded sandstone monoliths; trough cross-bedded channels with bioturbation; crossbedded deeply incised channels with a variety of isolated, enigmatic burrows; planar tabular cross-bedded layers with 1-m wide circular structures; thin planar-tabular layers with *Skolithos*; and tabular layers with carbonized plant remains and *Zoophycos*. The massive sandstone deposits with burrows were interpreted as a shallow, offshore shelf depositional environment and the planar tabular cross-bedded structures were interpreted as a shallow, subtidal near-shore shelf environment (Boss and Blackstock, 2008).

CHAPTER TWO

METHODS AND STUDY AREA

The overall goals of this project were to successfully correlate outcrops across six sections along a NW-SE transect, to develop a more concrete stratigraphy of a selected stratigraphic interval, and to better understand the basinal, regional, and global geological conditions during deposition of the Pisco Formation across a geographically extensive region.

Field Methods

For the purpose of correlation, I first identified a laterally extensive and temporally constrained unit in the Pisco Basin that could be successfully correlated across significant distances. In order to do this, I identified two synchronous and laterally extensive beds that set the bounds for this unit. An excellent candidate for a synchronous bed is a tuff bed, a layer of ash that would have been deposited throughout the basin at the same time. Thus, a single tuff bed represents a single event, and provides a time marker that can be used anywhere in the basin where it is found. If two such tuff beds can be correlated across large distances, I can be confident that the unit between those layers is temporally constrained across those distances.

The unit was used to represent the same interval of time at any location in the basin, and allowed us to determine lateral variability in paleoenvironmental conditions. In order to identify the tuff layers bounding the units, I implemented several methods. The first method started by finding several prominent tuff layers in a well-exposed

outcrop of the Pisco Basin. These tuff layers were found by directly examining good outcrops in the field and walking those layers a certain distance to determine the degree of their lateral continuity. Since the goal was to identify a laterally extensive *section*, it was necessary to find at least two tuff layers, one that marked the bottom of the section and one that marked the top of the section. In addition, there were other laterally extensive tuff beds (and other types of continuous beds) *between* the two main tuff beds, which helped provide a more secure correlation.

Before my project began, Kevin Nick (Loma Linda University), Poma (Universidad Peruana Union), and Roberto Biaggi (Universidad Adventista del Rio Plata) conducted field work in the Pisco Formation (unpublished) and walked out some of the more prominent tuff layers to ascertain how continuous they are. This is the only certain way to correlate layers from one section to another. For my project, I identified other outcrops in the basin and determined how many of the tuff layers previously found were present in those outcrops. Other criteria used for identifying tuff layers (when walking them out was not possible or feasible) include appearance (color and weathering), mineralogy (e.g., biotite abundance), thickness (although this can often vary), ^{40}Ar - ^{39}Ar radiometric dates, and most importantly, associations with other lithologies and layers above and below. There are two ways to apply the last criterion. As an oversimplified illustration, consider a hypothetical tuff layer A immediately below another hypothetical tuff layer B in a given measured section. If two similar layers appear in another section and are separated by roughly the same vertical distance, I can assume that those layers are equivalent to layers A and B in the original section. Another way this principle can be applied is by noting the presence of a definite sequence of layers just above or below a

hypothetical tuff layer C. For example, if tuff layer C is immediately below a sequence containing coarse sandstone, diatomite, a massive bed, and another sandstone, the presence of this same sequence in another section in association with a similar tuff layer can be used as evidence that the tuff layer is the same as tuff layer C.

Another method I employed to correlate beds involved $^{40}\text{Ar}/^{39}\text{Ar}$ analysis of tuff beds suitable for radioisotope dating. Some of the tuff layers in the Pisco Formation contain abundant biotite or sanidine, two minerals often dated by the $^{40}\text{Ar}/^{39}\text{Ar}$ method to determine cooling ages of volcanic tuffs (Hora et al., 2010). I used these dates to help provide a starting point for locating my section within a given outcrop. For example, my research team identified a biotite-rich tuff layer present in all outcrops that I used to define the base of my section throughout the basin. This tuff layer has previously been submitted for $^{40}\text{Ar}/^{39}\text{Ar}$ analysis by Dr. Kevin Nick (unpublished data). Thus, when searching for this same layer in unmapped outcrops, I referred to $^{40}\text{Ar}/^{39}\text{Ar}$ analyses by Nick to test potential candidates. When the $^{40}\text{Ar}/^{39}\text{Ar}$ date agreed with dates obtained for the tuff in other locations, this became confirming evidence for my correlation. It also helped provide a stratigraphic context in situations where other indicators were not apparent initially.

Six outcrops were selected based on several factors, including the traceability of a mapable tuff unit, exposure of the upper and lower units bounding the section, ability to establish a significant distance of separation between outcrops, and the opportunity to correlate outcrops separated by the Ica River (see Fig. 1). After drawing a stratigraphic section for each of the six outcrops, I was able to correlate the relevant units across the

outcrops. Each section was plotted showing lithofacies, thicknesses, contacts, and sedimentary structures.

I measured each individual section and recorded important features in a field notebook. I took photos of a representative sample of the units in my section, recording vertical and lateral changes. Samples were collected from each unit and submitted for mineralogical and textural analyses. Based on these data, I defined facies and plotted the relevant data in correlated sections.

I measured magnetic susceptibility (MS) in two selected sections, one from a southern outcrop in my transect (Cerros La Yesera) and one from a northern outcrop (Cerro Ballena). I collected rock samples every 0.5 meters from the bottom to the top of the section and measured the MS with a Bartington MS II magnetic susceptibility meter. From these data, I created plots of magnetic susceptibility vs. height for each measured section. These data reveal the variation in susceptibility vertically in each section as well as how the vertical variation differs from one section to the next.

Once correlation of the six outcrops was complete and a stratigraphy defined, I was able to use the data to better understand lateral and vertical variability in sedimentological conditions, which enabled the development of a paleoenvironmental interpretation.

The lateral scale of variability in lithology was evident first from observations in the field. Using my correlation, I was able to see how the type, thickness, and existence of beds change from one outcrop to the other. At each outcrop, I identified sedimentary structures, such as ripple cross-bedding, sole structures, lag deposits, burrowing, graded bedding, soft-sediment deformation, and other indicators of depositional environment.

This enabled interpretation of the lateral variability of depositional conditions from one location to another.

In order to access the outcrops, the team I was a part of rented two four-wheel drive pick-ups and drove to dirt roads that run alongside the cerros (hills). Once entering the path, we used GPS to locate the individual outcrops that we studied, and drove as close as possible to the sites. At some places, we had to park the vehicles several hundred yards from the outcrop, and hike to the outcrop itself. We used typical field supplies, such as rock hammers, Brunton compasses, GPS devices, and sample bags. We also used two laser ranging devices for measuring vertical height of units in the outcrop. We collected various samples throughout each outcrop, placed them in bags, and marked them for identification and later storage in the laboratory at Loma Linda University.

Laboratory Work

I collected over one hundred samples from each of the six outcrops in the Pisco Formation. Ten of those samples were sent to an external laboratory, which prepared thin sections from them. Those thin sections were examined with a microscope and used to help describe the facies I defined. The samples used for thin sections were chosen to obtain a representative sample from outcrops in the south and north as well as common lithologies. Texture and percentages of different mineralogical and lithic components were estimated by visual inspection and a reticule. Thin sections were also made from a dark gray tuff, a biotite-rich dark tuff above it, and the $^{40}\text{Ar}/^{39}\text{Ar}$ -dated white tuff, because those units appeared in every outcrop and were used for correlation.

I also compared the mineral percentages and textures of units across the 30-km linear transect of the six outcrops (see Fig. 1). I prepared my collected samples for XRD analysis to determine the mineral percentages, and I examined textures and mineral distributions of these fine-grained rocks with light microscopy of thin sections. These data also formed the basis for defining the facies that cover a wide range of the sediment types in my section.

I prepared XRD slides for over 50 samples, including, most importantly, the samples used for thin sections and facies analysis. The slides were placed in a Siemens D500 x-ray diffractometer to determine the mineralogy of each sample. I prepared some of those samples for SEM analysis. I used the mineralogy data from XRD, chemical composition analysis from the SEM, and observations from microscopic analysis of the thin sections to describe lithologies. I used those data as well as field observations to describe and define the facies.

Grain sizes of 30 samples were measured with a Beckman Coulter LS 13-320 particle size analyzer. The machine generated normal distribution graphs revealing the volume percentages of particles of various diameters (see Appendix B).

I submitted several tuff samples to an external laboratory, the laboratory of Oregon State University's College of Earth, Ocean, and Atmospheric Sciences (COAS), for $^{40}\text{Ar}/^{39}\text{Ar}$ isotope dating.

All data are recorded in tables in the appendices and are archived in the Department of Earth and Biological Sciences (Loma Linda University).

Synthesis Work

After collecting and analyzing the data, I integrated these data sets to develop a complete paleoenvironmental interpretation. First, I used my correlation to determine how similar indicators of depositional conditions are from section to section. This lateral variability indicates whether any large-scale differences in sedimentation exist that can be correlated with distance from the shoreline, distance from sediment source, or other factors. The correlations also reveal what sedimentary processes were operating at each location along my transect, providing an overall picture of the paleoenvironment.

Specific sedimentary structures are features and attributes of the sedimentary deposits from which sedimentary processes can be inferred. Lithology, fossil content, and sedimentary structures provide important information on the depositional medium, depositional source, depositional energy, and depositional environment. I used the data from each section to determine the sedimentary processes operating at each location as well as how the processes interacted among locations so as to create an overall picture of paleoenvironment.

Using these data, I separated representative units of the formation into appropriate facies. These facies were used to infer additional information about the sedimentary processes, which suggest depositional environment. Finally, the interpretation of depositional environments combined with water depth indicators provide an essential step contributing toward the development of a basin analysis model.

This large body of varied data sets, gathered from multiple sections along a significantly wide transect in the Pisco Basin, enabled the development of a more

complete, large-scale depositional model of the Pisco Basin that is more thorough than has been possible to this point.

CHAPTER THREE

RESULTS

Map of Time Surface

A biotite-rich, white-colored tuff unit was identified and dated by the $^{40}\text{Ar}/^{39}\text{Ar}$ radioisotope method. I used this white tuff unit to define a time surface, the base of the section, and I designated it as T₁. After a lithologic package was identified, another single time surface was walked out over several field seasons. The result is a map of the outcrop trace of a tuff that occurs about one-fourth of the distance from the top of the studied section (Fig 3). The tuff is a distinctive unit of dark gray color that is approximately 20 cm thick and locally contains climbing wave ripple stratification and planar laminations. This tuff unit, which appears in all outcrops, is designated T₂ (numbering is based on stratigraphic order starting at the base of the section) and is typically 4 – 6 meters below another distinctive tuff (containing abundant large biotite crystals) that marks the top of the section, designated as T₃. The tuff crops out on at least six hills (studied here) and can be followed for approximately 30 kilometers from NW to SE and 8 kilometers from NE to SW.

Facies Descriptions

Multiple facies were identified and defined based on lithologies and sedimentary structures that are prominent in the studied outcrops of the Pisco Formation (see Fig. 4 for an example of an outcrop). Main lithologies include sandstones, tuffs, siltstones, and diatomite. Together, these represent the majority of sedimentary rocks within the time-bounded unit I studied in the formation. Some facies are more common in the three

northernmost sections and nearly absent in the southern sections, such as the coarse sandstones (see Fig 5). Some facies are more abundant in the southern sections, such as the diatomaceous siltstone. The tuff facies appears consistently in all sections (see Fig. 4 for examples).

A summary of the defined facies and their characteristics are given in Table 1.

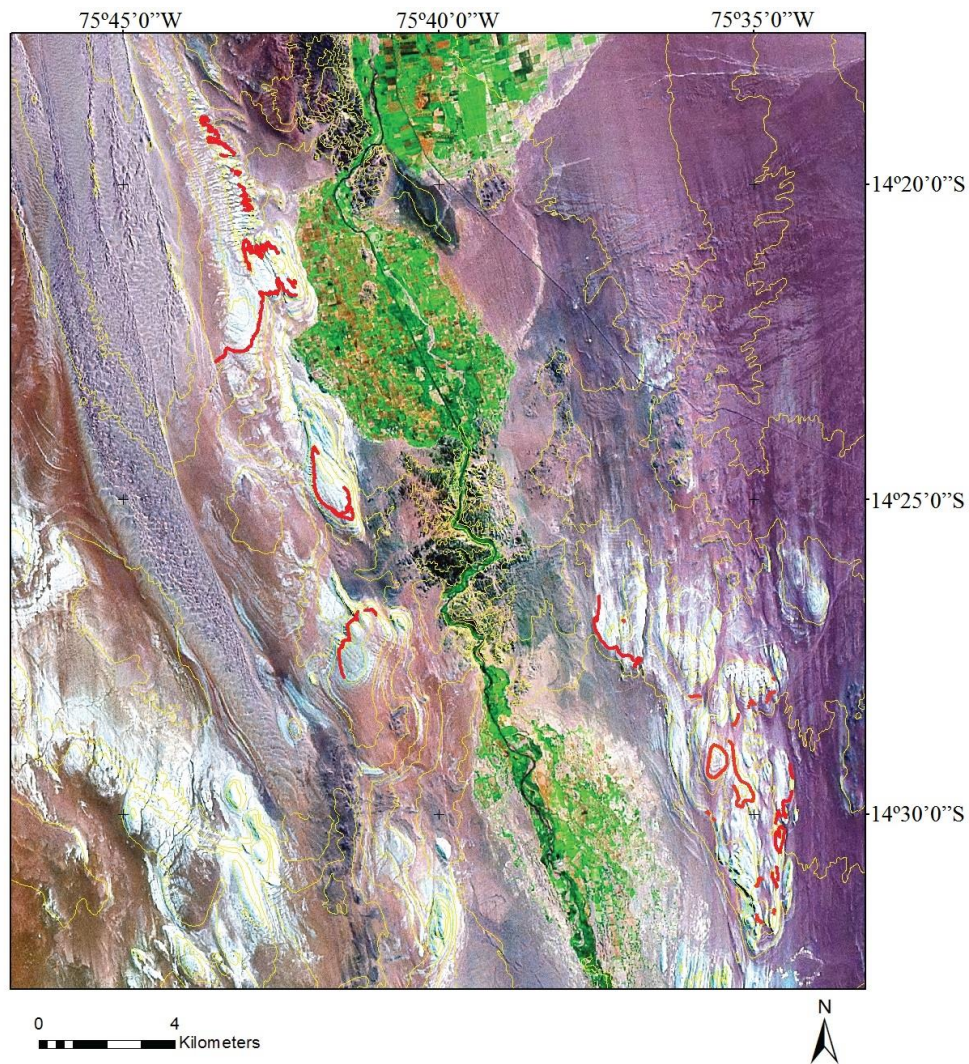


Figure 3. Map of the dark-gray tuff marker bed (T_2). This approximately 20-cm thick tuff as located and walked out across the Ica River Valley. Red lines are GPS tracks of outcrops of this tuff. I believe this is the extent of the exposure of this unit. Yellow lines are contours that highlight local relief. Contour lines are 50m in elevation. Base map is from Landsat imagery.

Table 1. Facies and their characteristics.

Facies	Thickness	Grain Size	MS Range	Sedimentary Structures
Sc Coarse Sandstone	0.16 to 0.9 m	0.2 - 2.0 mm	1.0 - 2.0 X 10 ⁻⁶ SI	Large wavy stratification, sharp base and long wavelength erosion at the base.
Sldp Planar Laminated Diatomaceous Siltstone	3.2 to 7.7 m	0.06 to 0.2 mm	N/A	Planar and wave-ripple laminations, gutter casts, scouring/scour fills, truncation of channels.
Sldm Massive Diatomaceous Siltstone	4.0 m	0.08 mm	1.6 - 1.9 X 10 ⁻⁶ SI	Some low amplitude hummocky cross-stratification, some sub-parallel structures.
Sld Diatomaceous Siltstone	1.9 m	Not measured	N/A	Hummocky and swaley cross stratification, burrows, climbing wave ripples, articulated whale skeletons, cross-bedding, scour fills, channel fill, truncation of channels, fish coprolites, fish scales, and wave ripple laminations.
Sfsl Fine Sand Siltstone	<0.1 to 0.9 m	0.1 mm	N/A	Planar laminations.
T Tuff	0.15 - 0.25 m	0.04 to 0.2 mm	10 - 30 X 10 ⁻⁵ SI	Planar laminations, burrows, trough cross-bedding, climbing wave ripples (in T ₂ only), wave ripple cross laminations, dune cross laminations, and hummocky cross-stratification.



Figure 4. Outcrop photograph of Cerro Ballena, with the visible dark gray tuff T_2 unit (tuff bed near the top of the photo that extends across the entire outcrop, indicated by the arrows). This is an example of the T_s facies. Bed is 20 cm thick.

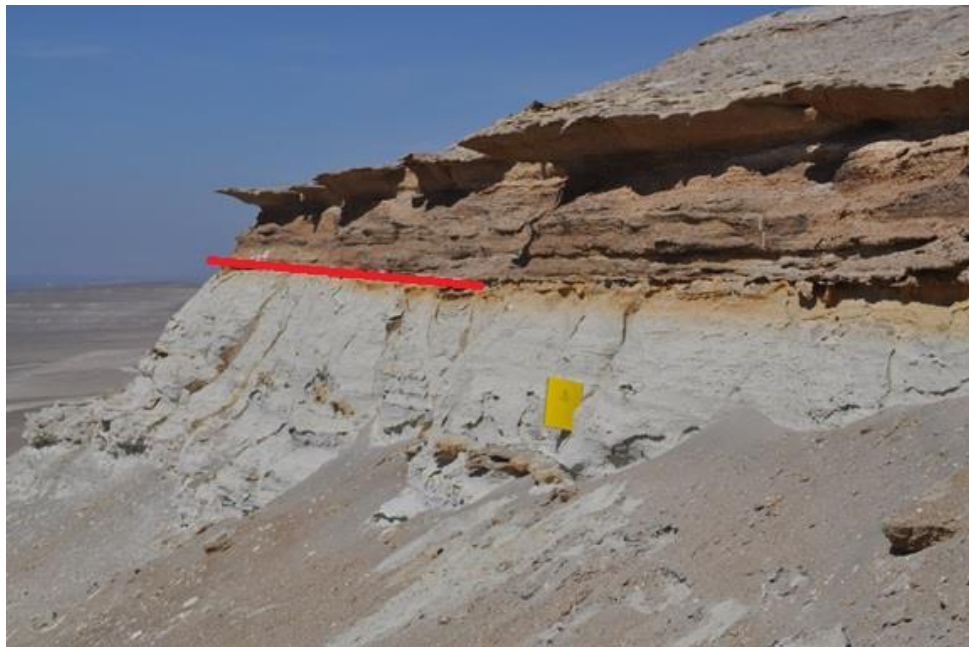


Figure 5. Outcrop photograph of Cerro Ballena North, showing another common facies, coarse sandstone (upper section of the outcrop). Note the contrast between the coarse sandstone on the top and the finer-grained diatomaceous siltstone on the bottom (contact between the two lithologies is highlighted in red). Field notebook is 28 cm tall.

Facies Sc: Coarse Sandstone

This facies consists of a light to medium brown-colored coarse sandstone that occurs in several beds up to one meter thick in both northernmost sections, Cerro Ballena and Cerro Ballena North, where the thickest beds reside. The beds occur especially from 3 meters to 14 meters above the base of each of those two sections. The facies is a coarse sandstone with angular pebbles, and locally contains abundant mollusk shells. In some places, the facies includes thin interbeds of clay, and is sometimes found in association with fine sandstone. In some places, the rock is stained orange to pink. Facies is often interbedded with the dominant lithology of diatomaceous siltstone (Sld). Large wavy stratification often characterizes the beds of this facies (see Fig. 6).

One unit containing this facies (represented by sample O11-51B) is bounded by an erosional surface above, and lies within diatomaceous siltstone (the most common lithology in the section) that contains articulated whale skeletons and abundant sedimentary structures such as ripples and cross-bedding. Sometimes straight-crested megaripples were observed within the bed.

The sand grains average one millimeter (between 0.6 and 2 mm in most cases) in diameter. The sorting is moderate, sphericity is moderate, and the grains are sub-rounded to rounded.

Detrital components are mostly volcanic rock fragments (65-95%) and sometimes include up to 35% bivalve shells, some of which are partially dissolved or replaced by gypsum (Fig. 7). Other detrital grains are small amounts of quartz (<1% - 10%) and feldspar dominated by plagioclase (1%-15%). In thin section, the feldspar crystals embedded within the volcanic rock fragments can be clearly seen. There is up to 30%

bone fragments and up to 10% clay pellets appear deformed around the bone fragments. Small amounts (about 1% each) of deformed mudstone and sandstone rock fragments are also present.



Figure 6. Field photograph of the coarse sandstone facies (Sc) in Cerro Ballena North. Scale bars are one centimeter each. Notice the coarse sandstone beds starting at the ruler, sandwiching another unit containing gypsum.

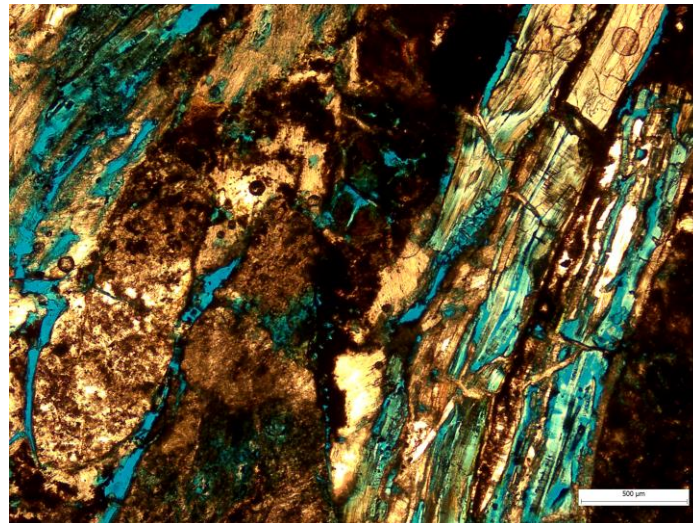


Figure 7. Thin section of Sample P11-33B in plain-polarized light, a sample from Cerro Ballena North. Dark grains are volcanic rock fragments (VRFs), lighter-colored elongated objects (especially seen on the right side of the photo) are bivalve shells. Some of the bivalves are replaced by gypsum. Also the darker material around some of the VRFs is iron oxide alteration. Scale bar represents 500 μm .

I found evidence of halite as an original cement. In sample P11-35A, pores with rectangular outlines are observed within anhydrite cement, suggesting that they formed after halite (original cement) was dissolved. Present cements visible include gypsum and anhydrite. Cement is white to grayish in color, but sometimes no cement is visible. In some locations, thin section analysis reveals circumgranular porosity around detrital grains. Some darker grains show signs of weathering and replacement by clay. Mudstone pellets show signs of being “squeezed” and deformed, and biotite shows expansion and weathering.

Facies Sldp: Planar-Laminated Diatomaceous Siltstone

This facies is a light brownish, sometimes pinkish-colored siltstone rich in diatomaceous material, and typically occurs in thick beds up to 7.7 meters thick. It occurs in one of the southernmost outcrops (Cerro Hueco La Zorra), at 4.5 meters and at 17 meters above the base. Sedimentary structures associated with the facies include planar laminations, gutter casts, scouring and scour fills, truncation of channels, and wave ripple laminations. Thin beds of secondary gypsum occur throughout this unit. The facies is often pinkish gray in color, and contains fish coprolites and scales.

The planar laminated diatomaceous siltstone is part of the broader category of diatomaceous siltstone facies Sld, which is abundant in the southernmost outcrops, Cerro Hueco La Zorra and Cerro La Yeseras South.

Two samples from Cerro Hueco La Zorra represent this facies. The grain sizes range from about 60 to 200 microns on average. The grains are poorly to moderately sorted, have low to moderate sphericity, and are subangular to subrounded. In the upper

unit in Cerro Hueco La Zorra (O11-33D), grains have a preferred orientation evident in thin section (see Fig. 8). In the lower unit (O11-29F), grain orientation is random, with no oriented structure or fabric.

Detrital components are a mixture of silt and sand-sized grains in a matrix of clay and diatoms. The detrital components consist of glass shards (30%), feldspar (~15%), hexagonal quartz (~1%), biotite (0-1%), fish scales (0 – 1%), and bone fragments (0 – 1%). (Percentages are given relative to total volume.) Clay comprises 17% and diatoms comprise 20% of the rock space.

Total porosity is 5 to 10% of the rock. Some pores are oversized. The porosity is 2 – 10% intergranular and 90 – 98% microporosity. No cements are observed.

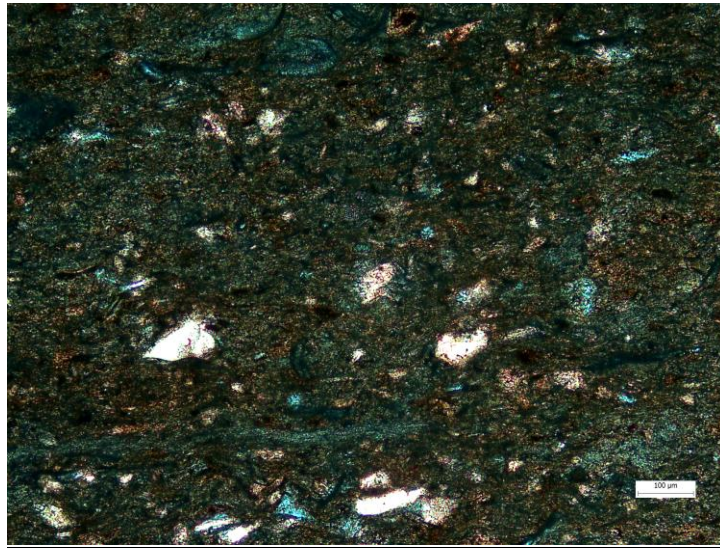


Figure 8. Thin section of Sample O11-33D from Cerro Hueco La Zorra. The dominant mineral grains are feldspar with diatom matrix. Blue-stained epoxy fills intergranular pores in diatoms and micropores between grains (PPL). Scale bar is 100 μm .

Facies Sldm: Massive Diatomaceous Siltstone

This facies consists of massive diatomaceous siltstone, which is often a light tan-colored brown with pinkish staining. This unit is the dominant lithology that comprises the majority of the outcrops. The representative bed is in Cerro Ballena, about 16 meters above the base, and spans a large portion of the section (four meters). The primary sample is mostly from a massive and fractured unit with minimal sedimentary structures. Sub-parallel laminae are evident, and there is low-amplitude hummocky cross-stratification in some locations.

Detrital composition is about 57% diatomaceous material, 32% feldspar, and 3% tephra fragments (see Fig. 9). Replacement phases compose 7-8% of the composition of the facies, with 2-3% replaced by clay. The average grain size is approximately 80 microns. Grains are moderately well-sorted and subangular to subrounded. Feldspar grains have generally low sphericity (Fig. 9). Porosity is 98% microporosity and 2% intragranular porosity.

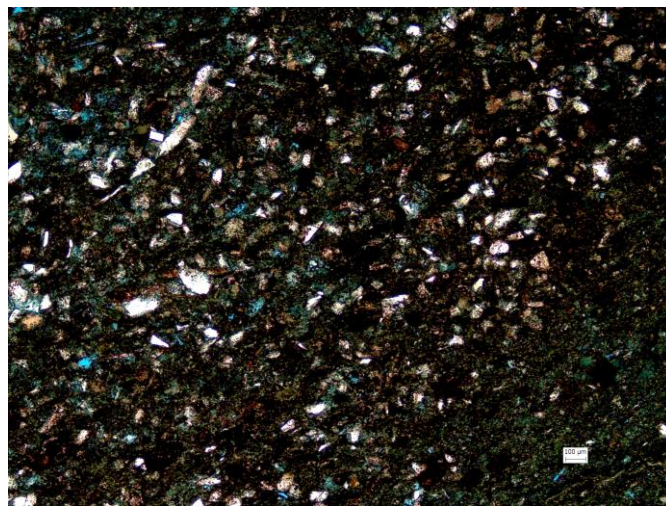


Figure 9. Thin section of Sample O11-51C from Cerro Ballena showing abundant feldspar grains and a few glass shards. Scale bar represents 100 μm .

Facies Sld: Diatomaceous Siltstone with Climbing Wave Ripples

This facies is represented by a light brown diatomaceous siltstone sample found in a unit near the white tuff at the base of Cerro Blanco South with a thickness of about 2 meters, but it typically comprises a majority of the outcrop (see Fig. 10). It contains biotite crystals visible to the naked eye and exhibits burrows and climbing wave ripples. Articulated whale skeletons and abundant sedimentary structures, such as cross-bedding, planar laminations, and 5 cm deep scour fills, hummocky cross-stratification, and swaley cross stratification are also found. Channel and channel fill, truncation of channels, fish coprolites, fish scales, and wave ripple laminations also appear. See Figure 11 for a photograph of some of the sedimentary structures found in this facies. The facies is mostly composed of diatomite. Detrital composition is about 70% diatomite, 15% glass shards (refer to Fig. 12), 5% a dark-colored manganese rich mineral, and 1% feldspar. Orange-colored iron stain is locally present. The detrital components are well-sorted and rounded and have low to moderate sphericity. Porosity comprises 5% of the sample.

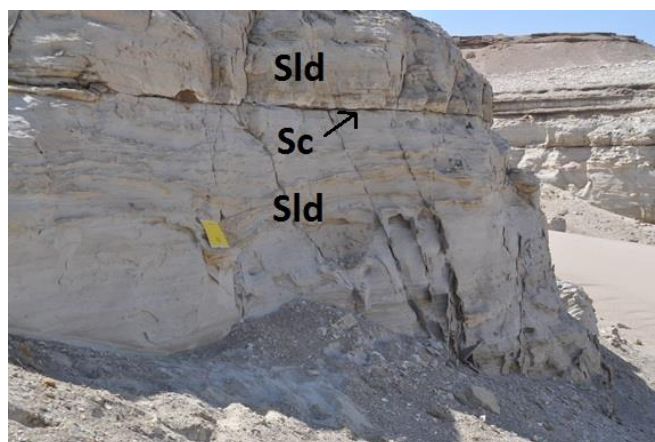


Figure 10. Field photograph of the outcrop at Cerro Ballena North, showing a coarse sandstone facies (Sc) bed within a larger unit of this diatomaceous siltstone facies (Sld). The Sld unit contains thin beds that have drapes and laminae of gypsum. Field notebook is 28 cm long, and marks the location of a channel.



Figure 11. Photo of medium-gray tuffaceous siltstone Sld, showing gutter casts and channels (20 centimeters deep and 50 centimeters wide) near the base. From Cerro Ballena South.

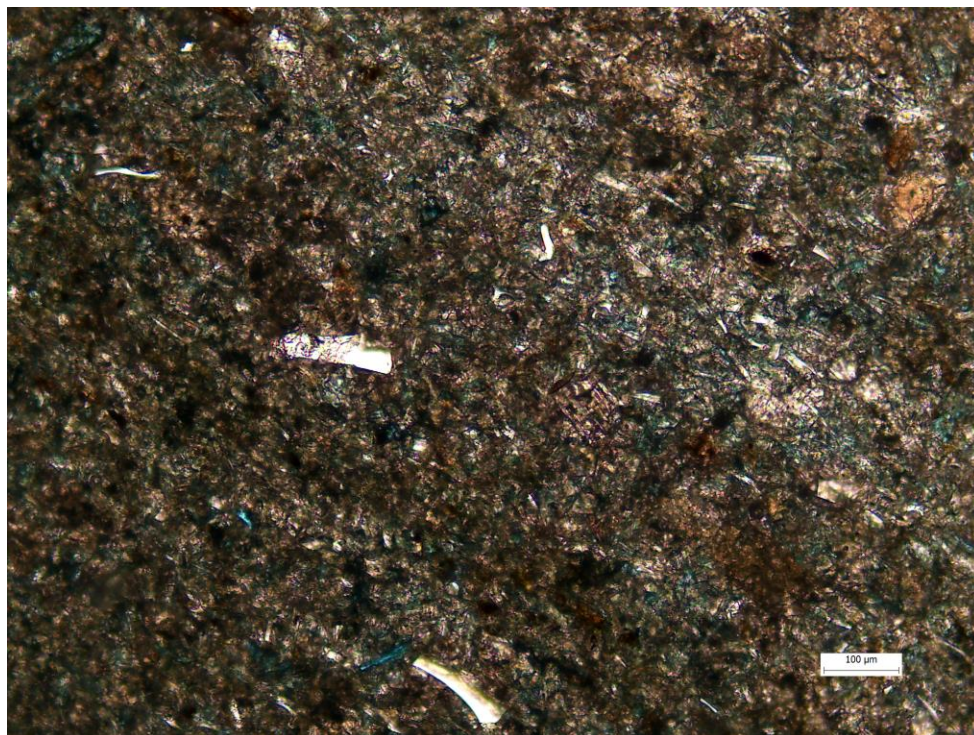


Figure 12. A thin section of sample P11-15B from Cerro Blanco, showing glass shards. Bedding crosses from upper left to lower right. (PPL.) Scale bar is 100 μm .

Facies Sfs1: (Planar-Laminated) Fine Sand to Siltstone

This facies is represented by a light brown-colored rock composed of silt and very fine sand, located near the base of Cerro Ballena North. Its thickness ranges from <0.1 to 0.9 meters, and it is characterized by planar laminations. The representative sample collected is located near the white tuff complex that defines the base of Cerro Ballena North and serves as a time marker for all of the sections.

The average grain size of the facies sample is 97 μm . Grains are moderately to well-sorted, have moderate sphericity, and are subrounded. The facies contains approximately 68% detrital material, 2% intergranular clay, and 30% porosity. The most abundant detrital material is volcanic rock fragments (29% of total rock) (Fig. 13). Other detrital components include glass shards (17%), calcite and phosphatic shells (2%), and feldspar (1%). The porosity is 50% microporosity and 50% intergranular. The volcanic rock fragments are altered and appear very dark in thin section. In stereoscope, they are dark, rounded grains. No cements were identified.

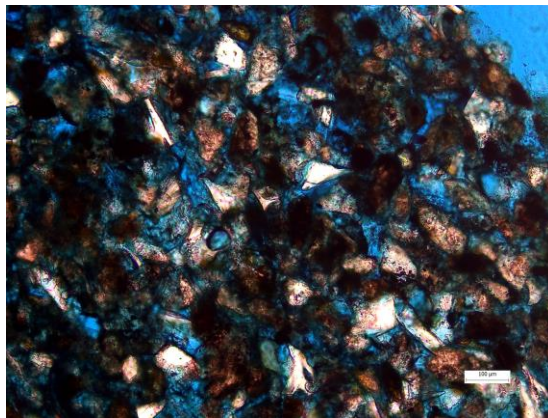


Figure 13. Thin section of sample P11-31D from Cerro Ballena North. Glass shards and volcanic rock fragments (dark brown grains) are the dominant components of this rock. Scale bar is 100 μm .

Facies T: Tuff

This facies includes two types of tuffs: T_s, tuff with sedimentary structures such as planar laminations and climbing wave ripples (Fig. 14), and T_m, massive tuff without visible sedimentary structures. The T_s facies comprises two of the time marker units, T₁ (a biotite-rich, white-colored, ⁴⁰Ar/³⁹Ar-dated tuff) and T₂ (the mapped dark gray tuff), and other tuffs within the section (see Fig. 15). T_m comprises the time marker unit at the top of the section (T₃), a biotite-rich dark-colored tuff, which was also dated by the ⁴⁰Ar/³⁹Ar method. The thickness of T_s is usually about 0.15 – 0.25 meters and the thickness of T_m is about 0.15 meters. Tuff in the T₂ and T₃ units is classified as crystal tuff. T₁ beds are classified as vitric tuff with some crystals.

T_s often occurs at the base of each section as a white-colored tuff and sometimes contains abundant biotite crystals visible to the naked eye. Many sedimentary structures such as planar laminations, wave ripple cross laminations, bioturbation, burrows, trough cross-bedding climbing wave ripples (in the dark gray tuff T₂ time horizon only), and soft-sediment deformation are evident. Climbing wave ripples are found in some T_s beds (only the beds associated with the T₂ time marker unit).

A representative bed of the T_s facies is a light-gray tuff found in the middle of the section in Cerros La Yesera South, underlying a thin claystone and overlying a thin medium-gray tuff in the middle of the section (see Fig. 15 for thin section). (This tuff bed is not used as a time marker for correlation between outcrops.) At the microscopic scale, no oriented structure or fabric is apparent.

This representative T_s sample consists of 50% detrital material, 40% diagenetic material, and 10% porosity (Fig. 15). Some of the pores appear oversized in thin section.

Detrital components include feldspar (15%), quartz (5%), volcanic rock fragments (15%), and glass shards (15%). Biotite, glauconite, and zircon occur in minor amounts. Between detrital grains are clay (20%) and cement (15%) (mostly anhydrite). The clay present was most likely from weathered volcanic rock fragments. The porosity is 100% intergranular.



Figure 14. Photo of white tuff T_1 at base of section, showing in-phase wave ripples and small burrows. From Cerro Ballena South.

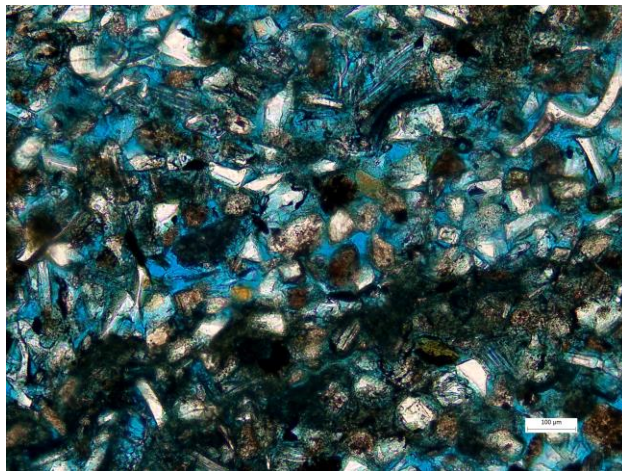


Figure 15. Thin section of sample O11-53E of a light gray tuff of facies T_s in the middle of the section in Cerro La Yeseras. PPL. Scale bar is 100 μm .

Sections

Refer to Figures 16-22 for lithological and sedimentological details of the six outcrops I examined from south to north. All of the sections have at least one white-colored tuff that contains biotite crystals visible to the naked eye, which was used to define the base of the sections. This time marker unit has been referred to as T₁. All of the sections also contain a thick, dark gray tuff (T₂) and a biotite-rich tuff (T₃) at the top that is 3-6 meters above the mapped dark gray tuff. I used both of these tuff units to correlate all six sections. Since all sections are bounded above and below by the same units, they are assumed to cover the same stratigraphic interval.

The six outcrops I examined lie along a NW-SE linear transect approximately 30 kilometers long (see Fig. 1). On average, the sections are 28.4 meters thick (average of 18.5, 23.5, 27, 31, 36, and 34.5 meters).

In general, the three southernmost sections are thicker (31 – 36 meters) and characterized by finer grain sizes, a higher percentage of diatomaceous material, and more dark-colored tuffs. In general, the three northernmost sections are not as thick (19 – 27 meters) and are characterized by a substantial increase in coarse clastic and bioclastic material. I observed abundant shells (associated with coarse sandstone) in only the northernmost section, Cerro Ballena North.

Legend for Measured Sections

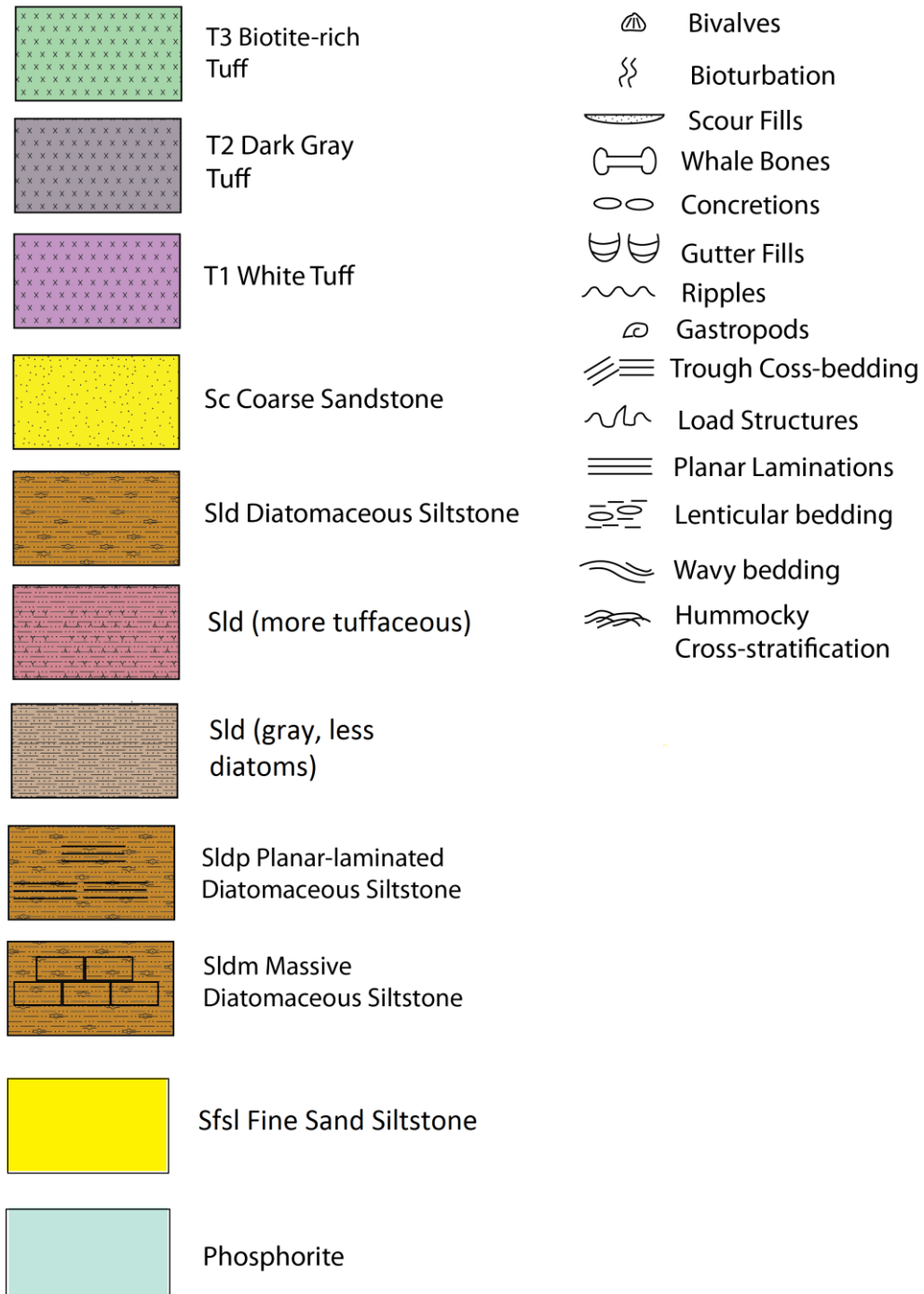
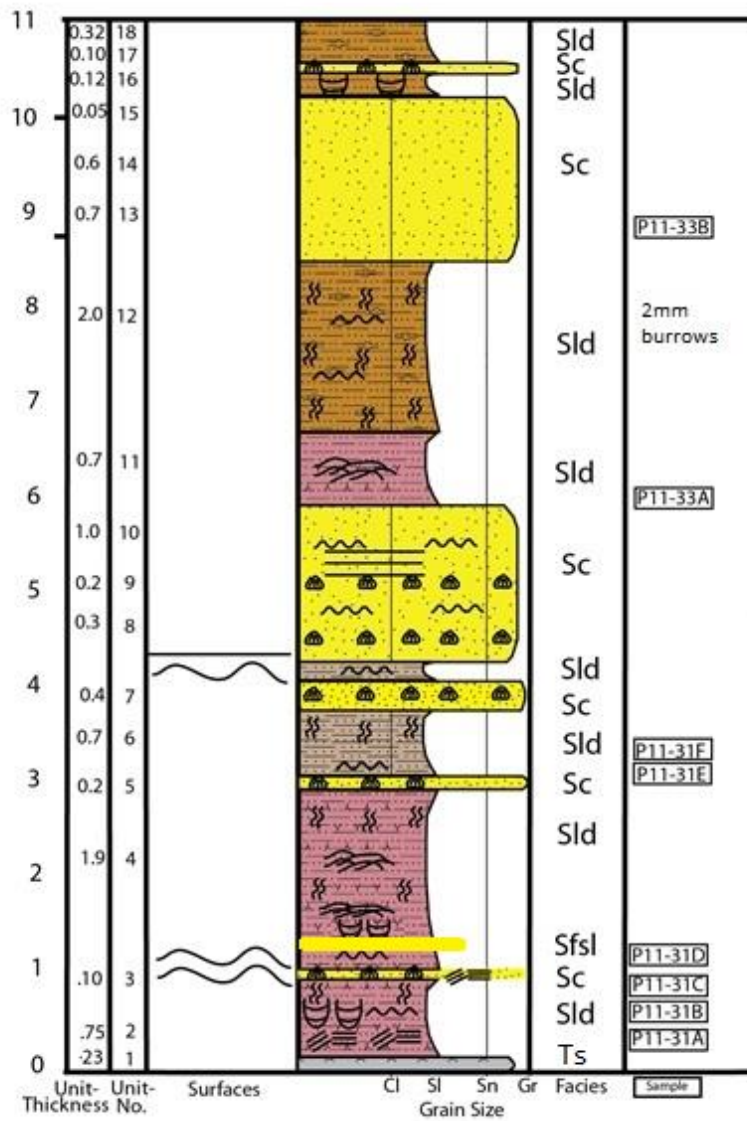


Figure 16. The legend for stratigraphic sections.

Cerro Ballena North Stratigraphic Section

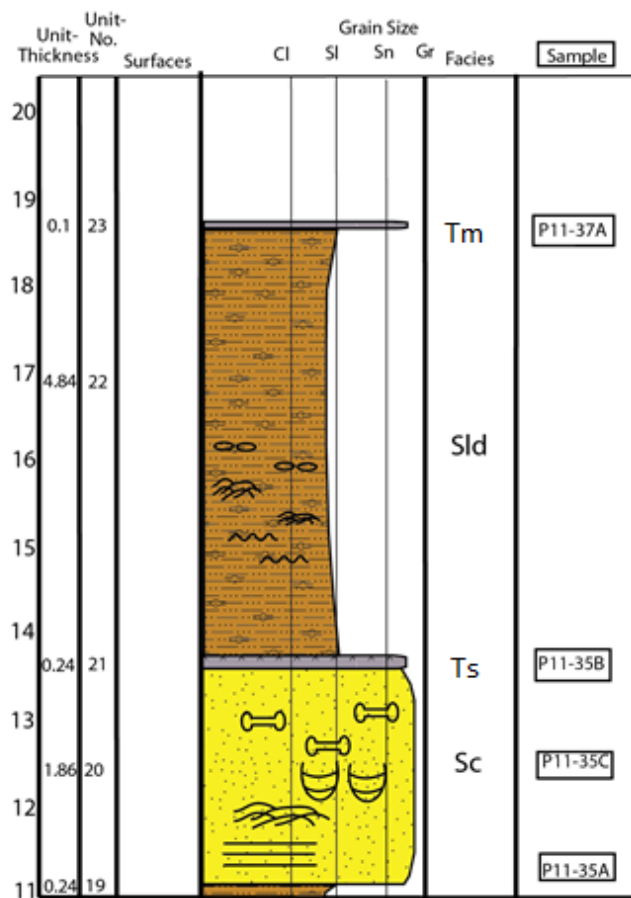
Continued on following page



A

Figure 17. A and B. Cerro Ballena North Lower and Upper Sections

Cerro Ballena North Stratigraphic Section



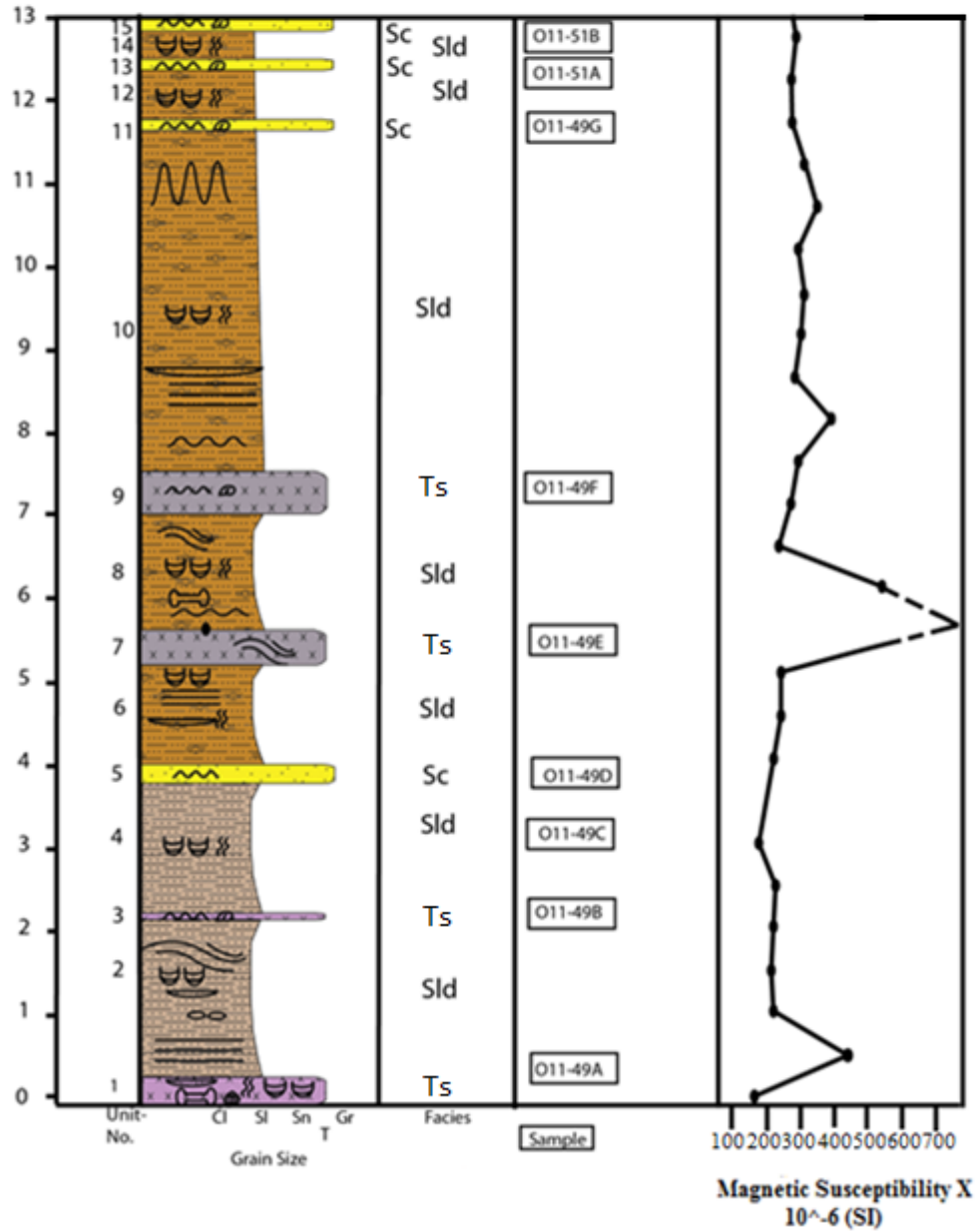
Continued from previous page

B

Figure 17. A and B. Cerro Ballena North Lower and Upper Sections

Cerro Ballena Stratigraphic Section

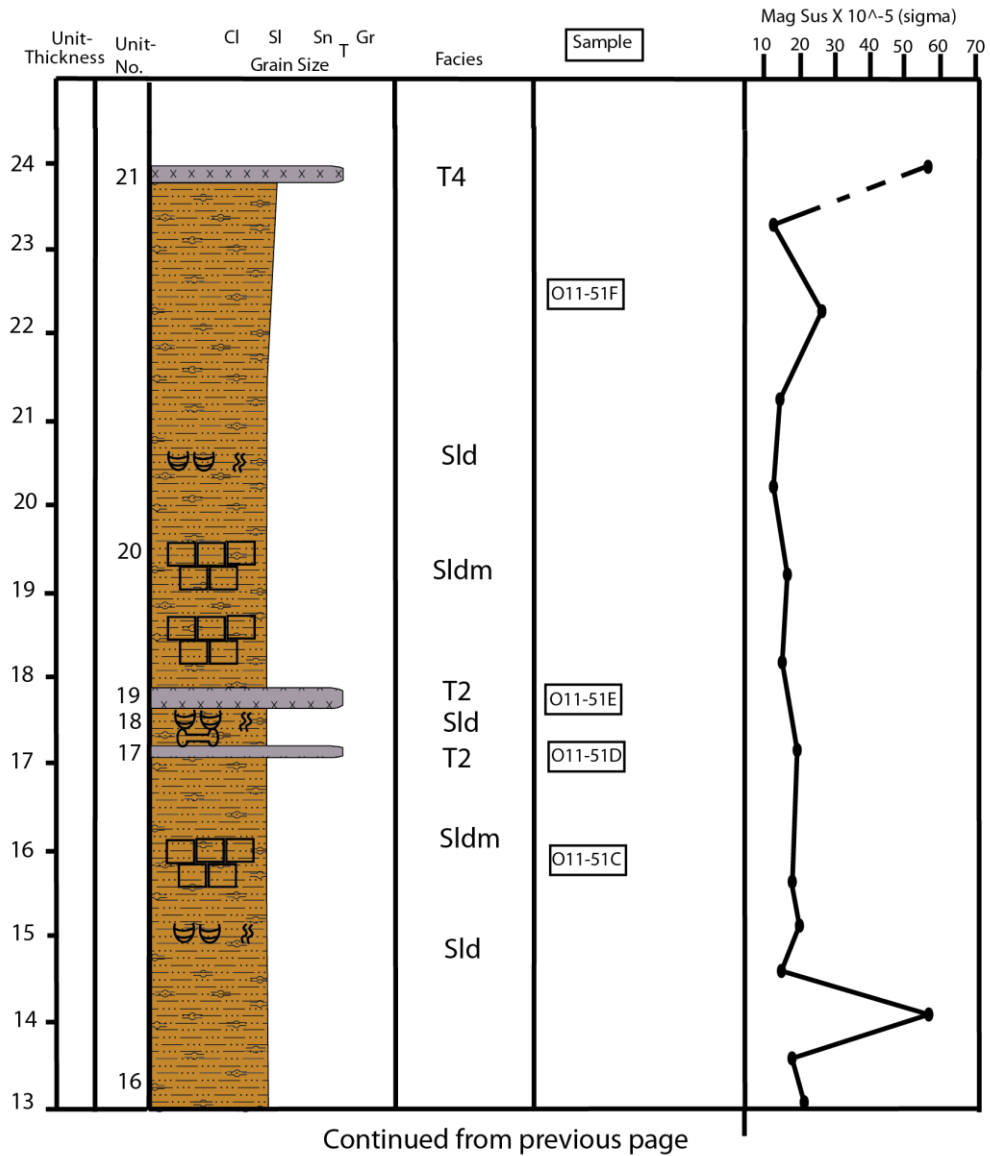
Continued on following page



A

Figure 18 A and B. Cerro Ballena Lower and Upper Sections

Cerro Ballena Stratigraphic Section

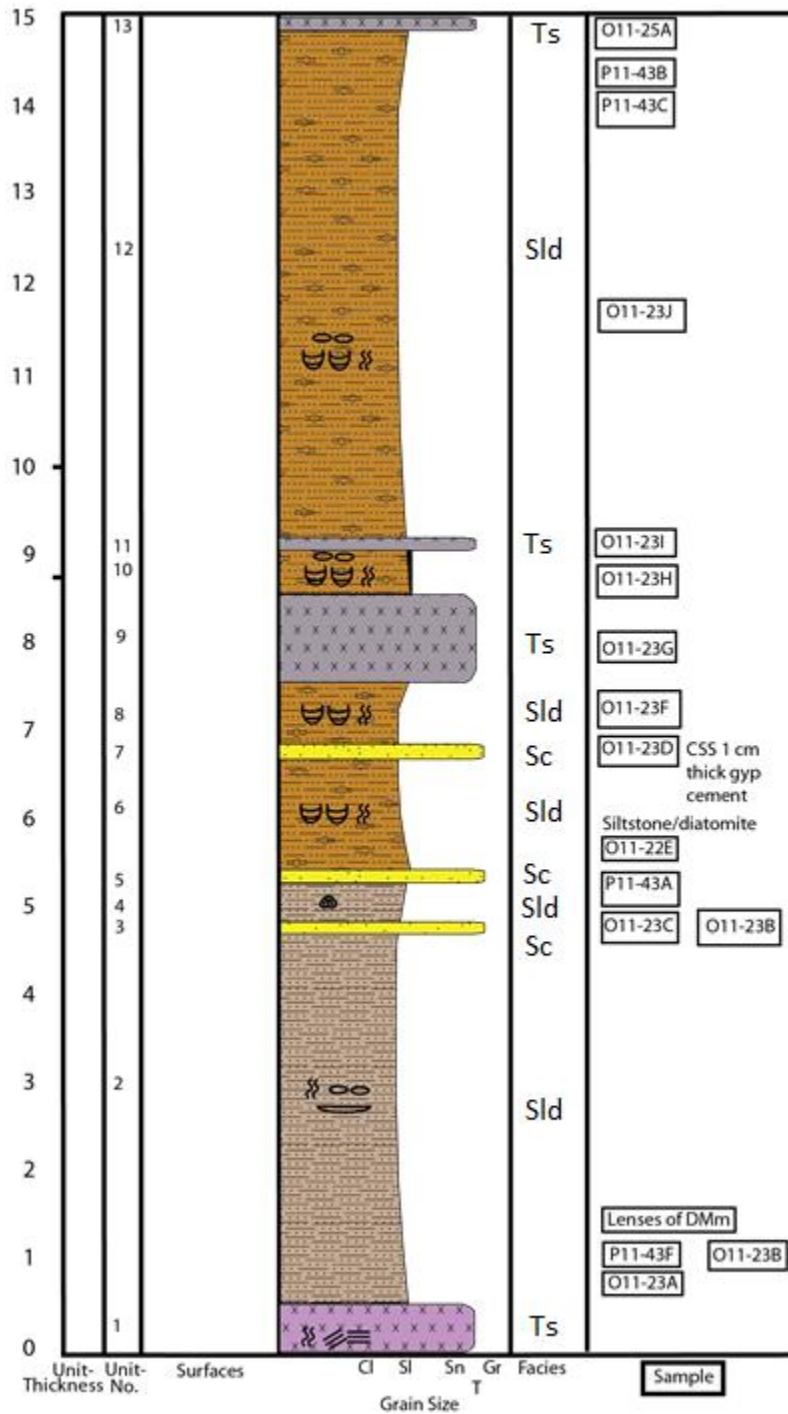


B

Figure 18 A and B. Cerro Ballena Lower and Upper Sections

Cerro Ballena S Stratigraphic Section

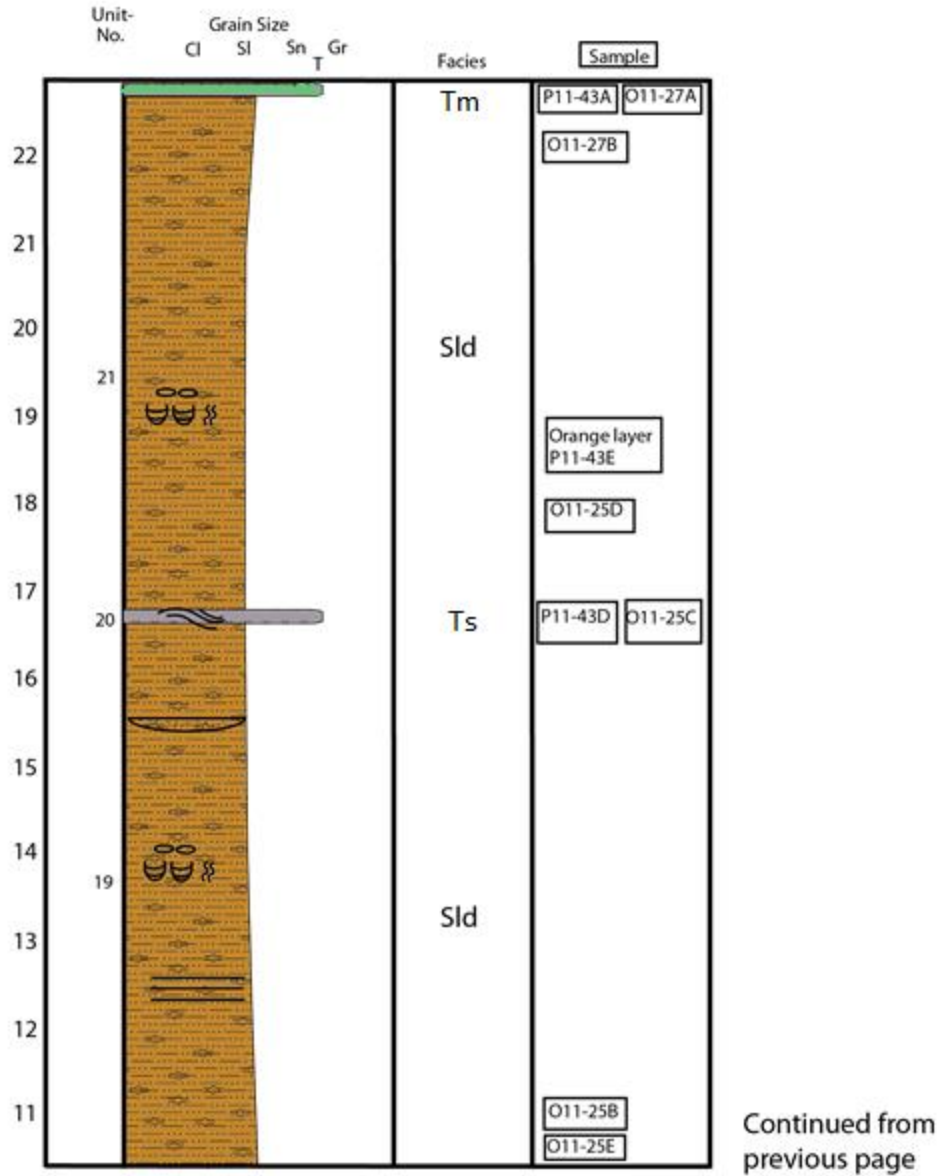
Continued on following page



A

Figure 19 A and B. Cerro Ballena South Lower and Upper Sections

Cerro Ballena S Stratigraphic Section

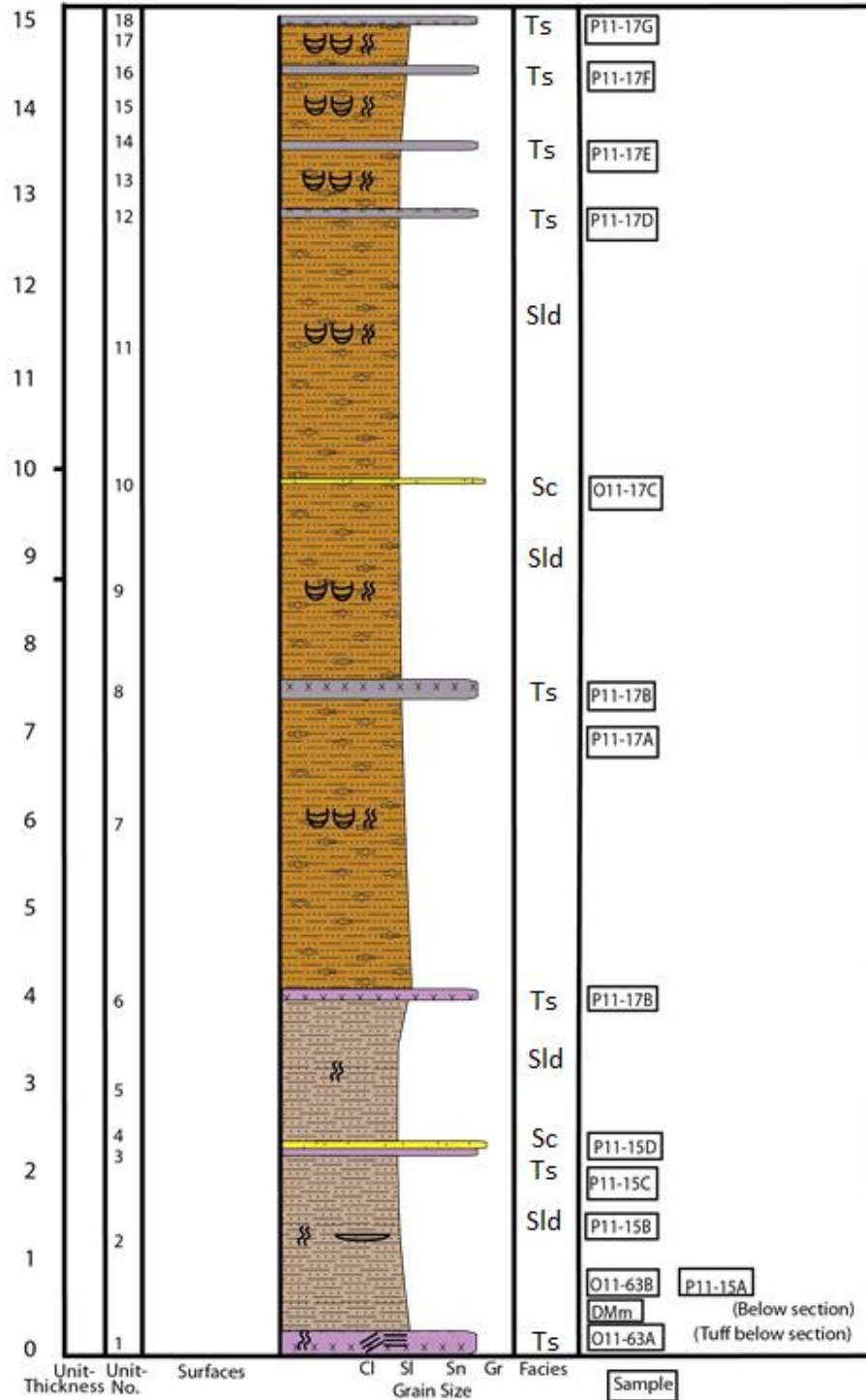


B

Figure 19 A and B. Cerro Ballena South Lower and Upper Sections

Cerro Blanco South Stratigraphic Section

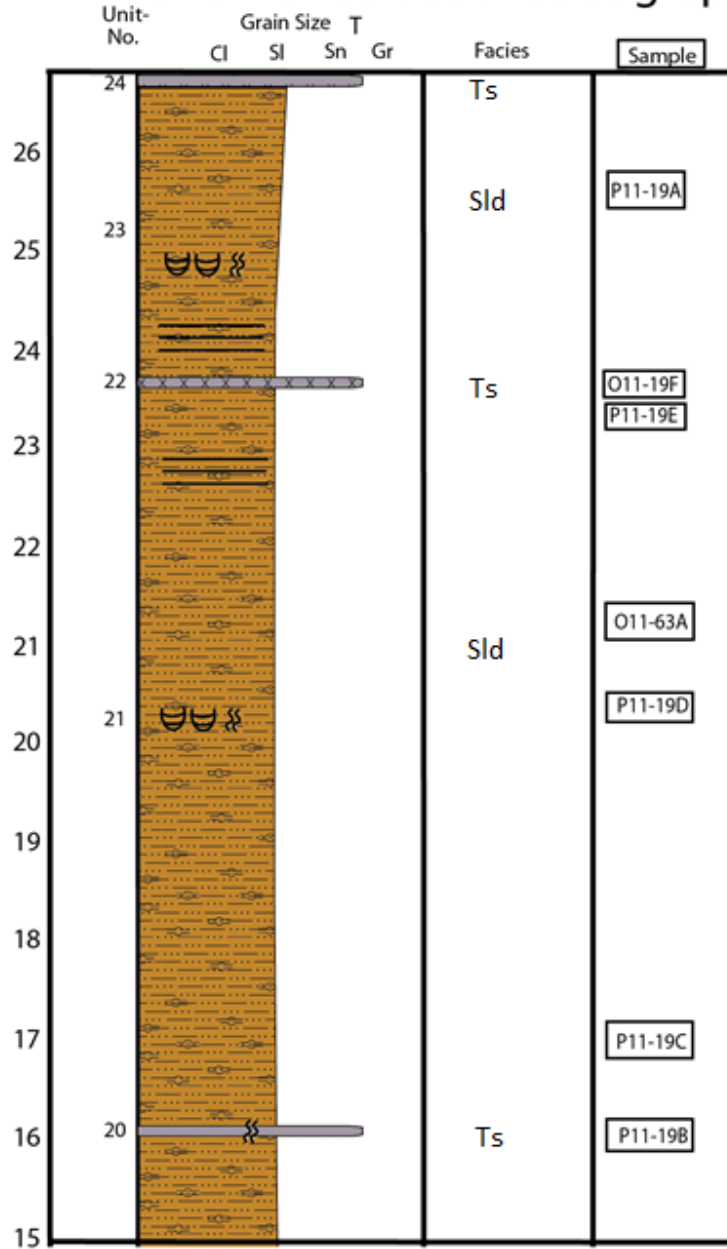
Continued on following page



A

Figure 20. A and B. Cerro Blanco South Lower and Upper.

Cerro Blanco South Stratigraphic Section



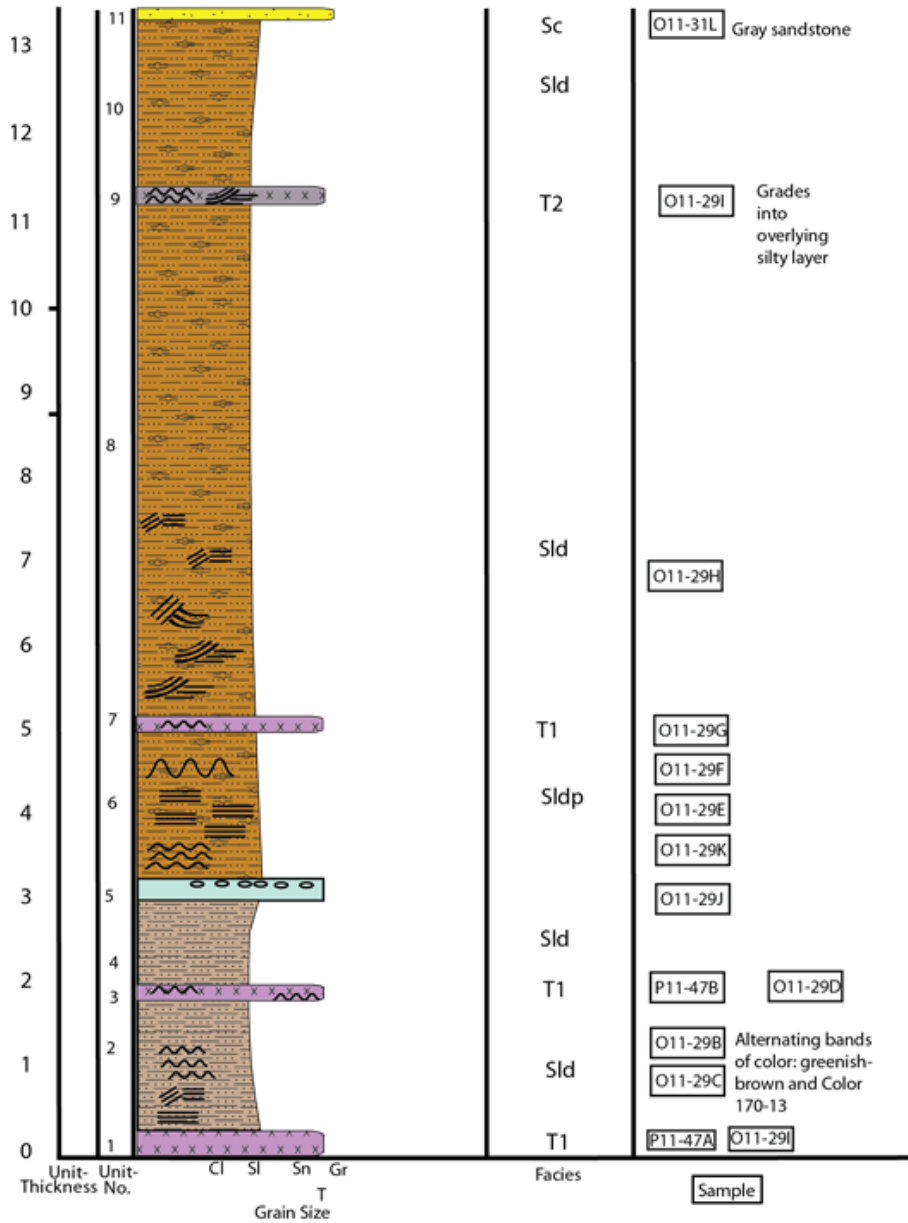
Continued from previous page

B

Figure 20. A and B. Cerro Blanco South Lower and Upper.

Cerro Hueco La Zorra Stratigraphic Section

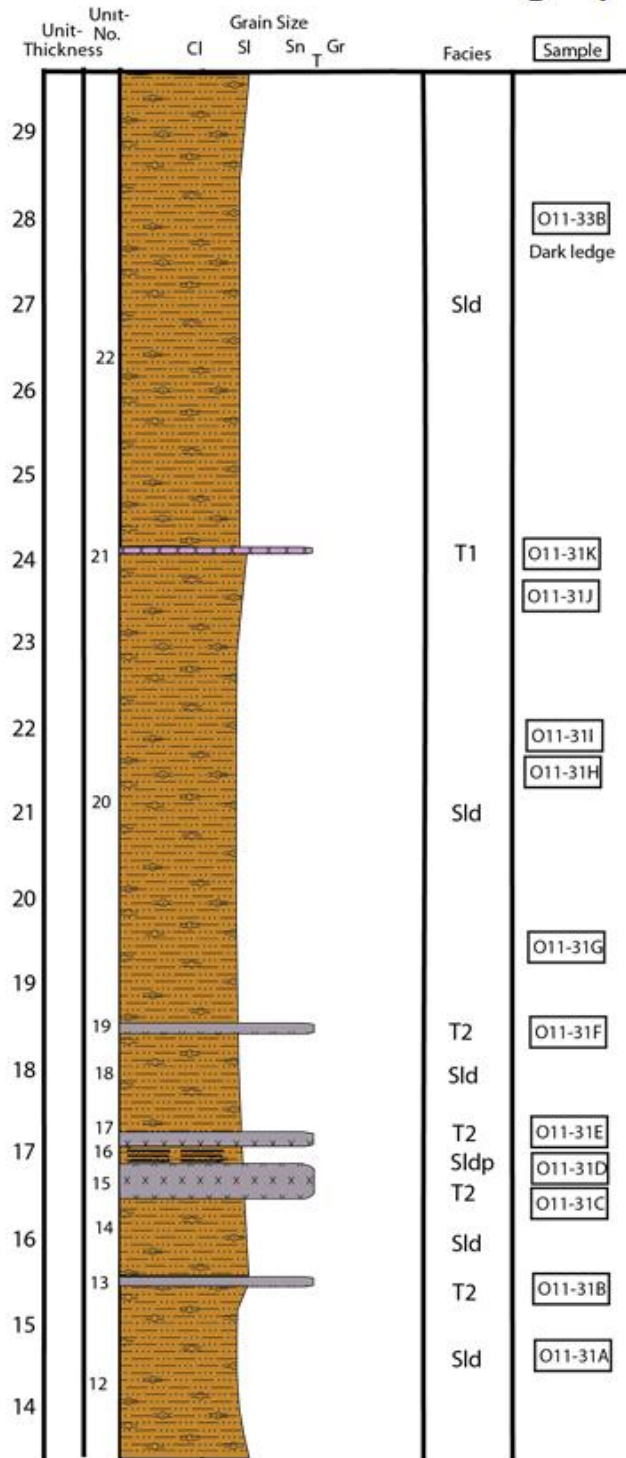
Continued on following page



A

Figure 21. A, B, and C. Cerro Hueco La Zorra Lower, Middle, and Upper Sections, respectively.

Cerro Hueco La Zorra Stratigraphic Section

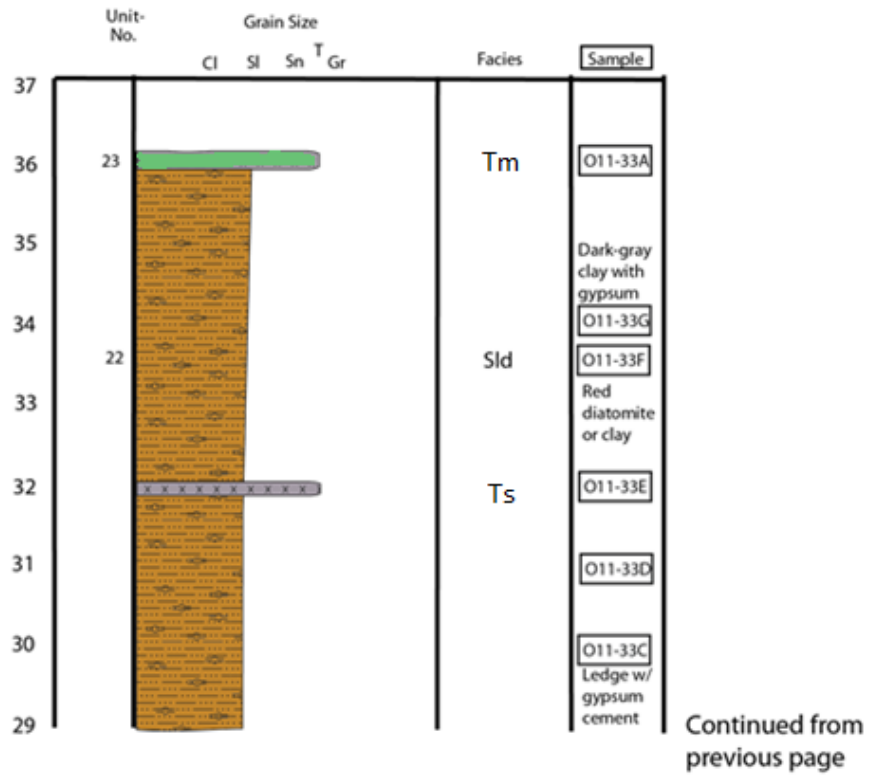


Continued from previous page

B

Figure 21. A, B, and C. Cerro Hueco La Zorra Lower, Middle, and Upper Sections, respectively.

Cerro Hueco La Zorra Stratigraphic Section

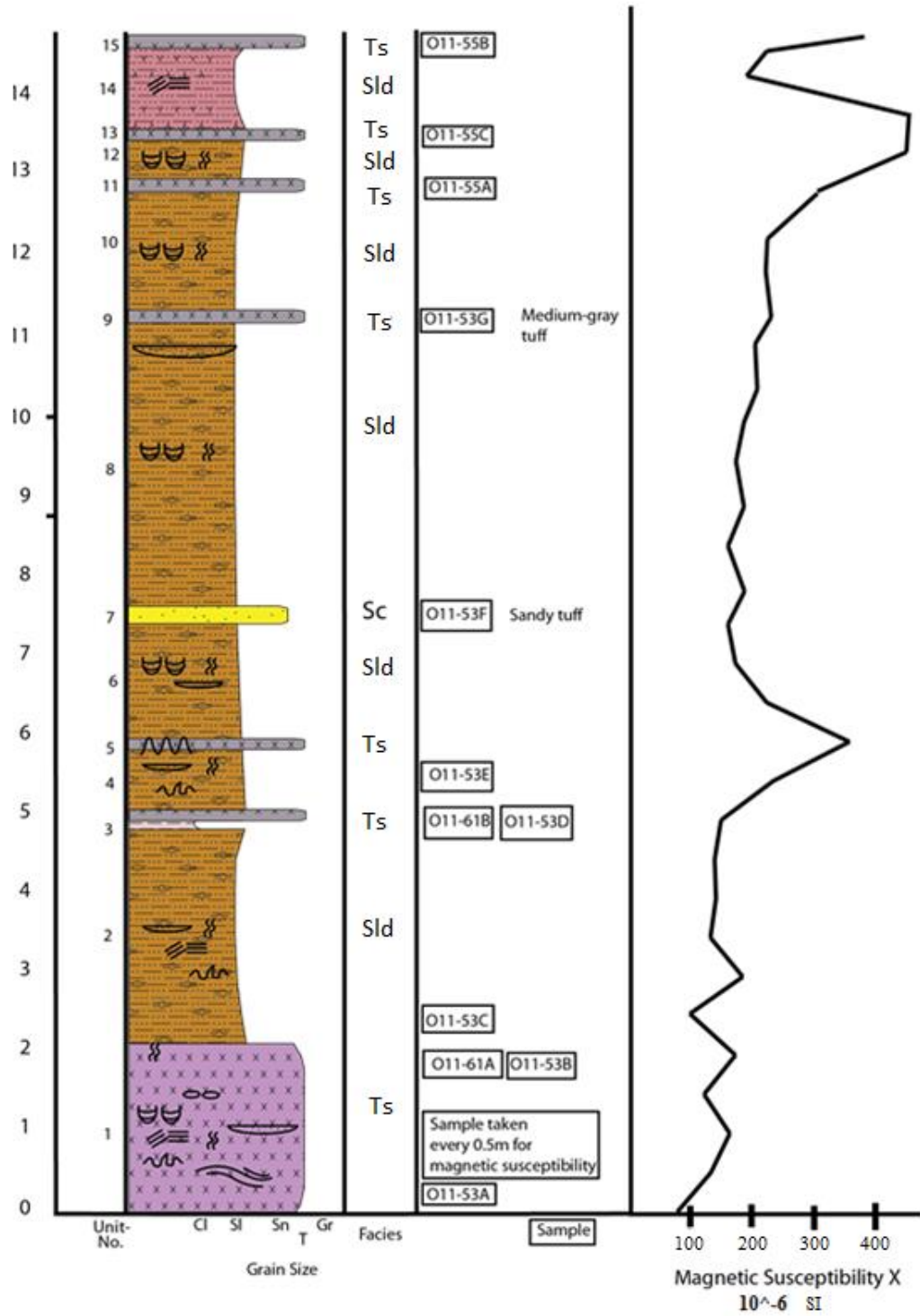


C

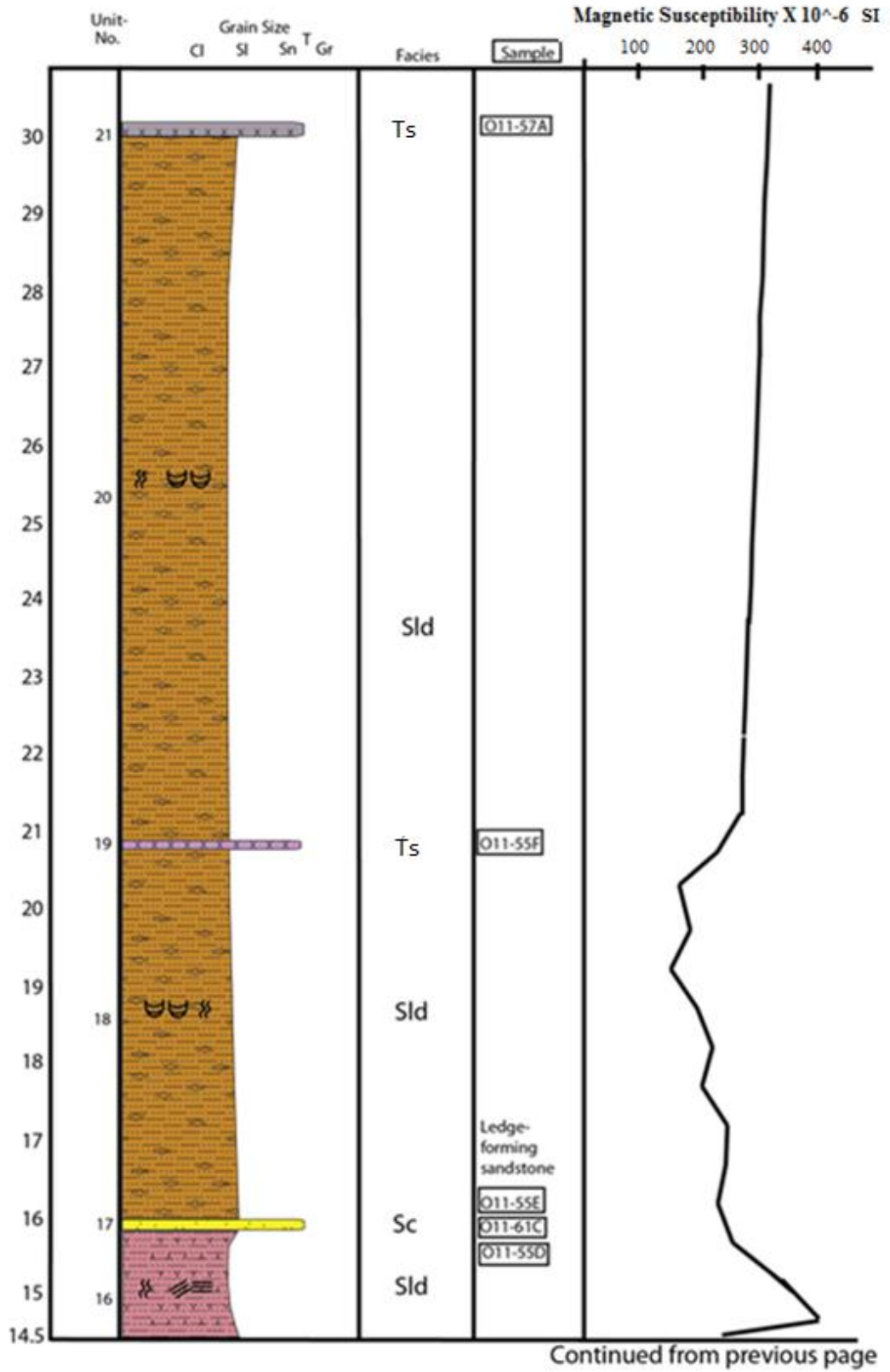
Figure 21. A, B, and C. Cerro Hueco La Zorra Lower, Middle, and Upper Sections, respectively.

Cerro Yeseras South Stratigraphic Section

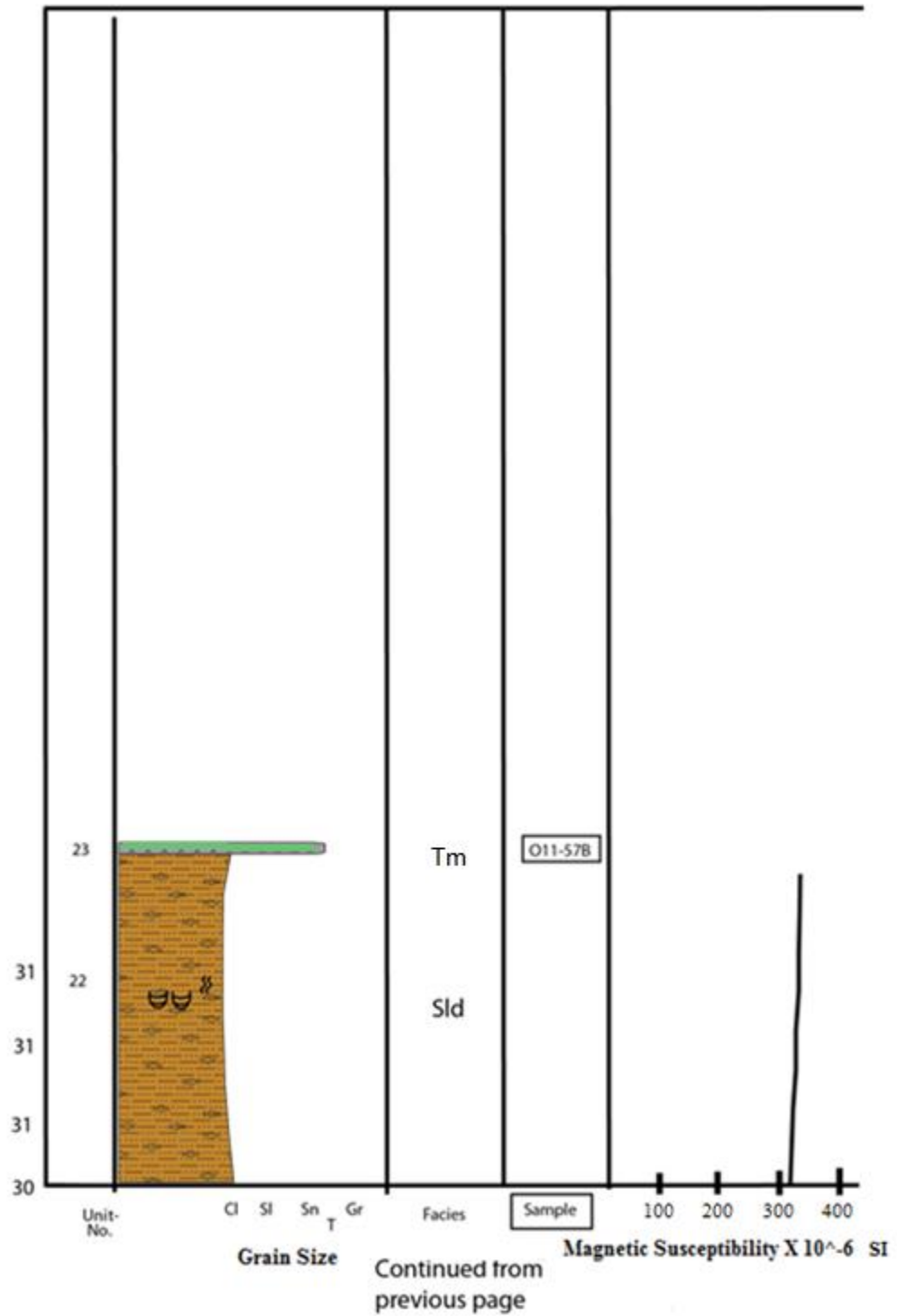
Continued on following page



A
 Figures 22. A, B, and C. Cerro La Yeseras Lower, Middle, and Upper Sections.



B
 Figures 22. A, B, and C. Cerro La Yeseras Lower, Middle, and Upper Sections.



C

Figures 22. A, B, and C. Cerro La Yeseras Lower, Middle, and Upper Sections.

Measured $^{40}\text{Ar}/^{39}\text{Ar}$ Dates of Tuffs

Samples of the tuff units used as time markers were collected for $^{40}\text{Ar}/^{39}\text{Ar}$ dating, and the dates were used to put layers in a general stratigraphic context. This was done to confirm the correlation and to help establish the boundaries of the time unit to be measured. Specifically, the $^{40}\text{Ar}/^{39}\text{Ar}$ radioisotope measurements of the upper (T_2 and T_3) and lower (T_1) tuffs define the boundaries of the time surface-bounded unit. Specific lithostratigraphic patterns were identified and correlated after this context was established. The dated samples are presented here. Dated samples include one from the top of the study interval, one from near the top, and three from near the base (refer to Table 2).

The white tuff unit T_1 used to define the base of the section was radiometrically dated in three areas within the Ica River Valley (refer to Figures 23-27, the $^{40}\text{Ar}/^{39}\text{Ar}$ graphs). The T_3 unit defining the top of the section and a T_s facies bed within the section were also dated.

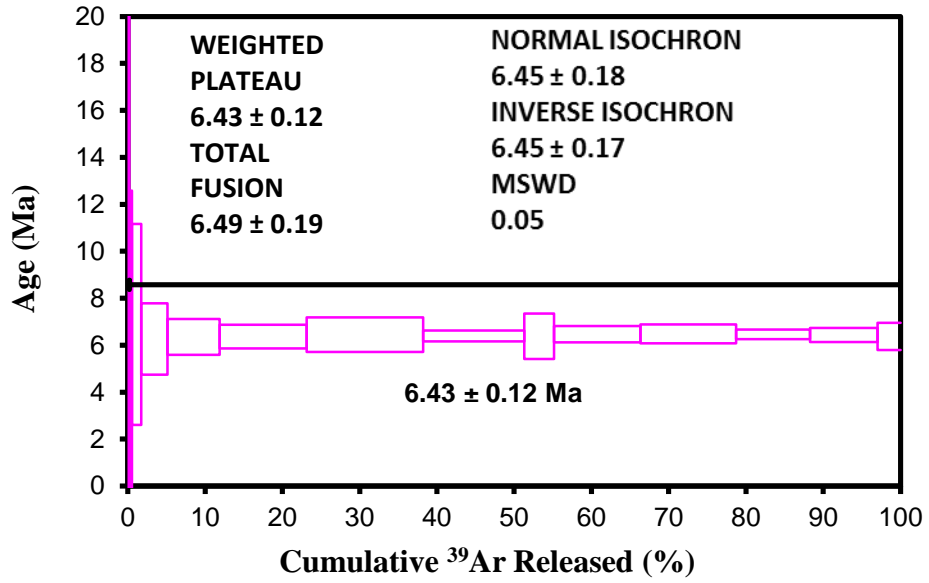
The $^{40}\text{Ar}/^{39}\text{Ar}$ radiometric age results are summarized in Table 2 below. Starting from the base of the study interval, the two samples of T_1 taken from Cerro Blanco and shown in the table, A07-36A and A07-35E, yielded dates of 6.82 ± 0.07 Ma and 6.75 ± 0.13 Ma, respectively. Another T_1 tuff sample taken from near Cerro Ballena, A03-139C, yielded an age of 6.87 ± 0.04 Ma. A white T_s bed in the middle of the section at Cerro La Yeseras, A07-27B, was dated at 7.12 ± 0.09 Ma. At the top of the interval studied, the dark T_3 tuff with visible biotite crystals yielded an $^{40}\text{Ar}/^{39}\text{Ar}$ age of 6.43 ± 0.12 Ma.

Table 2. $^{40}\text{Ar}/^{39}\text{Ar}$ radiometric age results.

Sample	Sample Description	Weighted Plateau Age (Ma \pm 2 σ)	MSWD	Inverse Isochron Age (Ma \pm 2 σ)	Latitude (deg S)	Longitude (deg W)	Elevation (m)
A07-77A	Upper time marker (biotite-rich tuff), Cerro Ballena	6.43 \pm 0.12	0.04	6.45 \pm 0.17	14.34598	75.71836	436
A07-27B	Tuff unit (white tuff), Cerros La Yesera	7.12 \pm 0.09	0.23	7.12 \pm 0.11	14.52842	75.57885	422
A07-36A	Lower time marker (white tuff), Cerro Blanco	6.82 \pm 0.07	0.08	6.82 \pm 0.18	14.39817	75.7013	496
A07-35E	Lower time marker (white tuff), Cerro Blanco	6.75 \pm 0.13	0.02	6.74 \pm 0.35	14.39551	75.70151	476
A03-139C	Lower time marker (white tuff), Cerro Ballena	6.87 \pm 0.04	0.23	6.79 \pm 0.12	14.36266	75.71173	467

As noted, a sample from a white T_s tuff within the section at Cerro La Yeseras (between the time markers T₁ and T₃) and yielded an $^{40}\text{Ar}/^{39}\text{Ar}$ age of 7.12 \pm 0.09 Ma. These ages from different outcrops and different stratigraphic levels in the section all fall within a relatively small range (7.12 Ma – 6.43 Ma = 0.69 Ma). The average yielded age for the lower time marker, the T₁ unit, is 6.81 \pm 0.49 Ma.

A



B

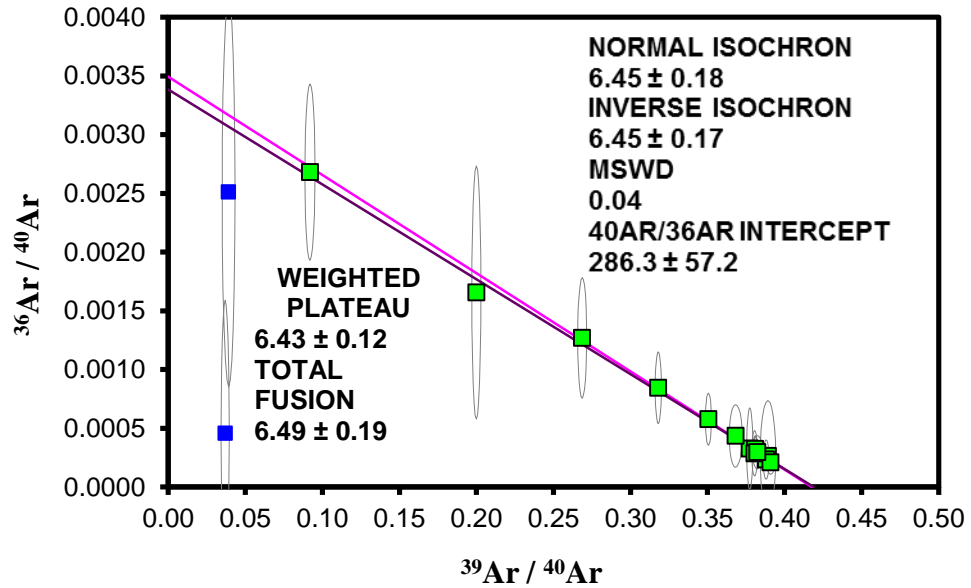


Figure 23. $^{40}\text{Ar}/^{39}\text{Ar}$ weighted plateau (A) and inverse isochron (B) plots for Sample A07-77A. This is the dark-colored biotite-rich tuff (the T_3 unit) at the top of the section. Sample is from Cerro Ballena South. Ages calculated by several methods are written in the box of the graph. Each pink box is a radiometric age with variance for each heating step. Green squares indicate data points used for the line of best fit, and blue squares indicate outliers that were not used in the line. Ellipses around the data points show confidence interval.

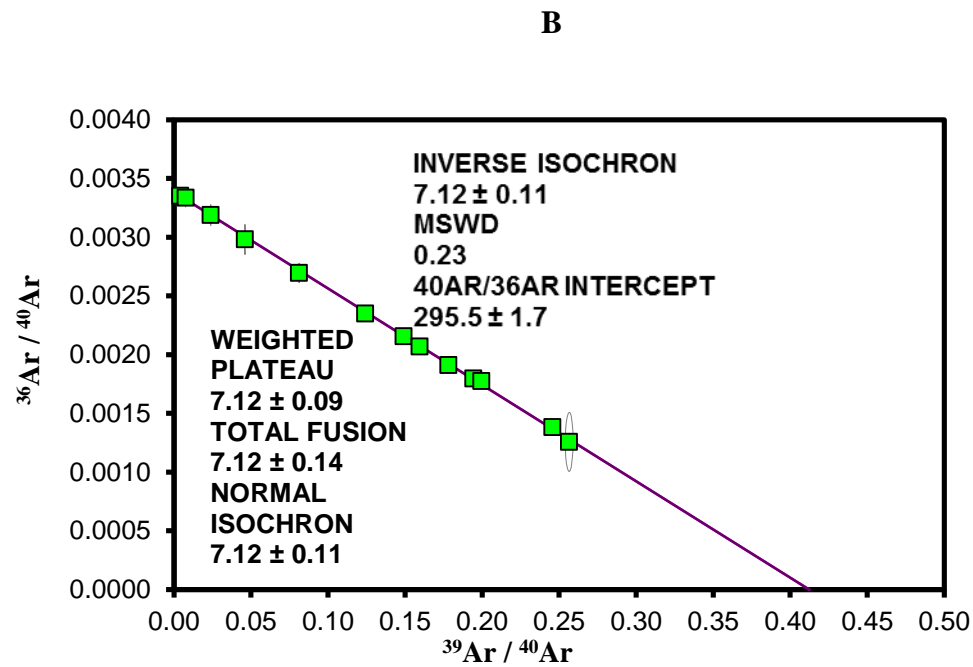
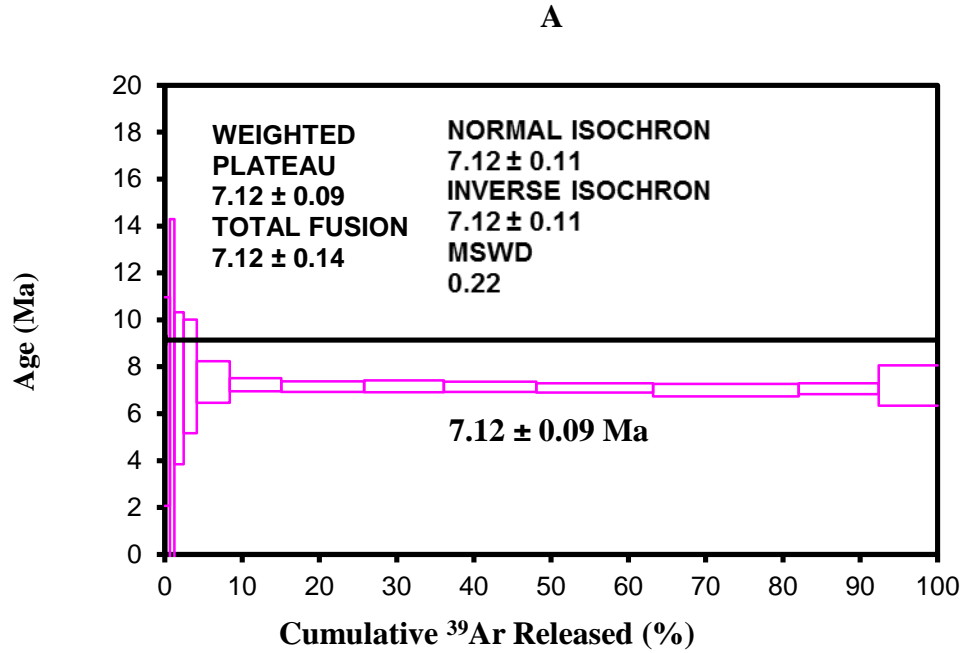
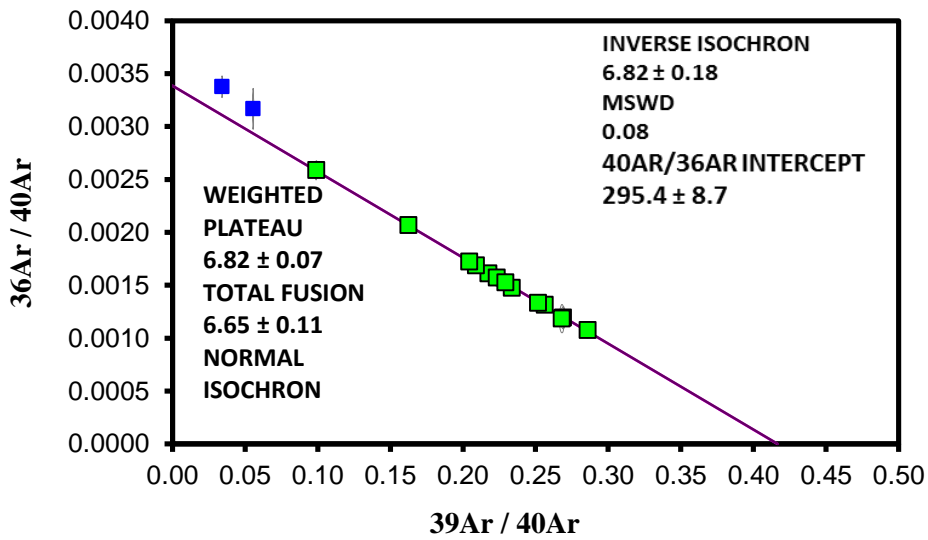
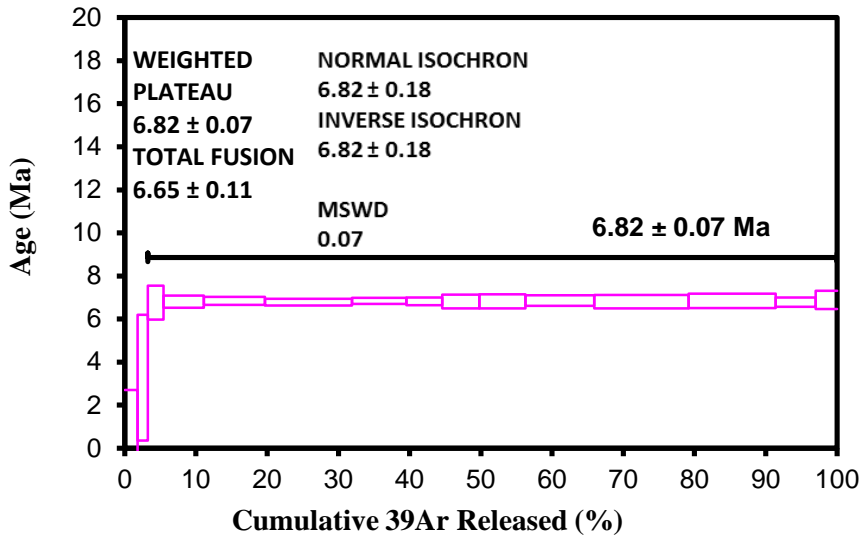


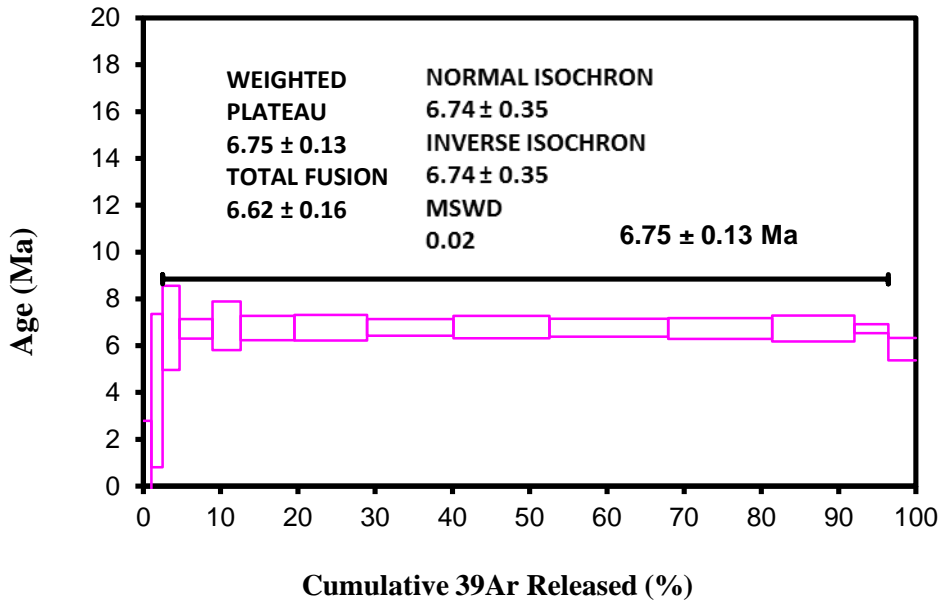
Figure 24. $^{40}\text{Ar}/^{39}\text{Ar}$ weighted plateau (A) and inverse isochron (B) plots for Sample A07-27B. This is a white-colored tuff between the upper and lower time markers. Sample is from Cerros La Yesera. Ages calculated by several methods are written in the box of the graph. Green squares indicate data points used for the line of best fit. Ellipses around the data points show confidence interval.



B

Figure 25. $^{40}\text{Ar}/^{39}\text{Ar}$ weighted plateau (A) and inverse isochron (B) plots for Sample A07-36A, the white tuff at base of the section. Sample is from Cerro Blanco. Ages calculated by several methods are written in the box of the graph. Each pink box is a radiometric age with variance for each heating step. Green squares indicate data points used for the line of best fit, and blue squares indicate outliers that were not used in the line. Ellipses around the data points show confidence interval.

A



B

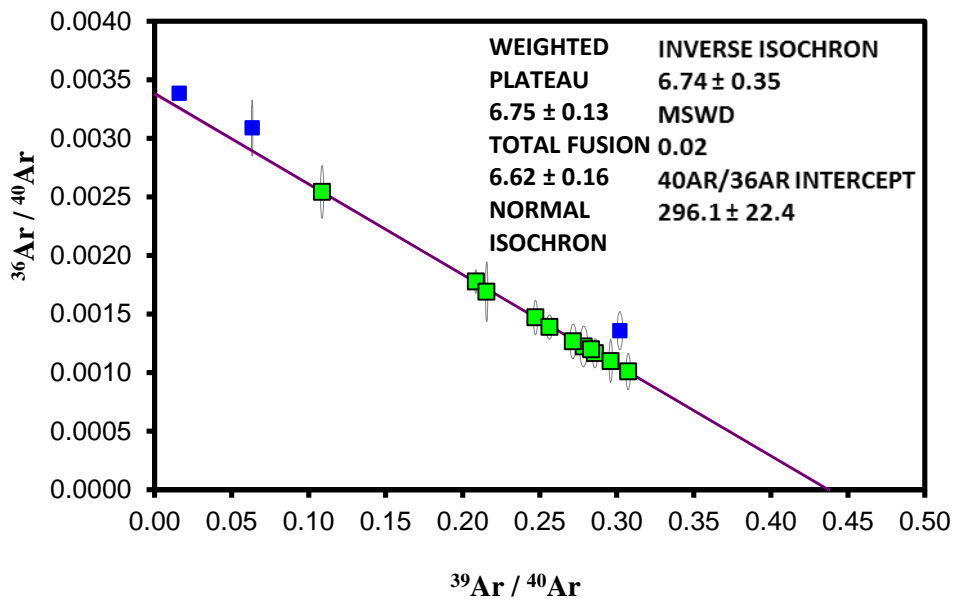
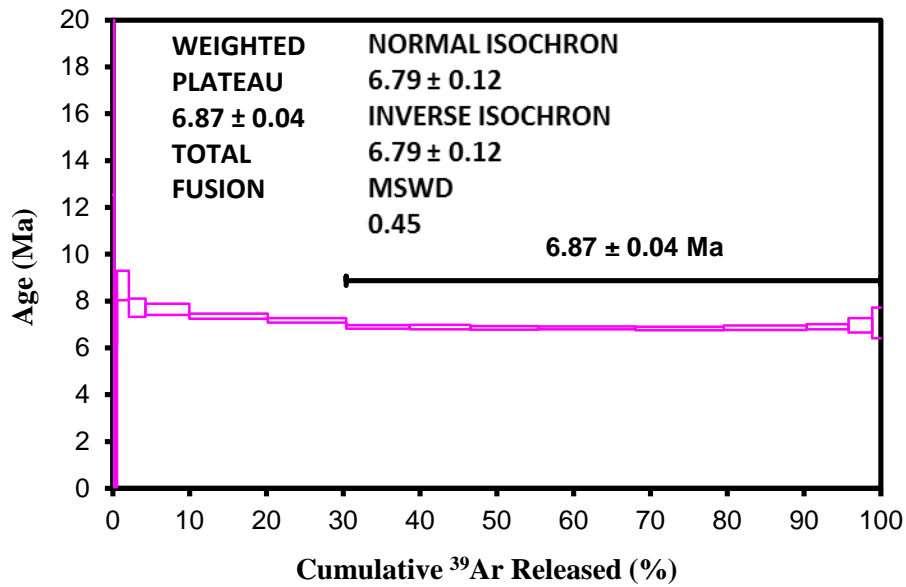


Figure 26. $^{40}\text{Ar}/^{39}\text{Ar}$ weighted plateau (A) and inverse isochron (B) plots for Sample A07-35E. This is the white tuff at the base of the section. Sample is from Cerro Blanco. Ages calculated by several methods are written in the box of the graph. Each pink box is a radiometric age with variance for each heating step. Green squares indicate data points used for the line of best fit, and blue squares indicate outliers that were not used in the line. Ellipses around the data points show confidence interval.

A



B

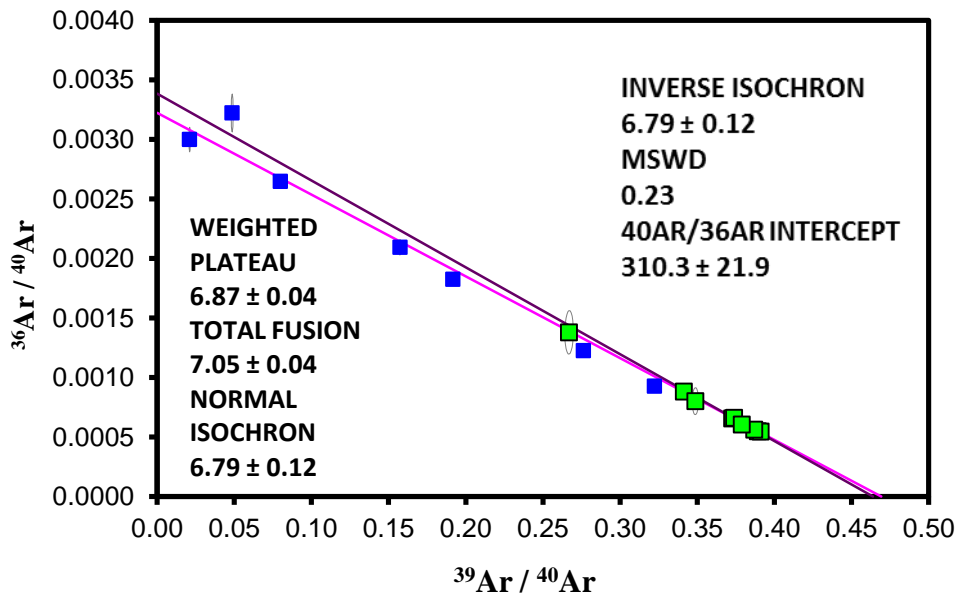


Figure 27. $^{40}\text{Ar}/^{39}\text{Ar}$ weighted plateau (A) and inverse isochron (B) for Sample A07-139C. This is the white tuff at the base of the section. Sample is from Cerro Ballena. Ages calculated by several methods are written in the box of the graph. Each pink box is a radiometric age with variance for each heating step. Green squares indicate data points used for the line of best fit, and blue squares indicate outliers that were not used in the line. Ellipses around the data points show confidence interval.

A summary of the mean age results is reproduced below in order of stratigraphic height (Table 3).

Table 3. Summary of $^{40}\text{Ar}/^{39}\text{Ar}$ Ages of Tuffs

Unit	Facies/Unit	$^{40}\text{Ar}/^{39}\text{Ar}$ Age	Location
White Tuff (Lower Bound)	T _s /T ₁	6.81 ± 0.24 Ma	Cerro Blanco and Cerro Ballena
White Tuff within section	T _s /NA	7.12 ± 0.11 Ma	Cerro La Yeseras
Biotite-rich Dark Tuff (Upper Bound)	T _m /T ₃	6.43 ± 0.12 Ma	Cerro Ballena North

Magnetic Susceptibility

To better understand environmental and sedimentological conditions during deposition, I took magnetic susceptibility measurements of two selected sections, one from a southern outcrop in my transect (Cerro La Yeseras) and one from a northern outcrop (Cerro Ballena). I collected sediment samples every 0.5 meters from the bottom to top of each section. The results are displayed as graphs in Figure 28 below. The two graphs for the two sections are placed side by side for comparison.

In Cerro Ballena, with the exception of five spikes, the magnetic susceptibility values fluctuate slightly between 50 and 300 X 10⁻⁶ SI. A spike occurs at 0 – 1 meters, two at 5 – 7 meters, one at 14 meters, and one at 23 – 24 meters. These spikes correspond with a white-colored T_s complex, dark gray T_s beds, a concretion, and the tuff unit T₃ (which defines the top of the section), respectively.

In Cerros La Yesera, the values generally fluctuate between 50 and 200 X 10⁻⁶ SI near the bottom 12 meters and top 15 meters, the majority of which is the dominant pink-colored diatomaceous mudstone. A thick light gray-colored T_s tuff sits at 5-6 meters from the base, and corresponds with the spike in the susceptibility value. The value gradually increases and decreases because of the thickness of the tuff, and presumably because the tuff grades into the beds above it. Two other noticeable spikes in susceptibility, at about 13 m and 15 m, are associated with a gray T_s tuff complex. Another spike emerges at about 23 meters, although no tuff is present at that height. However, an orange, Fe-stained concretion ledge sits at that height. From 13 m to 20 m, the values are generally higher than at the bottom and top 10 meters. This interval is characterized by many dark-colored T_s tuff beds. Values of MS show a similar gradual

increase and decrease above average values from 5 – 20 meters in the Cerros La Yeseras section and from 7 – 14 meters in the Cerro Ballena section.

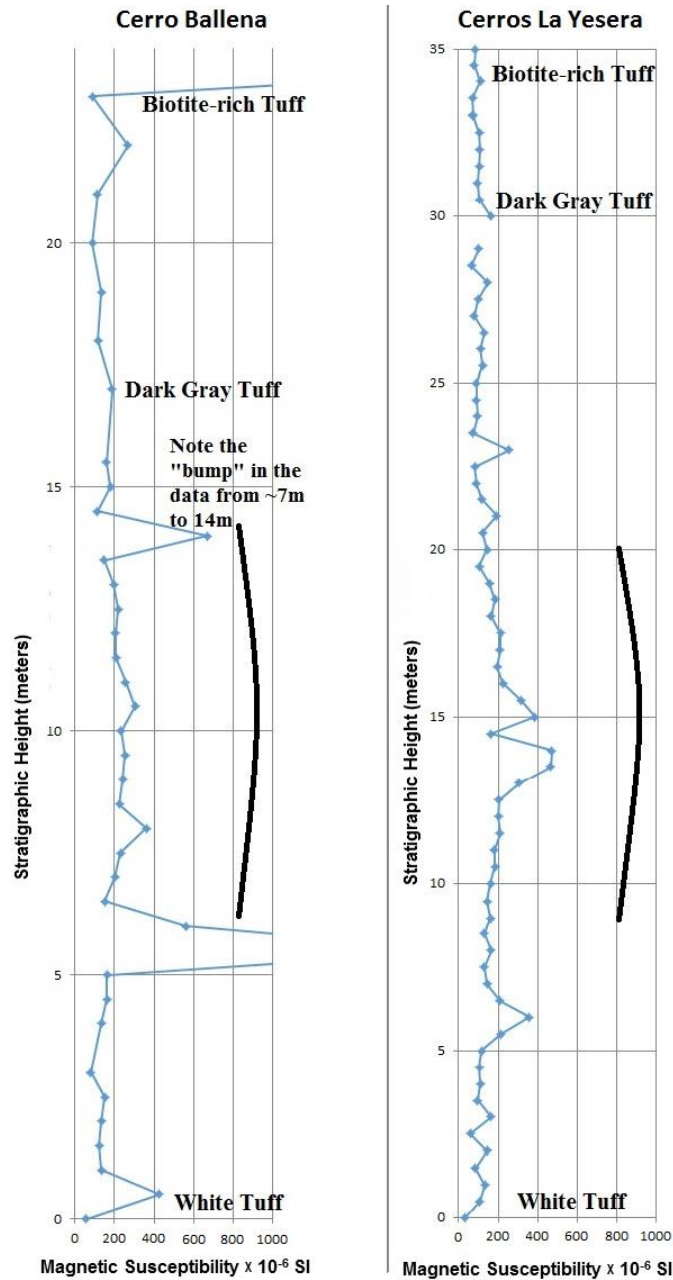


Figure 28. Magnetic susceptibility plots, side by side, at Cerros La Yesera and Cerro Ballena. Since both sections are assumed to represent the same stratigraphic interval, the vertical scales are calibrated to each other. Note the “curve” in magnetic susceptibility (increasing and decreasing values, with a relative maximum in the middle) that appears in the same relative position stratigraphically.

CHAPTER FOUR: DISCUSSION

Map

It is important to note the level of completeness of the map for the Ica River Valley (see Fig. 3). As the map shows, the dark gray tuff marking the top of the section (unit T₂) can only be observed in select geographic regions in the modern topography. Further west and southwest, we could not locate any signs of the tuff, due to modern erosion. The reason for concluding that modern erosion is responsible is the presence of Jurassic volcanics and older sedimentary rocks exposed at the surface in this region to the west. The fact that these older rocks are exposed in the vicinity suggests erosion was active and removed much of the more modern sediments. We also could not locate the tuff in any location to the east, possibly due to burial or ancient erosion.

Similarly, the ⁴⁰Ar/³⁹Ar-dated white tuff (T₁) that defined the base of the section seemed to be missing in some locations. In some places, the T₁ unit was completely eroded away (see Fig. 14). In Cerro Hueco La Zorra, there were multiple white T_s tuffs of the same lithology at the approximate vertical distance of 27 meters below the top of the section. Specifically, there are two biotite-rich white T_s tuff units: one 31 meters below the top of the section, and another 36 meters below. Another white-gray T_s tuff is present between those two tuffs (at 34 meters below the top of the section), but it did not contain significant amounts of biotite. It is assumed that one of those three tuff beds is equivalent to the time marker unit T₁ in the other outcrops.

Structure Implications

The elevation of the dark gray tuff (T₂ unit) above sea level varies from location to location. The T₂ unit at the southernmost outcrop at Cerro La Yeseras South has an elevation of about 396 meters (1300 feet). Further north on Cerro La Yeseras, the elevation is about 320 meters (1050 feet).

To the west lies Cerro Hueco La Zorra, Cerro Blanco, and the outcrops in Cerro Ballena further north. As in Cerro La Yeseras to the east, the elevation of the T₂ unit decreases from south to north. The elevation is about 550 meters (1800 feet) at Cerro Hueco La Zorra, about 520 meters (1700 feet) in Cerro Blanco, and about 415 meters (1365 feet) in Cerro Ballena North. These elevation differences are due to uplift that has occurred in the region.

The decrease in elevation from south to north in Cerro La Yeseras is interesting in light of the fact that the ancient shoreline lies to the north of Cerro La Yeseras. This is opposite to what is expected without uplift, as elevation should *increase* as one draws closer to the shore. Likewise, elevation decreases shoreward from Cerro Hueco La Zorra in the south to Cerro Ballena in the north. This shows the effect of differential uplift increasing toward the modern coast.

Paleoenvironmental Interpretation of Facies

Interpretation of Facies Sc (Coarse Sandstone)

This facies is a *clastic-rich, coarse-grained facies*, which occurs in the three northernmost outcrops, especially in the two northernmost outcrops, Cerro Ballena North and Cerro Ballena. This facies is interpreted as shallow-water (nearshore) coarse-grained

sediments that accumulated near various islands that existed west of the ancient shoreline and were subsequent reworked by wave action. Several reasons exist for this interpretation. First, these sediments are much coarser than those in sections further south, indicating a more nearshore environment. The units containing this facies also pinch out from north to south. Cerro Ballena and Cerro Ballena North sections are also located near a group of Jurassic volcanic hills, which have been interpreted as ancient islands. These observations suggest that the facies represents nearshore sediments that accumulated near various islands west of the main shoreline.

The megaripple structure within this facies (see Fig. 6) and the coarse grain size in the facies (often ~1 mm in diameter, coarse to very coarse sandstone) suggest a high energy environment, while the moderate sorting, moderate sphericity, and sub-roundedness indicate that the sediments were not reworked significantly. The immature sandstone with fossil fragments and bone fragments support the interpretation of high energy, only slightly reworked sediment.

The abundance of sedimentary structures in the surrounding facies (the S1d) and the lack of burrowing are also consistent with an upper shoreface environment. Some bedforms of the dunes observed were straightcrested or megarippled, which require relatively strong currents, consistent with shallower water.

Candidates for provenance include both local sources and distant sources. The lack of quartz suggests a short transport distance, and thus a local provenance. The Andes Mountains is one possible local source. However, the sediments did not likely originate from the Andes Mountains, since the Andes are dominated by coarse-grained plutonic rocks with large amounts of quartz and feldspar.

Weathering occurred before or shortly after deposition (i.e., weathering did not occur in modern times). The volcanic rock fragments in the sandstones are rounded and weathered. The general roundedness of the grains suggests much movement during transport, but since the transport distance was not very great, the movement is likely due to wave action.

Interpretation of Facies Sldp

This facies is a finer-grained facies that dominates in the southernmost outcrops, Cerro Hueco La Zorra and Cerro La Yeseras South. The specific sedimentary structures (planar laminations, gutter casts, scouring and scour fills, truncations, and wave ripple laminations), which are abundant, indicate wave reworking above storm wave base. The predominance of fine-grained particles and the lower relative abundance of clastics in the outcrops to the south suggest a greater water depth than the water depth during deposition of the northern sections (Cerro Ballena N, NN, and NNN). Thus, these outcrops were deposited further from shore.

Interpretation of Facies Sldm

This facies is a fine-grained facies that differs from Sldp and other Sld in that it lacks abundant sedimentary structures, and exhibits a massive and/or tabular structure. The existence of some sedimentary structures such as hummocky cross-stratification suggests a similar environment as Sldp, and is at least below fair weather base (Dott and Bourgeois, 1982). Burrows also occur in some cases. Massive structures with burrowing has been interpreted by others as deposited in a shallow offshore shelf (Boss and

Blackstock, 2008). Thus, this facies is interpreted as sediments deposited between fair weather base and storm weather base, but further from shore than the Sc facies.

Interpretation of Facies Sld

This facies represents any diatomaceous siltstone that does not fit easily into the category of Sldp or Sldm. The depositional environment is interpreted to be similar to those two facies, and the existence of wave ripple laminations, gutter casts, and scour fills suggest wave reworking above storm wave base. However, the environment is still further from shore than the Sc facies, as suggested by finer grain sizes.

A key component of this facies is diatomaceous material. The diatoms could have either accumulated or been transported from elsewhere. Brand et al. (2004) provide evidence from the abundance of whale fossil preservation in the Pisco Formation and the lack of repeating primary laminations to suggest that the diatoms accumulated through rapid burial. They suggest that the diatoms were laterally advected by currents from the Pacific Ocean while settling out, and redeposited in the shallow, protected bays of the Pisco Basin.

Interpretation of Facies Sfs1: Fine Sandy Siltstone

This facies contains finer-grained material than the Sc facies but coarser-grained material than the Sld facies. The presence of some coarse-grained material (fine sand), the abundance of planar laminations, and the proximity to the reworked white T₁ tuff unit together suggest this facies was deposited closer to shore than the Sld facies, but in deeper water than the Sc facies. This facies is found in the northernmost section, Cerro

Ballena North, where the Sc facies is most abundant. Since this outcrop is located closest to shore (i.e., the shore of the Jurassic volcanic islands), I would possibly expect coarser-grained material to be mixed in with the siltaceous material, unlike in other outcrops further from the shore. Since this facies is lacking the coarse material found in Sc, it was likely deposited in deeper water. This interpretation is consistent with the fact that the host unit sits near the base of the section.

Interpretation of Facies T

This facies represents all of the distinct tuff beds found in the section, including T_s and T_m. Each tuff unit, such as the white T₁ unit and the dark gray T₂ unit, exhibit consistent thicknesses and similar compositions across outcrops, suggesting that they are air-fall, volcanic tuffs. The air fall nature of the T facies is discussed more fully in the Stratigraphic Sections and Correlation section. The crystals and lithics mixed in with the ash (as seen in thin sections such as Fig. 15) represent either the volcanic source and/or reworking and mixing with other sediments.

Post-Depositional Processes

Sometime after deposition, the water receded, the environment dried out, and calcium sulfate (gypsum) precipitated out of the water, leaving behind abundant gypsum deposits in the form of cement and fractures fill just below the biotite-rich tuff that defines the top of the section. These deposits occur in all outcrops, and are most abundant in Cerro Blanco. Halite deposits also formed closer to the shore as the

environment dried out, which are present in some of the Sc beds in the northernmost outcrop, Cerro Ballena North.

Provenance

Tuffs

Candidates for provenance include both local sources and distant sources. Since the tuffs appear to be air-fall tuffs, volcanoes are the likely source. The crystals and lithics mixed in with the ash represent either the volcanic source and/or reworking/mixing with other sediments.

As seen in the Facies Descriptions section, tuff samples from both south and north (including the mapped tuff) each consist of a similar quartz-feldspar-lithic ratio: approximately 4% quartz, at least double the amount of feldspar, and a much greater percentage (>30%) of lithics.

Sandstones and Siltstones

The abundance of volcanic rock fragments and glass in the sandstone and siltstone samples collected suggest an origin from the weathering of volcanic rocks (see Figs. 7, 12, and 13). The nearest volcanic sources are Jurassic-age volcanoes approximately 2 kilometers from Cerro Ballena, and are thus a likely provenance for these sediments.

Sandstone is most abundant in Cerro Ballena North, and the sandstones there generally have a high percentage of lithics (60 – 95% volcanic rock fragments), a lower amount of feldspar (~1%), and an even lower amount of quartz (<1%). According to Dickinson et al. (1983), this suggests a provenance of an undissected arc to possibly a transitional arc, consistent with the origin of tuffs in an arc setting.

The feldspar in the sandstones appear to be partially weathered (see Fig. 29). In addition, the sandstone facies Sc are moderately to well-sorted and rounded, indicating transport distance and/or wave action.

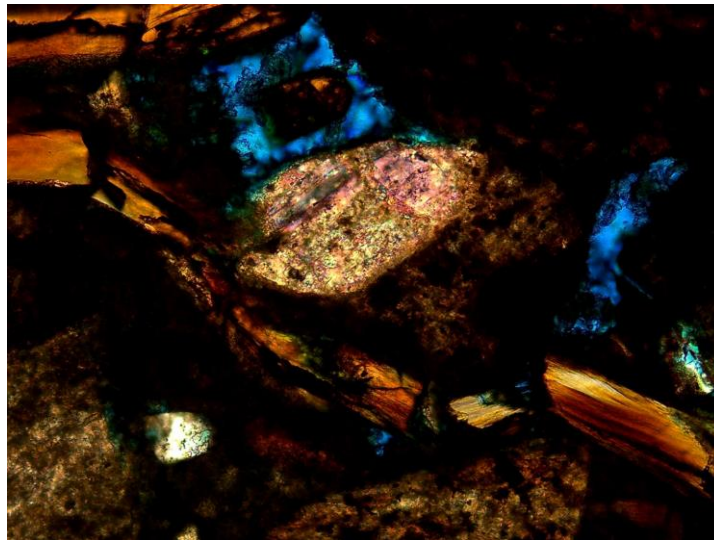


Figure 29. Thin section of Sc (Coarse Sandstone), from Cerro Ballena North, showing weathered feldspar grains. Sample from approximately three meters above the base of the section.

Overall, it appears that the majority of the sediments (which make up the sandstones and siltstones) originated from the weathering of volcanoes in an undissected or transitional volcanic arc. The nearest volcanoes are the Jurassic volcanoes about two kilometers north of Cerro Ballena. Features such as weathered feldspar, rounded grains, and sorting reflect the transport distance as well as the effects of wave action. This is consistent with the hypothesis that the provenance of these sediments is the Jurassic volcanoes a few kilometers to the north.

Diatoms

Diatoms are a significant component of the sediment of the Pisco Formation, and appear in the Sld, Sldm, and Sldp facies, which together comprise the majority of the sediment in my unit. The diatoms most likely first formed in the Pacific Ocean during a time of significant nutrient supply and were advected by currents and redeposited in the shallow, protected bays of the Pisco Basin (Brand et al., 2004).

Stratigraphic Sections and Correlation

This study provides the first detailed regional time correlation of a unit within the Pisco Formation. No previous researcher has attempted a correlation of this extent in the formation. In order to understand the depositional history and to track changes horizontally, it is imperative to establish a stratigraphic context for each of the sections examined. Not only must I know the timespan covered, but I also must know where the sections are located in relation to one another. Correlation also helps illuminate the differences in processes occurring at the same time in different locations in the basin. See Figure 30 for a proposed correlation of the six studied outcrops.

Identification of Tuffs with Unique Characteristics and Dates

My correlation covers a linear transect that is approximately 30 kilometers long. I chose to base the correlation on three ubiquitous tuff units, two of which were subjected to $^{40}\text{Ar}/^{39}\text{Ar}$ dating. A thick, dark gray tuff (unit T₂) that occurs in all six outcrops (see Fig. 31A and B) in association with a biotite-rich T₃ tuff (see Fig. 31C and D) was mapped. This tuff couplet was used to define the top of the section in each outcrop. The

$^{40}\text{Ar}/^{39}\text{Ar}$ -dated biotite-rich, thick white tuff (T_1) with abundant sedimentary structures such as hummocky cross-stratification is also exposed in outcrop all along the transect (see Fig. 32A and B). I used this unit to designate the base of the section. The ubiquity and excellent exposure of these units made them good time markers for correlation and for identifying the same clearly defined bounded time unit in each outcrop.

In addition to the tuff time marker units, other types of units are found in several of the sections, and some are continuous units that span all of the outcrops (refer to Fig. 30). One of the most prominent class of these units is the Sc facies (coarse sandstones), which mostly appear in the three northernmost sections (the Cerro Ballena sections). Many of the Sc sandstones near the top of Cerro Ballena North continue south through Cerro Ballena. One of the sandstone units may extend all the way to Cerro Ballena South as well, as Figure 30 shows.

The Dark Gray Tuff and Correlation of the Top of the Section

The two tuff units used to define the top of the section (the dark gray T_2 and biotite-rich T_3 unit) are separated by approximately 4.7 meters (the average of 6, 3, 6, 5, 4, and 4 meters for each of the six sections). This rough consistency across all outcrops supports the correlation.

Other gray T_s tuffs below the time marker T_2 tuff provide further confirmation of correlation (refer to Fig. 30). Near the top of the three southernmost sections (Cerro Yesera South, Cerro Hueco La Zorra, and Cerro Blanco South), multiple gray T_s tuffs appear below the two upper time markers (T_2 and T_3). The occurrence of these tuffs in the same general placement below the T_2/T_3 couplet in multiple sections further

strengthens the correlation from section to section.

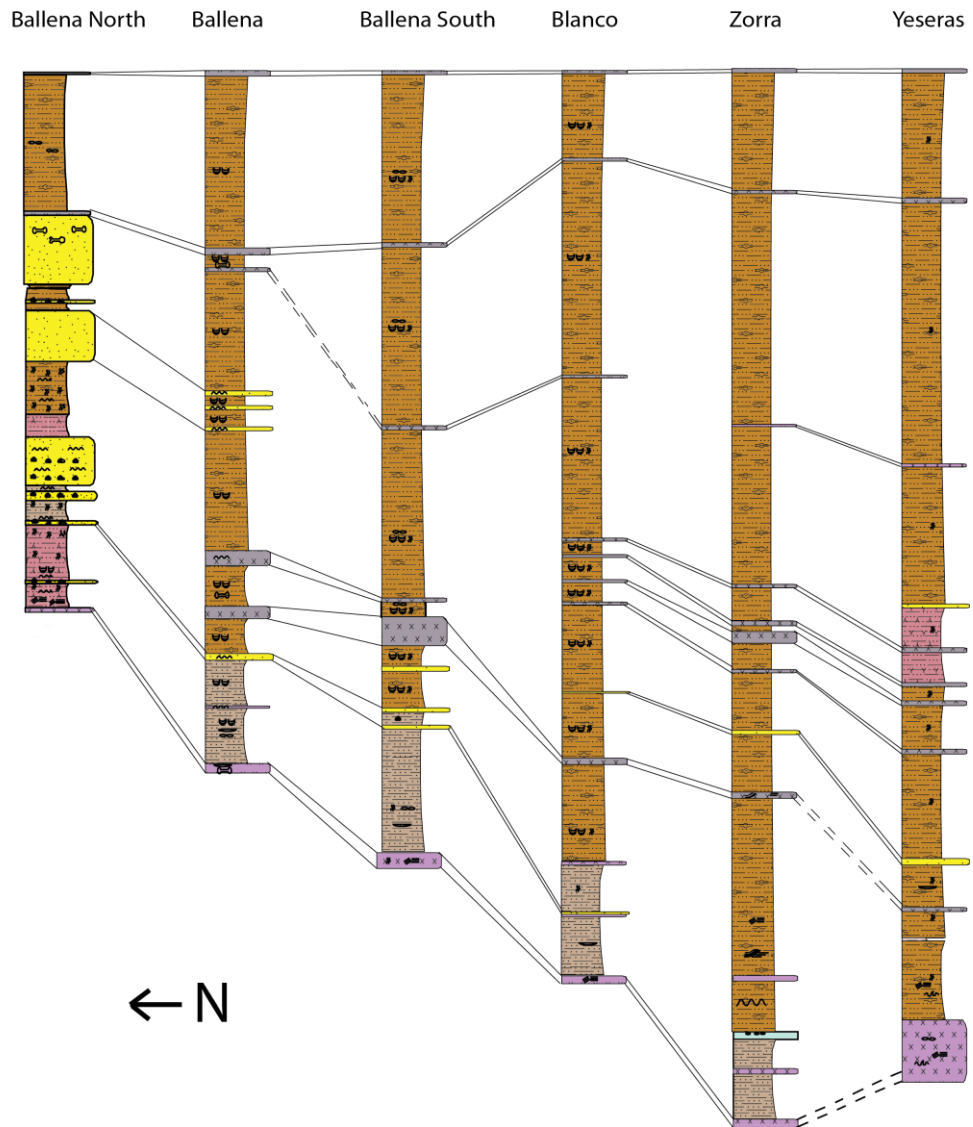


Figure 30. Correlation Panel for all sections, based on the correlation methods as described in this section. Notice that T₃, the biotite-rich dark tuff (uppermost unit), T₂, the thick dark gray tuff (second to highest unit in all outcrops), and T₁, the dated white tuff (lowermost unit), appear in all sections, providing a well-defined interval of time across the study area.

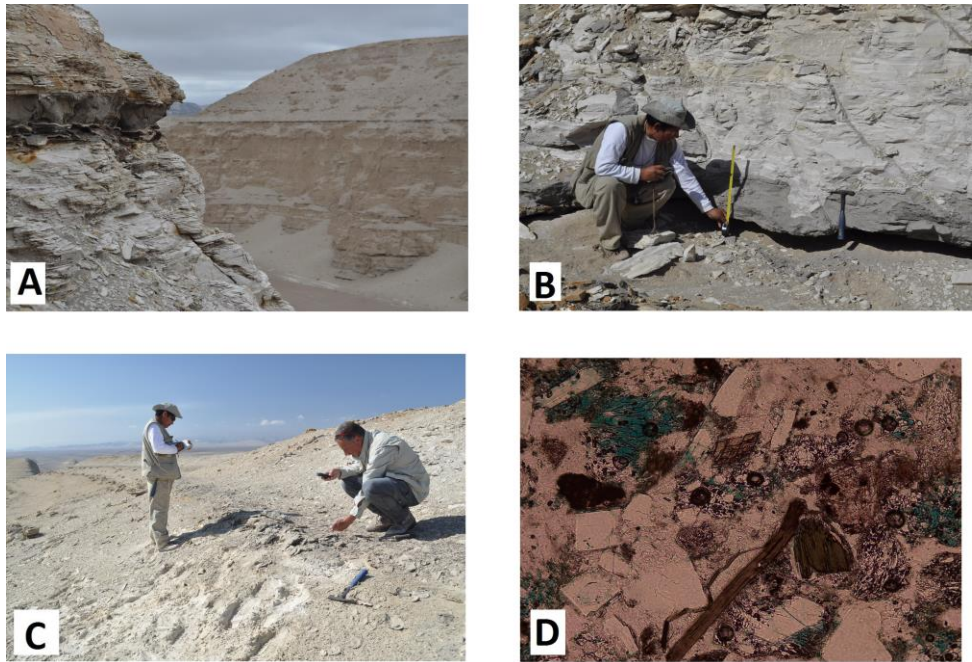


Figure 31. Photographs of upper tuffs (dark gray T₂ tuff and biotite-rich dark T₃ tuff). A. Dark Gray Tuff (T₂) in the context of the outcrop. Cerro Hueco La Zorra. B. Closer view of the Dark Gray Tuff (T₂), with person pointing at the base of the unit. Cerro La Yeseras. C. Close view of the T₃ biotite-rich tuff defining the top of the section. Typical view in weathered exposures shows a dark bench. Cerro La Yeseras. D. Thin section of biotite-rich tuff defining the top of the section, showing biotite crystals, quartz grains, plagioclase feldspar grains, amphibole (with the 60⁰ and 120⁰ cleavage), and volcanic ash. Cemented by calcite (pink-stained in thin section). From Cerro Ballena. Sample A11-20B.

The Dated White Tuff and Correlation of the Base of the Sections

The lower bound of each section was chosen to be a radiometrically dated white-colored tuff bed (T₁) that is rich in visible biotite crystals (see Fig. 32D). These characteristics were used to identify the same ⁴⁰Ar/³⁹Ar-dated white tuff (T₁) in each outcrop. Cerro Hueco La Zorra is the only section that presents difficulty in identifying the tuff, because of two biotite-rich white T₁ tuffs close to one another stratigraphically.

The white T₁ tuffs defining the base of each section are located at 18.5, 23.5, 27, 31, 36, and 34.5 meters below the biotite-rich gray T₃ tuff defining the top of the section. Although these distances do vary, they all exhibit a consistent pattern: the thicker the section, the greater the distance between the tuff couplet at the top (T₂ and T₃) and the white T₁ tuff candidate. This consistency in the distance from the top of the outcrop to the white T₁ tuff helps establish a reasonable correlation. In addition, the white T₁ tuff identified as the base at each location exhibited similar sedimentary structures to one another, such as planar laminations, climbing wave-ripple laminations, wave ripple laminations, cross-bedding, and burrowing at the top of some erosional surfaces (Fig. 32B).

In some places, the dated white T₁ tuff was completely eroded away (Fig. 32C), limiting the ability to use it for correlation. In Cerro Hueco La Zorra, there are two biotite-rich white T_s tuffs: one 31 meters below the top of the section, and another 36 meters below. Another white-gray T_s tuff is present between those two tuffs (at 34 meters below the top of the section), but it did not contain significant amounts of biotite. However, the presence of white T_s units at the same approximate stratigraphic placement as the basal T₁ unit of the other outcrops supports the proposed correlation. At least one of these T_s units are likely to be the same white T₁ tuff unit that exists at the base of all of the other outcrops.

An orange, brownish, or pink weathering occurs on and above the white T₁ tuff bed at the bottom of several sections (refer to Fig. 32C and 33), providing an additional link connecting the sections at their base.

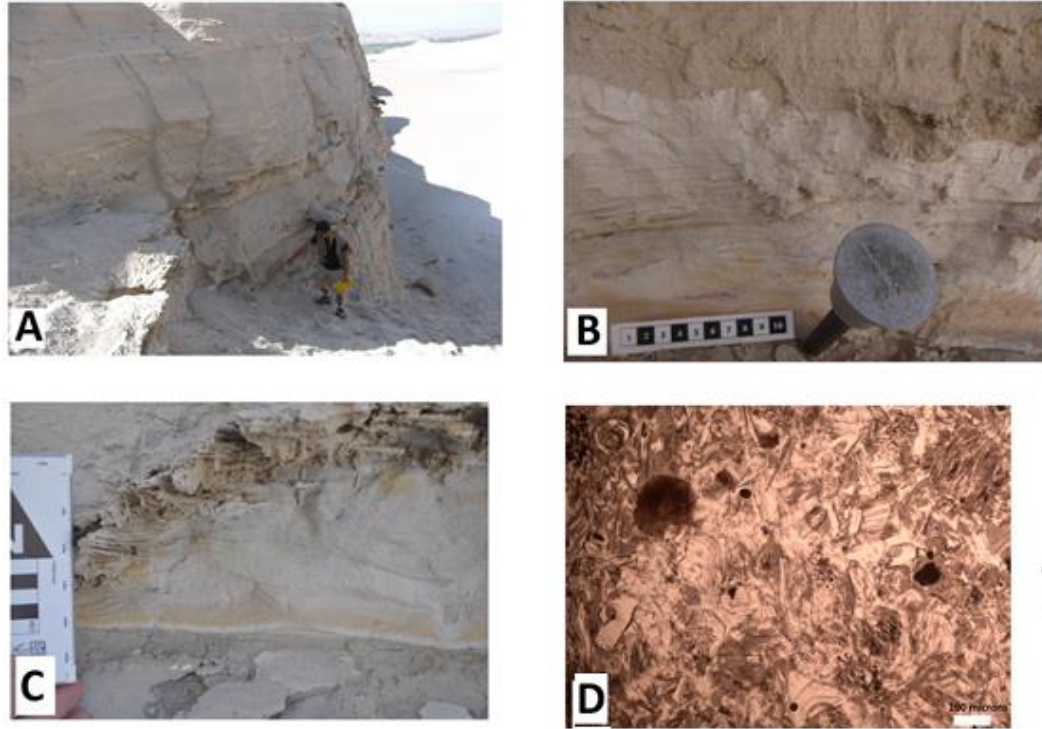


Figure 32. White-colored, biotite-rich tuff (T_1) that defines the base of the section and appears in all outcrops. A. The tuff in outcrop. The person is pointing at the location of the tuff. B. A closer view of the tuff, showing laminations, hummocky cross-stratification, and bioturbation. The stake is a marker indicating where samples were collected for $^{40}\text{Ar}/^{39}\text{Ar}$ dating. C. Close-up view of the tuff showing erosion that causes the unit to pinch out at places. D. Thin section photograph of the tuff in plain polarized light (PPL). The white bar is 100 μm .

Are the Tuffs Airfall?

The first piece of evidence that one of the upper time markers, the dark gray T_2 tuff, is most likely an air fall tuff, is a consistent thickness (approximately 15 centimeters) across all six outcrops, about 30 kilometers of distance. Its composition is also consistent from outcrop to outcrop, with little to no impurities.

The $^{40}\text{Ar}/^{39}\text{Ar}$ -dated biotite-rich white T_1 tuff at the base of the section is also mostly pure, but its thickness varies slightly across the transect. Some of this is due to erosion, and some of it is due to uncertainty in identifying its placement in one of the

outcrops (Cerro Hueco La Zorra). The white T₁ tuff is approximately 0.25 meter thick in all of the outcrops, except in Cerro Ballena South, where it is 60% thicker, approximately 0.4 meters. The general uniformity in thickness suggests that the T₁ tuff beds are airfall tuffs as well. Local reworking may explain thickness variations in T₁.

Additionally, in Cerro La Yeseras (the southernmost section), I observed a complex of white-colored T_s tuffs approximately two meters thick in total. It is uncertain whether the entire complex at Cerro La Yeseras is the ⁴⁰Ar/³⁹Ar-dated white tuff (the T₁ unit defined at Cerro Ballena South) or just one of the white T_s tuffs at the bottom. Barring this southernmost section, the thickness of the white T₁ tuff used to define the base of the section seems consistent across the transect, supporting the interpretation that it is an air-fall tuff.

In the dark gray T₂ tuff, some of the volcanic glass appeared in a dumbbell shape under thin section (see Fig. 34), supporting the idea that the ash particles had been flying through the air immediately before deposition.

Correlation of the Top vs. the Base

The section is defined by two principal time markers: the two dark tuffs at the top and the ⁴⁰Ar/³⁹Ar-dated biotite-rich white tuff at the base. As previously mentioned, the principal unit (T₂) was walked out and mapped across the linear transect (Fig. 3), so it serves as a reliable time marker that correlates all six sections. The lower time marker, the ⁴⁰Ar/³⁹Ar-dated biotite-rich white tuff (T₁), also seems to provide a reliable correlation for the base of the section, though this correlation is not as secure in all outcrops as the top of the section (the primary exception is Cerro Hueco La Zorra).

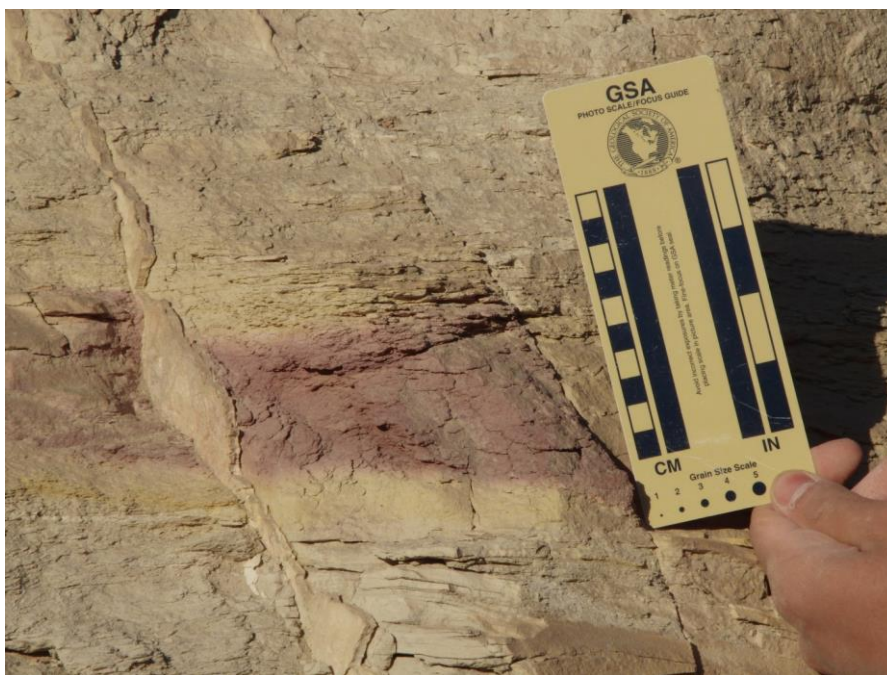


Figure 33. Red-pink coloration approximately five meters above the white tuff (T₁) at the base of Cerro Ballena. GPS: 14.32544⁰ S, 75.72437⁰ W.

In Cerro Ballena, the ⁴⁰Ar/³⁹Ar date for the T₁ tuff unit chosen was 6.87 ± 0.04 Ma, very close to the ⁴⁰Ar/³⁹Ar dates for the T₁ unit chosen at Cerro Blanco, 6.82 ± 0.07 Ma and 6.75 ± 0.13 Ma (refer to ⁴⁰Ar/³⁹Ar results, Table 2 and Figs. 23-27). In each outcrop, at least one biotite-rich white T_s tuff with the same features as the dated T₁ white tuff in Cerro Ballena South exists at the same general placement below the secure upper

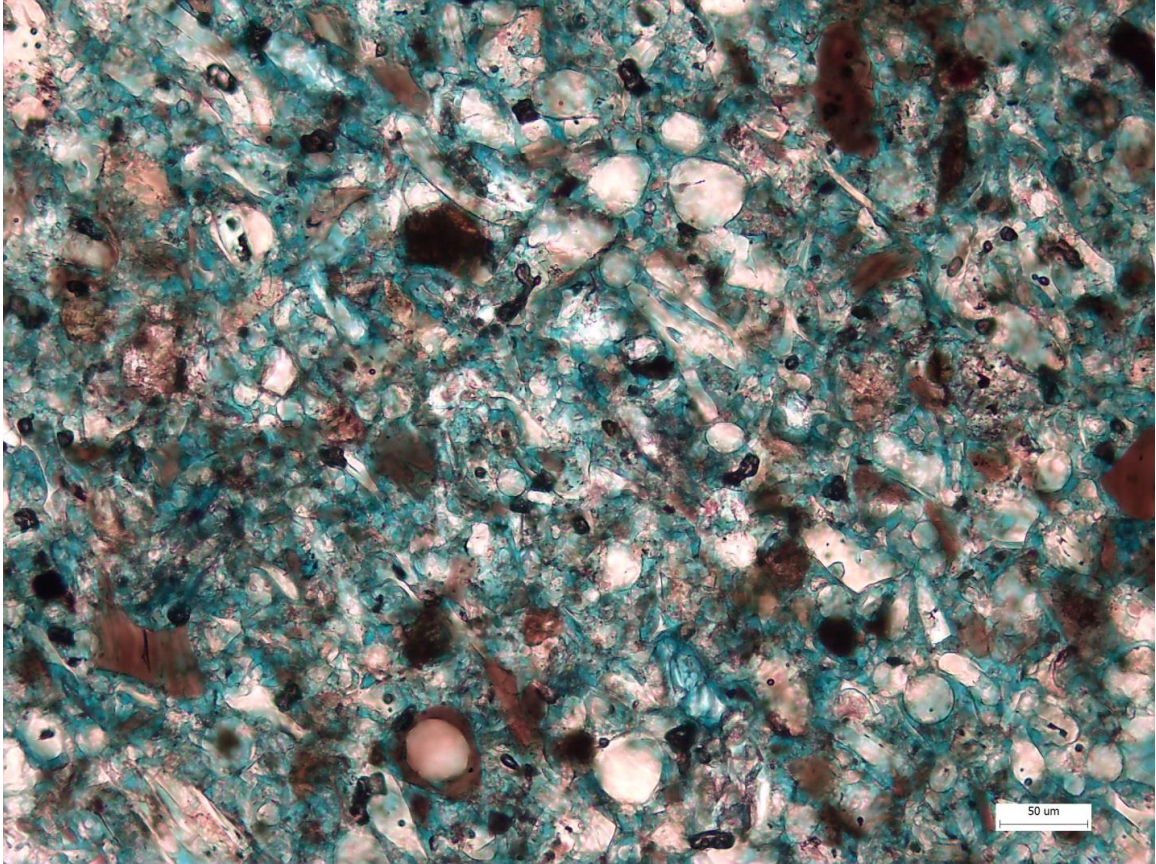


Figure 34. Thin section of dark gray T₂ tuff, showing weathered (brown) glass as well as feldspar, quartz, and gypsum cement. White ruler bar is 50 μm . Sample A11-16B. 14.52895⁰ S and 75.57892⁰ W.

time marker of the biotite-rich dark tuff (T₃), within a range of 18.5 meters (Cerro Ballena North) to 36 meters (Cerro Hueco La Zorra). In none of the sections (except Cerro Hueco La Zorra) do any other good candidates for the same white T₁ tuff appear. The problems associated with identifying the unique basal T₁ unit in Cerro Hueco La Zorra have been discussed. Overall, however, I believe I have properly identified this single white T₁ tuff in all six outcrops, and thus have a reasonably secure lower time marker for my section.

Correlating Units on Each Side of the Ica River

The Ica River runs from north to south and separates Cerro Hueco La Zorra, Cerro Ballena, and Cerro Blanco in the west from Cerro La Yeseras in the east. Cerro Hueco La Zorra in the west is nearly direct across the Ica River from the northern part of Cerro La Yeseras in the east.

The distinctive dark gray tuff (T₂) and the biotite-rich dark tuff (T₃) above it occur in proximity to each other in both Cerro Hueco La Zorra and Cerro La Yeseras. In each outcrop, they are separated by nearly the exact same vertical distance (about four meters).

As noted earlier, multiple gray T_s tuffs appear about halfway down these two sections (as well as in Cerro Blanco South). At least four distinct dark gray T_s tuffs occur between 17 and 21 meters below the top of Cerro Hueco La Zorra and four distinct dark gray T_s tuffs occur between 20 and 24 meters below the top of Cerro La Yeseras. Thus, it is likely that most or all of the four tuffs are continuous across the river between Zorra and Yeseras.

The ⁴⁰Ar/³⁹Ar-dated biotite-rich white T₁ tuff from Cerro Ballena South is identifiable in Cerro La Yeseras South, correlating outcrops east of the Ica River with outcrops west of the river. The white T₁ tuff was difficult to identify in Cerro Hueco La Zorra, but three candidates emerge, all within an expected vertical distance below the top of the section, between 31 and 36 meters below the T₃ unit (a biotite-rich dark tuff). This makes it likely the dated white T₁ tuff appears in Cerro Hueco La Zorra as well, since Cerro Hueco La Zorra is between Cerro Ballena and Cerro La Yeseras, both of which contain the dated white T₁ tuff.

The distance from the northernmost section examined (Cerro Ballena North) to the southernmost section (Cerro La Yeseras South) is approximately 30 kilometers. This study is the first study of the Pisco Basin to correlate sections across this distance. Thus, this study develops the most laterally extensive stratigraphy of a portion of the Pisco Formation to date.

$^{40}\text{Ar}/^{39}\text{Ar}$ Dates of Tuffs

As outlined in the Results section, several tuffs within the section were dated by the $^{40}\text{Ar}/^{39}\text{Ar}$ radioisotope method. Refer to Table 3 for the mean age results of each unit.

The fact that these ages from several outcrops and different stratigraphic levels in the section all fall within a relatively small range (7.12 Ma – 6.43 Ma = 0.69 Ma) indicates that the bounds for the section designated on each outcrop are most likely accurate, and that each section examined represents the same stratigraphic interval. That is, the correlation is most likely accurate. Therefore, the two important time markers that were dated by the $^{40}\text{Ar}/^{39}\text{Ar}$ method (T_1 and T_3) each represent a single event that serves as a reliable correlation across the outcrops.

The $^{40}\text{Ar}/^{39}\text{Ar}$ dates are consistent with stratigraphic order, with the exception of one measurement. An interesting anomaly in the correlation is the older $^{40}\text{Ar}/^{39}\text{Ar}$ age (7.12 Ma) yielded for the white T_s tuff that is stratigraphically higher than the lowest tuff, the T_1 bed, which yielded $^{40}\text{Ar}/^{39}\text{Ar}$ ages ranging from 6.75 to 6.87 Ma. The cause for the difference is possibly explained by the difference in methodology used to obtain the $^{40}\text{Ar}/^{39}\text{Ar}$ date from the “anomalously” old white tuff. Whereas all of the other samples’ $^{40}\text{Ar}/^{39}\text{Ar}$ ages were based on analysis of the *biotite* crystals found in them, the $^{40}\text{Ar}/^{39}\text{Ar}$

date for the “anomalously” old white tuff was based on analysis of the *sanidine* within the sample. However, it is known that coevally erupted biotite and sanidine often do not yield similar radiometric ages (Hora et al., 2010). It has been suggested that this is due to wrongly assuming that minerals contain no argon pre-eruption and that closure to diffusion occurs instantaneously at the time of eruption. However, it is interesting that typically sanidine ages are *younger* than biotite ages (due to extraneous argon within the biotite, from both initial non-zero concentration and externally sourced argon after eruption), whereas in my samples, the sanidine age was *older* than all of the biotite ages (even the ones that were from *lower* stratigraphic levels). Thus, this still represents a significant incongruence that will need further study and evaluation.

Magnetic Susceptibility

Using the magnetic susceptibility measurements taken from two selected sections (Cerro Ballena and Cerro La Yeseras), I was able to see whether or not there was any cyclical behavior in susceptibility, which would suggest cyclical conditions in sedimentation. Patterns in the magnetic susceptibility signal observed may also provide more details about the depositional environment and help correlate between the two sections.

Low-field magnetic susceptibility is the “induced magnetization of all minerals (diamagnetic, paramagnetic, antiferromagnetic, and ferrimagnetic) in the rock” (Richter et al., 1997). Magnetic susceptibility can be affected by “variations in the concentration of low-coercivity ferromagnetic magnetite grains and, to a lesser extent, of paramagnetic clays” (Riquier, et al. 2010). It often shows a negative correlation with calcium

carbonate concentration (Curry et al., 1995; Jovane et al., 2010), because carbonate rocks tend not to contain much magnetite (Richter et. al, 1997), but do contain diamagnetic minerals. However, it is important to note that even low concentration of ferromagnetic minerals in a rock body (such as magnetite) can produce a large magnetic susceptibility (Ibid).

Jovane et al. (2010) discuss one example of the association between magnetic susceptibility and carbonate dilution, noting that low carbonate content and relatively high magnetic susceptibility occur together, and indicate “warmer and wetter climates with associated enhanced chemical weathering and continental runoff.” This may indicate greater incoming solar radiation, or some other factor that affects climate. In addition, lower magnetic susceptibility suggests a colder and drier climate. Ellwood et al. (2011) used magnetic susceptibility data as an indicator of transgressive-regressive cycles associated with global sea level changes due to climate cycles.

Presumably, the inverse relationship between carbonate content and magnetic susceptibility in Jovane et al. (2010) is due to dilution, since a greater dilution of a sample with carbonate results in a lower percentage of siliciclastic material that contains the ferromagnetic minerals. In the Pisco Formation, diatoms are the cause of dilution, rather than carbonate. That is, a higher percentage of diatom in a rock is expected to be associated with a lower magnetic susceptibility. An increase in weathering results in a greater concentration of magnetite, and thus a higher magnetic susceptibility.

Magnetic susceptibility has also been used as a proxy for iron reduction induced by microbes (Mewafy et al., 2011). Magnetic susceptibility variations can also be used as proxies for climate and eustasy. However, the *magnitude* of magnetic susceptibility is not

important; rather, the *variations* in magnitude are.

After examining magnetic susceptibility measurements at Cerro Ballena and Cerro La Yeseras side by side, a mild correlation between the two sections becomes apparent (see Fig. 28). Approximately one-third of the way up the section in both outcrops, there is a slight increase in the magnetic susceptibility, followed by a slight decrease, as one moves up-section. This distinct pattern matches relatively well in both sections, and can be used to confirm the reliability of my correlation. This confirmation is significant, because the two outcrops are on different sides of the river (Cerro Ballena is on the west side, and Cerro La Yeseras is on the east side) and are separated by a relatively large distance. Several spikes in magnetic susceptibility also seem to match between the two sections (refer to Fig. 19). Thus, magnetic susceptibility adds to the strength of the correlation and further demonstrates that these outcrops are correlatable.

Surprisingly, however, with the exception of a few anomalously high magnetic susceptibility values (“spikes”), there are very few fluctuations when examining one section at a time. A more irregular signal was expected due to the differences in magnetite composition between tuffs and other units. My original expectation was that a strong irregular signal would provide a much clearer correlation between separated outcrops. This unexpected result requires explanation.

One possible explanation for the relative uniformity of magnetic susceptibility measurements is a mixing of magnetite with other sediments, resulting in homogenization of the magnetic susceptibility signal. Ultimately, a low magnetic susceptibility measurement implies a low magnetite concentration. Thus, either the source sediments themselves were low in magnetite, or the magnetite was oxidized during transport from a

distant source.

Some of the tuff units exhibit a relatively strong magnetic susceptibility, whereas other units exhibit much weaker susceptibility (refer to Fig. 18). However, non-tuff units such as the Sld facies often *contain* tuffaceous material (refer to Sections), which provides the magnetite. During deposition of these units, the ash supply from the source would eventually become depleted, and the ratio of ash to other sediment would decrease as deposition continues. Thus, one might expect a continuous decrease of magnetic susceptibility up section. The fact that magnetic susceptibility is relatively constant up section suggests that mixing of sediment and ash particles may have occurred during deposition. The non-tuff units that exhibit weak susceptibility may indicate complete homogenization over a large volume.

Paleoenvironmental Model

I used the data collected from all six sections to develop a paleoenvironmental model of the Pisco Formation for the studied time interval across the transect. The model is developed using interpretations of chemical environment, temperature and climate, and sedimentary processes over time. Burrowing and evaporite deposits are used to provide understanding of the chemistry of the environment. Thin sections and magnetic susceptibility measurements taken at certain outcrops are used to infer details about climate during deposition. Sedimentary structures and sedimentology of the sections are used to interpret sedimentary processes and depositional stages through time.

Chemistry

Burrows are abundant at the top of the white tuff unit, indicating an oxygen-rich chemical environment (Fig. 35). In contrast to sediments higher up in the section, no evaporite (gypsum) deposits exist, which is consistent with a subaqueous environment.

Burrows are abundant near the bottom of the second interval as well (e.g., three horizons of burrows at Cerro Ballena North at 7 meters from the base), indicating an oxygen-rich chemical environment. Evaporite deposits (gypsum veins) appear near the top of the interval in several of the sections, which indicates that the environment dried out at some point.



Figure 35. Photo of white tuff T₁, showing burrows at the top of the unit. From Cerro Ballena South.

Temperature/Climate

Thin sections of tuffs show significant weathering of feldspar and volcanic rock fragments (VRFs) compared to volcanic glass, whose structure is well-preserved (see Fig. 36). The fact that the feldspar and VRFs are altered indicates that some weathering has occurred, but the fact that the volcanic glass components (which are found in the same rock) are well-preserved indicates that weathering of the feldspar and VRFs occurred *before* deposition. From this, one can infer that the climate may have been relatively warm and wet just before or during this time interval of deposition, since physical and chemical weathering can occur at greater rates during warmer and more humid climates (e.g., Liu et al. 2014; Vogt et al., 2010).

The relatively warm climate evident in the weathering of feldspar and VRFs is consistent with previous published data that suggest warmer climates through the Middle and Late Miocene (LaRiviere et al. 2012).

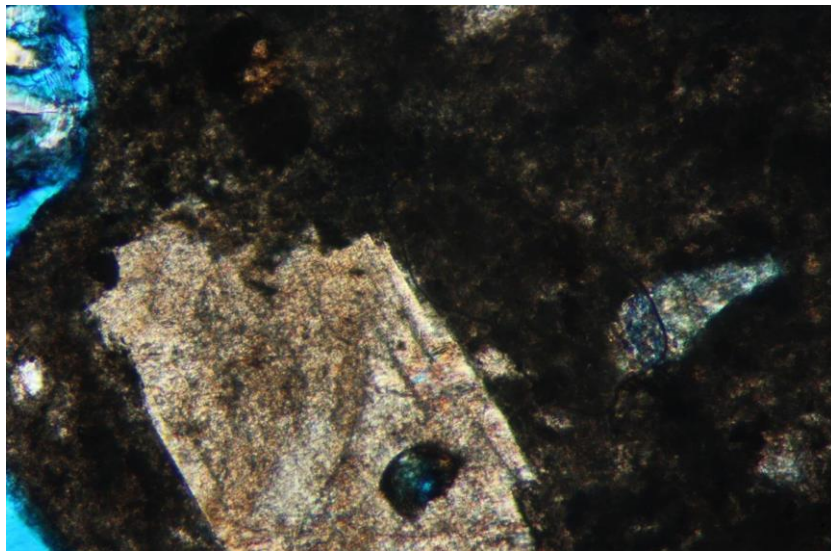


Figure 36. Thin section of a Sc coarse sandstone in CBN, 11.4 meters above the base of the section. Sample P11-35A. 32 X 0.006 magnification. Notice the volcanic rock fragment and the altered feldspar phenocryst.

Sedimentary Processes and Depositional Stages

Figure 30 shows each section side by side from north to south. I divide the unit into three separate time intervals, each representing a facies tract and bounded by distinct markers. The first time interval begins at the base of the section, at the T₁ unit in all outcrops, and ends at the Sc bed located at 3 meters from the base at Cerro Ballena North and 4 meters from the base at Cerro Ballena. In all other sections except Cerro La Yeseras, the interval ends at the transition from gray-colored, low-diatom Sld to abundant-diatom Sld. At Cerro La Yeseras, the interval includes only the Ts tuff complex at the base, including the T₁ unit. The second time interval begins at the transition from less diatom to more diatom in most of the sections, and ends at the dark gray T₂ tuff unit. The third time interval starts at the T₂ unit and ends at the T₃ unit at the top of each section.

The studied unit represents deposition over time that occurred in both the upper and lower shorefaces. The northern outcrops are shoreward, and the southern outcrops are basinward. The three northernmost sections (on Cerro Ballena), with a greater abundance of coarse-grained sediments, represent the upper shoreface and lower shoreface, and the diatom-rich southern sections (Cerro Blanco South, Cerro Hueco La Zorra, and Cerro La Yeseras South) represent the lower shoreface. The occurrence of deeper water sediments Cerro Hueco La Zorra and Cerro La Yeseras supports the interpretation that the ancient shoreline is toward the northwest.

Areas in the southern sections where bioturbation, ripples, and cross-beds occur are interpreted as “middle” shoreface. This is still within the upper shoreface, as indicated by the cross-bedding (Fraser and Hester, 1977), but closer to the lower

shoreface, suggested by the presence of bioturbation. These sedimentary structures appear in Cerro Hueco La Zorra approximately 11 meters from the bottom. Further north, abundant burrows and wave ripples occur near the base of Cerro Blanco South. Burrows exist about 14 meters and 21 meters above the base.

At approximately four meters from the base of the unit (as measured in Cerro Ballena), a Sc bed marks a sudden transition from coarse-grained, clastic-dominated sediment to finer-grained, more diatomaceous sediment. This boundary is interpreted as an increase in water depth, possibly due to a sea level rise (transgression). The first stratigraphic interval includes this first phase of deposition, up to the increase in water depth. The second stratigraphic interval runs from the onset of the water depth change to the primary correlative time marker of the sections examined: the thick, dark gray tuff (unit T₂), which occurs in all outcrops. I chose this as the next interval because it ends at a clear, presumably important time horizon that appears across the basin. The third interval covers the rest of the section, from the dark gray T₂ unit to the top of the section.

Figure 37 shows a summary of the paleoenvironmental interpretation of the section at the different time intervals.

Time Interval 1: From White Tuff to Onset of Sea Level Change at 4 m

In Cerro Ballena, a noticeable and sudden change in lithology occurs at approximately four meters from T₁ at the base of the section. The first four-meter interval consists of T₁, biotite-rich white tuff that defines the base of the section, as well as siltstone with tuffaceous material. At approximately 4 meters from the base sits a Sc bed. Immediately above the coarse sandstone, I observed a marked increase in

diatomaceous and finer-grained material to the top of the section. This section discusses the conditions and processes associated with the facies tract in this interval that extends from Cerro Ballena North in the north to Cerro La Yeseras in the South.

The white T₁ tuff at the base of the interval shows sedimentary structures in most outcrops. At Cerro Ballena North, the hummocky cross-stratification, gutter casts, and bioturbation from T₁ to the top of the interval suggest wave reworking in the intertidal zone. Continuing along the facies tract toward the south, similar sedimentary structures exist in the T₁ tuff bed, including climbing in-phase wave ripples with some small burrows at the top in Cerro Ballena South (see Fig. 35), also indicating wave reworking in the intertidal zone. All across the tract, gray Sld with less diatom dominates, suggesting upper shoreface.

The predominance of silt-sized sediment in this interval (across the entire facies tract) indicates a depth above storm weather wave base. The symmetrical ripples prominent in the white T₁ tuff in the northern part of the facies tract imply intense wave action, also indicating that the water depth during deposition was above storm wave base. Sedimentary structures are evident in the Sld overlying T₁ in the two northernmost sections. However, as one moves south along the facies tract, sedimentary structures become less common in the Sld. In the south, the existence of hummocky cross-stratification near the base (see Facies Sld description) and the lack of such structures higher up in the section suggest that the water depth increases up section. The depth at Cerro Blanco South is below the fair-weather wave base, due to the presence of hummocky cross-stratification (Dott and Bourgeois, 1982). Most likely, the sediment was deposited in the sea and subsequently reworked by wave action.

Diagrammatic Cross-section of Paleoenvironment Throughout Time for Studied Interval

Depositional Environment	Processes	Structures and Other Features
Storm reworking of shelf deposits	Unidirectional current in addition to oscillatory flow.	Asymmetrical Hummocky Cross-stratification
Fairly uniform across study area	Storm events above storm wave base and below fair weather base. Wave reworking	Ripples and hummocks (smaller in the north) Gutter casts and planar laminations
	Volcanic eruptions	Climbing wave ripples Mafic, dark gray tuff
Time Interval 3		
Upper to middle shoreface	Sea level rises again	Wave reworking (in the south), still relatively deep.
Above storm wave base	Sea level fall	Relative rarity of sedimentary structures and erosion surfaces in the north, but planar laminations and gutter casts in the south.
Continual volcanic eruptions	Wave action, eruptions, diatom deposition Relative sea level rise and transgression.	Larger, more prominent sedimentary structures and coarse sandstone beds (thin) relative to higher up in the section.
Water depth increases from Interval 1	(In the south, sea level rise occurs higher up in the section to line up with storm event that deposited coarse sand bed.)	Larger cross-beds and grain sizes (pebble-sized) in south. Scour fills, wave ripples, cross beds in tuffaceous material. Dominance of fine-grained material (diatom and silt). Sandstone gives way to finer-grained material. Planar laminations and wave ripple laminations.
Time Interval 2		
Shallow, high-energy (but becoming deeper near the top). Above storm-weather base (offshore transition zone).	Rip currents from storm surges	Stratigraphic interval height increases and sand percentage decreases toward the south.
	Wave reworking	Gutter casts, channels Hummocky cross-stratification Small burrows Climbing in-phase wave ripples
Time Interval 1		

Figure 37. Diagrammatic Summary of interpretation of paleoenvironment throughout time for studied interval.

Previous studies have suggested that hummocky cross-stratification forms near (and above) storm wave base, where unidirectional current speeds are low (forming low-angle, isotropic cross-stratification) and aggradation rate is high, which preserves hummocks (Dumas and Arnott, 2006).

Just above the white T₁ tuff in Cerro Ballena South, many sedimentary structures are observed, such as gutter casts and small channels (see Fig. 11). These structures are consistent with wave reworking, and indicate the occurrence of wave action during deposition of the entire 4 meter interval in the north. The gutter casts strongly indicate a

shallow, high-energy environment that can be explained by rip currents from storm surges all the way to mid-shelf.

Further south in the facies tract, water depth increases noticeably up section. Sand content decreases in the outcrops further south, as does the height of the interval. The sand content is replaced with relatively uniform fine-grained diatomaceous siltstone, indicating a water deepening south along the facies tract.

Time Interval 2: From Sea Level Change to Deposition of Dark Gray T₂ Tuff Unit

This time interval shows the most lateral variation across the facies tract from north to south.

At approximately 4 meters from the base of Cerro Ballena, a Sc coarse sandstone bed appears, which marks a transition into more diatomaceous and finer-grained material. The predominance of diatomaceous and finer-grained (silty) sediment in this interval (across the entire facies tract) indicates a deepening of the water. This represents a sea level rise and period of transgression. This event caused the tract to shift further from shore. Many scour fills, wave ripples, and cross-beds appear throughout the siltstone and tuffaceous beds at the bottom of this interval, indicating a time of wave action, volcanic eruptions, and diatom deposition.

In Cerro Ballena North, this interval contains thick, abundant Sc beds, which quickly pinches out toward the south, in Cerro Ballena. This suggests a basinward trend from north to south along the facies tract. (The exception is Cerro La Yeseras, which is considered to be closer to the mainline shore than Cerro Hueco La Zorra is to either the mainline shore or the Jurassic islands. Refer to the map in Figure 1. The greater

abundance of Sc and tuffaceous Sld in Cerro La Yeseras, relative to Cerro Hueco La Zorra, supports this interpretation.) The dramatic decrease of the Sc content basinward, leaving only one or two thin (0.1 – 0.2m) Sc beds in the three southernmost outcrops, is consistent with this interpretation.

The lack of T_s beds in the northern part of the facies tract (Cerro Ballena North) and the presence of tuffaceous Sld in their place suggest that the ash from erupting volcanoes was mixed with sediment that was being deposited near the shore. Further south in the facies tract, there is much less tuffaceous Sld. Instead, there are multiple distinct T_s beds. This lack of sediment and ash mixing indicate a decrease in sediment supply and/or depositional rate basinward. The continued abundance of dark gray T_s beds southward in the facies tract supports continual volcanic eruptions and ash deposition during relatively slow deposition of the Sld in a low energy environment. The abundance of diatom-dominated (as opposed to tuff-dominated) Sld southward supports relatively uniform conditions from Cerro Ballena to Cerro Yeseras in this interval.

The sedimentary structures in Cerro Ballena in the north (shoreward) become larger and more prominent further up-section, with a large channeling and cross-bedding, suggesting activity above storm wave base. This is consistent with the several thin Sc beds that lie just above the prominent sedimentary structures. This indicates either a higher energy hydrodynamic event such as a larger storm, or a drop in sea level beginning during this time, resulting in regression and shallowing. However, above the Sc sandstone units, the abundance of sedimentary structures lessens and erosional surfaces nearly disappear. In addition, the same dominant fine-grained lithology (Sld) persists throughout the rest of this interval, suggesting that sea level may not have

dropped, and that the coarser materials originated instead from storm events transporting sand further offshore.

Further basinward along the facies tract, in Cerro La Yeseras, the lower part of the interval contains fine-grained material (S1d), consistent with the evidence of sea level rise and increasing water depth seen in the northern Cerro Ballena outcrop. The transition likely occurs at about 5.9 meters from the base of the section, where a gray T_s bed lies that seems to correlate with a gray T_s bed in Cerro Ballena just above the Sc bed marking the transition. Just above this T_s bed in Cerro La Yeseras sits a Sc bed. At this horizon, a storm event occurred that resulted in agitation of the water and an increase in energy, transporting and depositing the coarser-grained sediments and causing mixing of silt with the ash (indicated by the presence of T_s beds sandwiched in tuffaceous S1d). The energy was even greater shoreward (at Cerro Ballena), resulting in the deposition of a coarser Sc sandstone unit, relative to the size of the sand grains in the Sc unit at Cerro La Yeseras.

The patterns in Cerro La Yeseras in the south exhibit a sea level fall and rise within an upper to middle shoreface environment just as Cerro Ballena in the north does. Gutter fills appear above the Sc sandstone in Cerro La Yeseras, which presumably formed during the storm event or sea level fall that is evident in the middle of the interval. Eventually, an increase in energy occurs, apparent by large trough cross beds and pebbles. Fine-grained diatomaceous siltstone (S1d) dominates the rest of the interval up to the dark gray T₂ tuff, which is consistent with the interpretation of sea level rise (or no change in sea level, but cessation of the storm event) during deposition. Two claystones (at 13.5 m and 16.3 m above the base) also support a low-energy environment, which was present at this location further from the shore. The same fine-grained pattern

occurs in this interval at Cerro Ballena as well as the other outcrops. Multiple dark-colored T_s tuff units in this interval appear in every outcrop, indicating a constant supply of ash due to one or more volcanic eruptions during deposition of the diatomaceous silt (S1d).

The abundant sedimentary structures near the base of the interval in Cerro La Yeseras (as seen in the outcrop), such as planar laminations and wave ripple cross-laminations, mark the time just before the energy levels began dropping due to the increase in water depth. Another possible interpretation is that the decrease in grain size allowed for the formation of sedimentary structures, despite the fact that water depth was increasing (and thus energy was decreasing). In fact, scouring occurs in the fine-grained diatomaceous silt and is prominent in this interval. Nevertheless, all of this indicates that the area in Cerro La Yeseras South was still well above storm wave base.

Sedimentary structures that occur near the top of the interval at Cerro La Yeseras (planar laminations and gutter casts) show that processes such as wave reworking continued all through deposition in the south end of the facies tract. However, the material in which these structures occur is fine-grained, meaning that the energy levels need not be very high, and water depth at the top of the interval may still be greater than water depth during Time Interval 1.

Time Interval 3: From Deposition of Dark Gray T₂ Tuff Unit to Deposition of Biotite-rich Tuff T₃

The final depositional interval starts at the deposition of the T₂ dark gray tuff (the primary unit used to correlate all of the sections) and ends at the top of the section, where

the biotite-rich T₃ tuff unit sits. The boundaries of this interval were chosen based on the ability to identify two distinct time markers that span all outcrops.

Volcanic eruptions mark the onset of this interval, resulting in the deposition of a more mafic, thick gray tuff across the basin. In both northern (Cerro Ballena North) and southern (Cerro Hueco La Zorra) sections, climbing wave ripples within the unit indicate continuing wave reworking during deposition. Gutter casts and planar laminations in both of these locations confirm this interpretation.

Above the dark gray T₂ tuff in Cerro Ballena North sit thin to thick laminae that are subhorizontal. At some places, ripples or small hummocks appear in small areas (see Figs. 38 and 39).



Figure 38. Cerro Ballena North. Hummocky cross-stratification in the unit above the dark gray tuff T₂.

The presence of hummocky-cross stratification in the north suggests the occurrence of storm events that generated oscillatory or multidirectional flow to form

these structures (Duke 1985). Previous studies have indicated that hummocky cross-stratification forms just above storm weather base (where aggradation is high enough to preserve the structures), and swaley cross-stratification occurs between storm weather and fair weather base (Dumas and Arnott, 2006). In Figure 38, the hummocky cross strata appear somewhat asymmetrical, which suggests the presence of a slight unidirectional current in addition to the oscillatory flow (Ibid).

The same study suggests that the oscillatory velocity required to generate such hummocks is 50 – 90 cm/second (Dumas and Arnott 2006). The asymmetry present in the hummocks within the section suggests that there was also a unidirectional component of flow with a velocity of 5 – 10 cm/s. These hummocks and swaley cross-stratification occur throughout the entire interval (see Fig. 39).



Figure 39. Cerro Ballena North, showing a large portion of the interval from the dark gray tuff T₂ to the top of the section. Note the hummocky cross-stratification that occurs throughout the interval.

The presence of the hummocky cross-stratification in this interval indicates that a storm event or events continued during deposition of the dark gray T₂ tuff and diatomaceous siltstone (S1d) above it. Basinward along the facies tract, in Cerro Ballena South, a fine-grained diatom-rich clay layer embedded within the diatomaceous siltstone S1d indicates transportation of clay particles from a different area. Most likely, the diatomaceous silt continued to deposit while the clay particles were being deposited.

This interval terminates with the deposition of the T₃ bed, a dark-colored tuff containing large and abundant biotite crystals. Planar laminations within the tuff imply that the storm event or events continued through the deposition of the tuff. The laminations were formed by movement of a storm current during ashfall.

The orange-colored, Fe-stained layer in all sections suggests oxidation of the iron within the diatomaceous silt. This iron-staining extends across the entire facies tract and occurs in all the outcrops in this interval.

These observations show that little change is evident southward along this facies tract. While there does appear to be less sedimentary structures in this interval as one moves basinward, the interval between T₂ and T₃ is characterized by fine-grained S1d, a lack of beds of any other facies, and some sedimentary structures. Even in the region closest to shore where thick Sc beds are abundant below (Cerro Ballena North), there is very little difference from the rest of the sections. This may suggest another transgression and rise in sea level. This interpretation is consistent with the presence of sedimentary structures such as hummocky cross-stratification in the S1d and climbing wave ripples in T₂, and planar laminations in T₃, which could have been caused by a storm event when the energy level increased temporarily.

CHAPTER FIVE

CONCLUSIONS

This research provides an important, original analysis of various aspects of the data related to the Pisco Formation. To provide a more comprehensive stratigraphy of the Pisco Formation, I correlated three time synchronous tuff units and one of those units was mapped across a distance of approximately 30 kilometers. I examined six outcrops in detail across four hills along a NW-SE linear transect, each of which covered a stratigraphic interval of approximately 30 meters. I successfully correlated the upper and lower units across each outcrop as well as several units between the upper and lower bounds.

The depositional environment is interpreted to be nearshore, including both upper and lower shoreface. The three northernmost sections (on Cerro Ballena) comprise most of the coarse-grained units in the Ica River Valley and represent the upper shoreface, and the fine-grained diatomaceous material occurs more abundantly in the southernmost sections (Blanco, Zorra, and Yeseras), representing the lower shoreface. Storm and surge structures such as large megaripples, hummocky and swaley cross-stratification, channeling, scouring, ripples, climbing wave ripples, cross-bedding, and planar laminations occur all throughout the valley. I identified and defined six facies of the Pisco Formation, representing coarse sandstones, diatomaceous siltstone, fine sand and silt, and two tuff facies.

The overall trend from south to north is an increase in clastics and average grain size, indicating an approach toward the shore. The shore is interpreted to be the Jurassic volcanic islands that sit to the west of the outcrops. The vertical trend in the northern

side of the Ica River Valley can be described in terms of energy levels, water depth, and distance from the shore. At least one change in relative sea level occurred during deposition of the section, and this is seen in the middle section, between the region closest to shore (Cerro Ballena North) and the regions in greater depths (Cerro Blanco, Cerro Hueco La Zorra, and Cerro La Yeseras South).

This study provides a more comprehensive correlation and paleoenvironmental interpretation of a specific time-bounded section across a long linear transect, providing the basis for further studies in the sedimentology, stratigraphy, and paelontology of the Pisco Formation and other analogous environments.

REFERENCES

- Boss, Stephen K., and Joshua M. Blackstock. "Enigmatic Trace Fossils And Depositional Setting Of The Clifty Formation (Devonian), Northwest Arkansas." *Abstracts With Programs - Geological Society Of America* 40.6 (2008): 231.
- Brand, Leonard R.; Esperante, Raul; Chadwick, Arthur V.; Porras, Orlando Poma; Alomia, Merling. "Fossil whale preservation implies high diatom accumulation rate in the Miocene-Pliocene Pisco Formation of Peru." *Geology* 2004 32 165-168.
- Brand, Leonard; Urbina, Mario; Carvajal, Cristian; DeVries, Thomas; and Esperante, Raul. "A Contribution To The Stratigraphy Of The Miocene/Pliocene Pisco Formation, Peru." *Journal Of Vertebrate Paleontology* 26.3, Suppl. (2006): 45.
- Brand, Leonard; Urbina, Mario; Chadwick, Arthur; DeVries, Thomas; and Esperante, Raul. "A high-resolution stratigraphic framework for the remarkable fossil cetacean assemblage of the Miocene/Pliocene Pisco Formation, Peru." *Journal of South American Earth Sciences* Vol. 31, Issue 4, April 2011.
- Bianucci, Giovanni, Olivier Lambert, and Klaas Post. "High concentration of longsnouted beaked whales (genus *Messapicetus*) from the Miocene of Peru." *Palaeontology* 53.5 (2010): 1077-1098.
- Boggs, Sam Jr. *Principles of Sedimentology and Stratigraphy*. Third Edition. Upper Saddle River, NJ: Prentice-Hall, Inc. 2001.
- Carvajal, Christian (2002). *Sedimentology and Paeloenvironments of the Miocene/Pliocene Pisco Fm., Peru*. M.S. Thesis. Loma Linda University: USA.
- Clarke, Julia A.; Ksepka, Daniel T.; Salas-Gismondi, Rodolfo; Altamirano, Ali J.; Shawkey, Matthew D.; D'Alba, Liliana; Vinther, Jakob; DeVries, Thomas J.; Baby, Patrice. "Fossil evidence for evolution of the shape and color of penguin feathers." *Science* 330.6006 (2010): 954-957.
- Curry, W.B., Shackleton, N.J., Richter, C., et al., 1995. *Proc. ODP, Init. Repts.*, 154: College Station, TX (Ocean Drilling Program). De Muizon, C. and DeVries, T.J. 1985. "Geology and paleontology of Late Cenozoic marine deposits in the Sacaco area (Peru)." *Geologische Rundschau*. 74 (3), 547-563.
<http://www.springerlink.com/content/v577k4282x20t5h1/>.
- DeVries, Thomas J. "Molluscan evidence bearing on Cenozoic warm upwelling off southern Peru." *Abstracts with Programs - Geological Society of America* 39.4 (2007): 78.
- DeVries, Thomas J., Lindsey T. Groves, and Mario Urbina. "A new Early Miocene *Muracypraea* Woodring, 1957 (Gastropoda, Cypraeidae) from the Pisco Basin of

- southern Peru." *Nautilus* 120.3 (2006): 101-105.
- De Silva, S.L. and Francis, P.W. "Correlation of Large Ignimbrites – Two Case Studies from the Central Andes of Northern Chile." *Journal of Volcanology and Geochemical Research* 37 (1989) 133-149.
- DeVries, T. J., and G. J. Vermeij. "Hermespina; New Genus Of Neogene Muricid Gastropod From Peru And Chile." *Journal Of Paleontology* 71.4 (1997): 610-615. <http://www.jstor.org/pss/1306581>.
- DeVries, Thomas J. "Molluscan evidence bearing on Cenozoic warm upwelling off southern Peru." *Abstracts with Programs - Geological Society of America* 39.4 (2007): 78.
- DeVries, T.J. and Schrader, H. 1997. "Middle Miocene marine sediments in the Pisco Basin (Peru)." *Boletín de la Sociedad Geológica del Perú* 87:1-13.
- DeVries T.J. "Oligocene deposition and Cenozoic sequence boundaries in the Pisco Basin (Peru)." *Journal of South American Earth Sciences*, Volume 11, Number 3, May 1998, pp. 217-231(15).
- Dickinson, W. R.; Beard, S. L.; Erjavec, J. L.; Fergusson, R. C.; Inman, K. F.; Knepp, R. A.; Linberg, F. A.; and Ryberg, P. T. "Provenance of North American Phanerozoic Sandstones in Relation to Tectonic Setting," *Geological Society of America Bulletin*, Vol. 94, No. 2, 1983, pp. 222-235.
- Duke, William L. "Hummocky cross-stratification, tropical hurricanes, and intense winter storms." *Sedimentology* Vol. 32, Issue 2, pages 167-194, April 1985.
- Dumas, Simone and Arnott, R.W.C. "Origin of hummocky and swaley cross-stratification – The controlling influence of unidirectional current strength and aggradation rate." *Geology* V. 34 No. 12 p. 1073-1076.
- Dunbar, Robert B.; Marty, Richard C.; Baker, Paul A. "Cenozoic marine sedimentation in the Sechura and Pisco basins, Peru." *Palaeogeography, Palaeoclimatology, Palaeoecology* 77.3-4 (1990): 235-261.
- Ehret, Dana J., Bruce J. Macfadden, and Rodolfo Salas-Gismondi. "Caught in the act; trophic interactions between a 4-million-year-old white shark (*Carcharodon*) and mysticete whale from Peru." *Palaios* 24.5 (2009a): 329-333.
- Ehret, Dana J., Gordon Hubbell, and Bruce J. MacFadden. "Exceptional preservation of the white shark *Carcharodon* (Lamniformes, Lamnidae) from the Early Pliocene of Peru." *Journal of Vertebrate Paleontology* 29.1 (2009b): 1-13.

- Ellwood, Brooks B.; Algeo, Thomas J.; El Hassani, Ahmed; Tomkin, Jonathan H.; Rowe, Harry D. "Defining the timing and duration of the Kacak Interval within the Eifelian/Givetian boundary GSSP, Mech Irdane, Morocco, using geochemical and magnetic susceptibility patterns." *Palaeogeography, Palaeoclimatology, Palaeoecology* 304.1-2 (2011): 74-84.
- Esperante, Raul; Brand, Leonard; Nick, Kevin E.; Poma, Orlando; Urbina, Mario. "Exceptional occurrence of fossil baleen in shallow marine sediments of the Neogene Pisco Formation, southern Peru." *Palaeogeography Palaeoclimatology, Palaeoecology* 257.3 (2008): 344-360.
- Fraser, GS; Hester, NC. "Sediments and sedimentary structures of a beach-ridge complex southwestern shore of Lake Michigan." *Journal of Sedimentary Petrology*. 47, 3, 1187-1200, Sept. 1, 1977.
- Gingras, M.K.; Pemberton, S.G.; Dashtgard, S.; Dafoe, L. "How fast do marine invertebrates burrow?" *Palaeogeography, Palaeoclimatology, Palaeoecology* 270:280-286, 2008.
- Hora, John M.; Singer, Brad S.; Jicha, Brian R.; Beard, Brian L.; Johnson, Clark M.; de Silva, Shan; Salisbury, Morgan. "Volcanic biotite-sanidine (super 40) Ar/ (super 39) Ar age discordances reflect Ar partitioning and pre-eruption closure in biotite." *Geology [Boulder]* 38.10 (2010): 923-926.
- Jovane, L, Sprovieri, M, Coccioni, R, Florindo, F, Marsili, A, & Laskar, J 2010, "Astronomical calibration of the Middle Eocene Contessa Highway section (Gubbio, Italy)," *Earth And Planetary Science Letters*, 298, 1-2, pp. 77-88.
- Kulm, L. D. ; Thornburg, T. M.; and Schrader, H.J. "Cenozoic structure, stratigraphy and tectonics of the central Peru forearc." *Geological Society, London, Special Publications* 1982, v. 10, p. 151-169.
- Leon, Walter; Aleman, Antenor; Rosell, Walter; and Torres, Victor. "Estratigraphia, Sedimentología y Evolución Tectónica de la Cuenca Pisco Oriental." Lima, Peru: Ingemmet. Dirección de Geología Regional. 2008.
- Liu, J; Jianhui, Chen; Kandasamy, Selvaraj; Qinghai, Xu ; Zongli, Wang; Fahu, Chen. "Chemical Weathering over the last 1200 years recorded in the sediments of Gonghai Lake Lvliang Mountains, north China; a high-resolution proxy of past climate." *Boreas*. Norway, 43, 4, 914-923, Oct. 1, 2014.
- Machare, J., and E. Fourtanier. "Datations Des Formations Tertiaires Du Bassin De Pisco (Perou) A Partir D'associations De Diatomees." ["Dating of Tertiary Pisco Basin (Peru) from Associations of Diatoms."] *Comptes Rendus De L'academie Des*

Sciences, Serie 2, Mecanique, Physique, Chimie, Sciences De L'univers, Sciences De La Terre 305.5 (1987): 407-412.

- Maracco, R.; De Muzion, C.. 1988. "Le Bassin Pisco, basin cenozoique d'avant arc de la cote du Perou Central: analyse geodynamique de son remplissage." ["Pisco Basin, Cenozoic basin before the arc rating of Central Peru: analysis geodynamics of its filling."] *Geodynamique*. 3 (1-2), 3-19.
- Marty, R.C. 1989. "Stratigraphy and chemical sedimentology of the Cenozoic biogenic sediments from the Pisco and Sechura basins, Peru." PhD. Thesis, Rice University, Houston, Texas, US.
- Mertz, Dieter. "Mikropalaeontologische Und Sedimentologische Untersuchung Der Pisco-Formation Suedperus." ["Micropaleontological and sedimentological investigation of the Pisco Formation of southern Peru."] *Palaeontographica. Abteilung B: Palaeophytologie* 118, Part 1-3.(1966): 1-48.
- Mewafy, Farag M.; Estella A. Atekwana; D. Dale Werkema Jr.; Lee D. Slater; Dimitrios Ntarlagiannis; André Revil; Magnus Skold; and Geoffrey N. Delin. "Magnetic susceptibility as a proxy for investigating microbially mediated iron reduction." *Geophysical Research Letters*, Vol. 38, L21402, 5 PP., 2011).
- Muizon, Christian de; Devries, Thomas J. "Geology and paleontology of Late Cenozoic marine deposits in the Sacaco area (Peru)." *Geologische Rundschau* Volume 74, Number 3, 547-563 (1985).
- Mutterlose, Joerg, and Kurt Wiedenroth. "Early Cretaceous (Valanginian-Hauterivian) Belemnites From Western Morocco; Stratigraphy And Palaeoecology." *Cretaceous Research* 29.5-6 (2008): 814-829.
- Nick, Kevin E., and Benjamin L. Clausen. "Tephrochronology And High Resolution Correlation In The Upper Pisco Formation, Miocene, Peru." *Abstracts With Programs - Geological Society Of America* 42.5 (2010): 432.
- Noble, Donald C.; McKee, Edwin H.; Farrar, Edward; Petersen, Ulrich. "Episodic Cenozoic Volcanism and Tectonism in the Andes in Peru." *Earth and Planetary Science Letters* 21 (1974) 213-220.
- Parham, James F., and Nicholas D. Pyenson. "New sea turtle from the Miocene of Peru and the iterative evolution of feeding ecomorphologies since the Cretaceous." *Journal of Paleontology* 84.2 (2010): 231-247.
- Reumer, Jelle; Bianucci, Giovanni; Post, Klaas; de Muizon, Christian; Salas-Gismondi, Rodolfo; Urbina, Mario; Reumer, Jelle. "The giant bite of a new raptorial sperm whale from the Miocene Epoch of Peru." *Nature [London]* 466.7302 (2010): 105-108.

- Richter, Carl, Jean-Pierre Valet, and Peter A. Solheid. "Rock Magnetic Properties of Sediments from Deara Rise (Site 929): Implications for the Origin of the Magnetic Susceptibility Signal." In Shackleton, N.J., Curry, W.B., Richter, C., and Bralower, T.J. (Eds.), 1997 *Proceedings of the Ocean Drilling Program, Scientific Results*, Vol. 154.
- Riquier, Laurent; Olivier Averbuch; Xavier Devleeschouwer; and Nicolas Tribouvillard. 2010 "Diagenetic versus detrital origin of the magnetic susceptibility variations in some carbonate Frasnian-Famennian boundary sections from northern Africa and Western Europe; implications for paleoenvironmental reconstructions." *International Journal of Earth Sciences = Geologische Rundschau* 99.Suppl. 1 (2010): 57-73
- Stucchi, Marcelo, and Mario Urbina. "Ramphastosula (Aves, Sulidae); a new genus from the Early Pliocene of the Pisco Formation, Peru." *Journal of Vertebrate Paleontology* 24.4 (2004): 974-978.
- Takahashi, Osamu and Matsukawa, Masaki. "Takahashi, Osamu, and Masaki Matsukawa. "Oceanward Shifting Of The Hauterivian (Early Cretaceous) Arc-Trench System In East Asia." *Geosciences Journal [Seoul]* 4.3 (2000): 187-199.
- Uhen, Mark D.; Pyenson, Nicholas D.; Devries, Thomas J.; Urbina, Mario; Renne, Paul R. "New Middle Eocene whales from the Pisco Basin of Peru." *Journal of Paleontology* 85.5 (2011): 955-969.
- Urbina, Mario, and Marcelo Stucchi. "Los cormoranes (Aves, Phalacrocoracidae) del Mio-Plioceno de la formacion Pisco, Peru." *Boletin de la Sociedad Geologica del Peru* 99.(2005): 41-49.
- Vogt, T; Clauer, N; Larque, P. "Impact of climate and related weathering processes on the authigenesis of clay minerals; examples from circum-Baikal region, Siberia." *Catena [Giessen]*. International, 80, 1, 53-64, Jan. 15, 2010.
- Walker, Luke J.; Wilkinson, Bruce; and Ivany, Linda C. "Continental Drift And Phanerozoic Carbonate Accumulation In Shallow-Shelf And Deep-Marine Settings." *Journal Of Geology* 110.1 (2002): 75-87.
- Wang, Dong'an, and Ruijun Chen. "The Characteristics Of Sedimentary Rock And Its Lithofacies Changes In The Karakoram Region." *Dizhi Kexue = Scientia Geologica Sinica* 30.3 (1995): 291-301.
- Witkowski, Jakub, David M. Harwood, and Karen Chin. "Taxonomic Composition, Paleoecology And Biostratigraphy Of Late Cretaceous Diatoms From Devon Island, Nunavut, Canadian High Arctic." *Cretaceous Research* 32.3 (2011): 277-300.

APPENDIX A

SAMPLE DESCRIPTIONS AND DATA FROM EACH FACIES

I recognized and identified six facies within my section. Table 2 in the Results chapter displays the facies with important characteristics of each facies.

Facies Sc: Coarse Sandstone

P11-33B: CBN

Sampling Site Information

From Cerro Ballena North, located at 14.30663⁰ S, 75.73250⁰ W. Originates from a unit that sits 8.7 meters above white tuff, which may be the same marker bed as the one dated at 6.9 Ma and considered the base of the section. The base of the bed is 4.9 meters below the marker bed T₂ and 10 meters below the T₃ marker bed, which is considered the top of the section.

Outcrop Features

The unit is 0.9 meters thick and contains coarse sandstone with abundant mollusks (coquina). It contains a thin clay interbed at 0.7 meters from the bottom of the bed. The bed is overlain by very fine sandstone with no visible sedimentary structures, and contains some Fe staining and pink-colored stain of unknown origin. It is underlain by a very fine sandstone with silt that is planar-laminated and wave-ripple cross laminated.

Petrography

The sample is composed of 90% detrital components, 10% intergranular components, 1% cement (100% gypsum), and 9% porosity. The detrital components are

composed of 65% volcanic rock fragments and 35% bivalves (some partially dissolved or replaced by gypsum). The porosity is 100% intergranular.

Texture

The average grain size is estimated to be 1.19 mm (from the average of grains with diameters 978, 892, 1579, 1065, 1430 mm). The grains are moderately sorted, well-rounded, and have moderate sphericity.

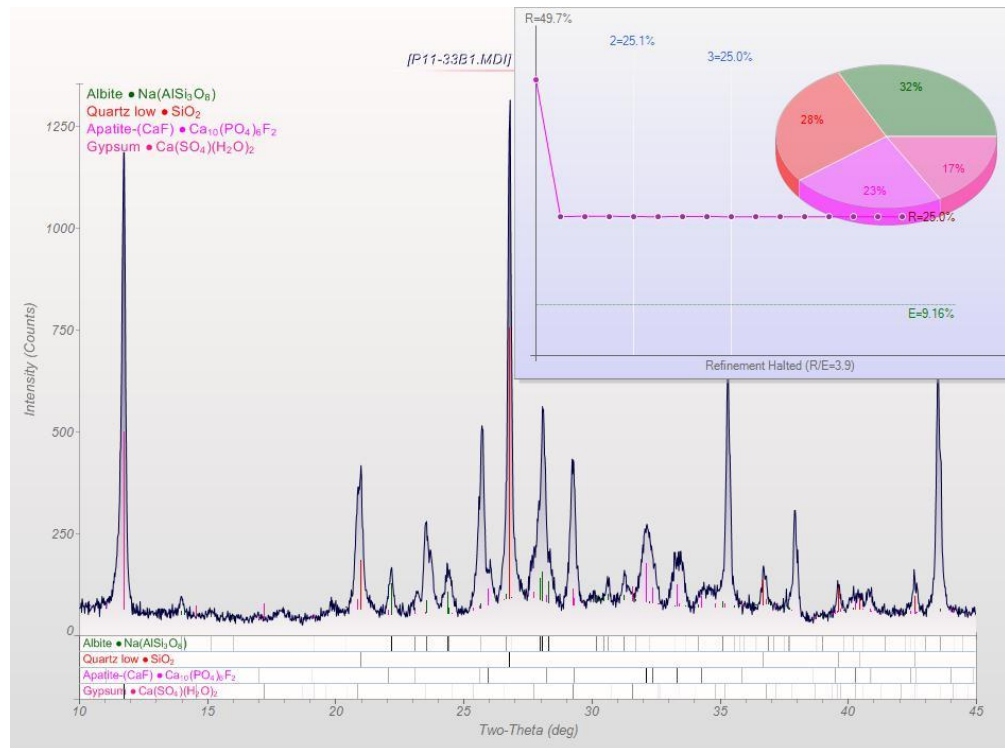


Figure A1. X-ray diffraction mineralogy of Sample P11-33B.

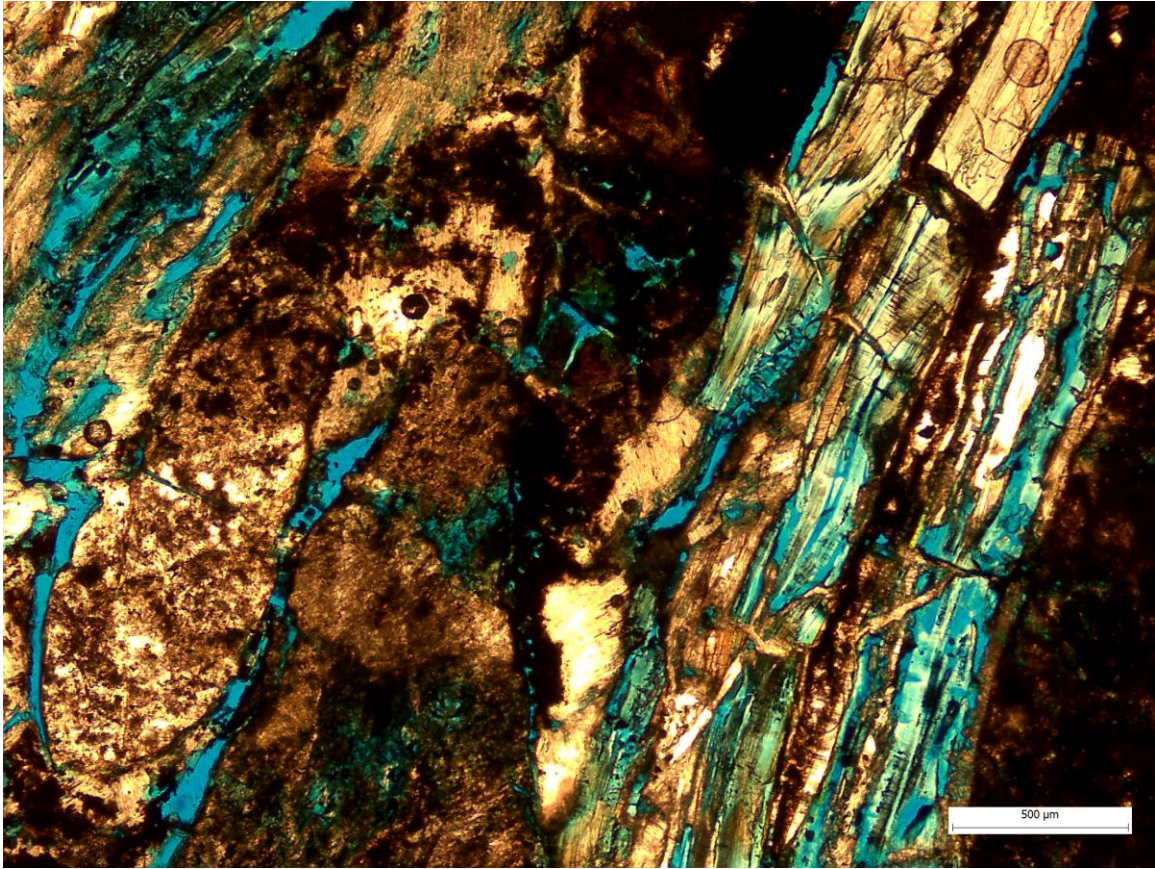


Figure A2. Thin section of Sample P11-33B. Dark grains volcanic rock fragments (VRFs), lighter-colored elongated objects (especially seen on the right side of the photo) are bivalve shells. Some of the bivalves replaced by gypsum. Also the darker material around some of the VRFs may be hematite (as also seen in the reddish tint in some of the shells under microscope).

P11-35A: CBN

Sampling Site Information

This sample was taken from Cerro Ballena North, with GPS coordinates of 14.306663⁰ S, 75.73250⁰ W. The unit sits 11.4 meters above the white tuff considered the base of the section. It sits 2.2 meters below marker bed “dark gray tuff” and 7.5 meters below the biotite-rich dark tuff, which is considered the top of the section.

Outcrop Features

The unit is 0.24 meters thick, and is a very coarse sandstone with angular pebbles. Unlike other similar sandstones in the vicinity, it does not contain mollusks. It has a sharp base, and the cements are visible at the surface and white in color. Pink diatomaceous mudstone occurs below, and contains scouring with planar lamination fill as well as planar laminations. The bed is overlain by Pink Diatomaceous Mudstone (PDM) above, which contains an articulated whale skeleton (the only one observed in the outcrop).

Petrography

The sample is composed of 62% detrital material, 25% cement (mostly anhydrite), and 13% porosity (some pores exist within the anhydrite cement). The detrital components are separated into dark volcanic rock fragments (60%), some of which include phenocrysts, plagioclase (~1%, many residing in the rock fragments), and quartz (<1%). The porosity appears to be 100% Intercrystalline, and resides within the anhydrite. Some of the pores are rectangular, indicating that they may have formed after the dissolution of halite cement.

Texture

The average grain size in the sample is estimated to be between 0.6 and 2 mm. The grains are moderately sorted, well-rounded, and have moderate sphericity.

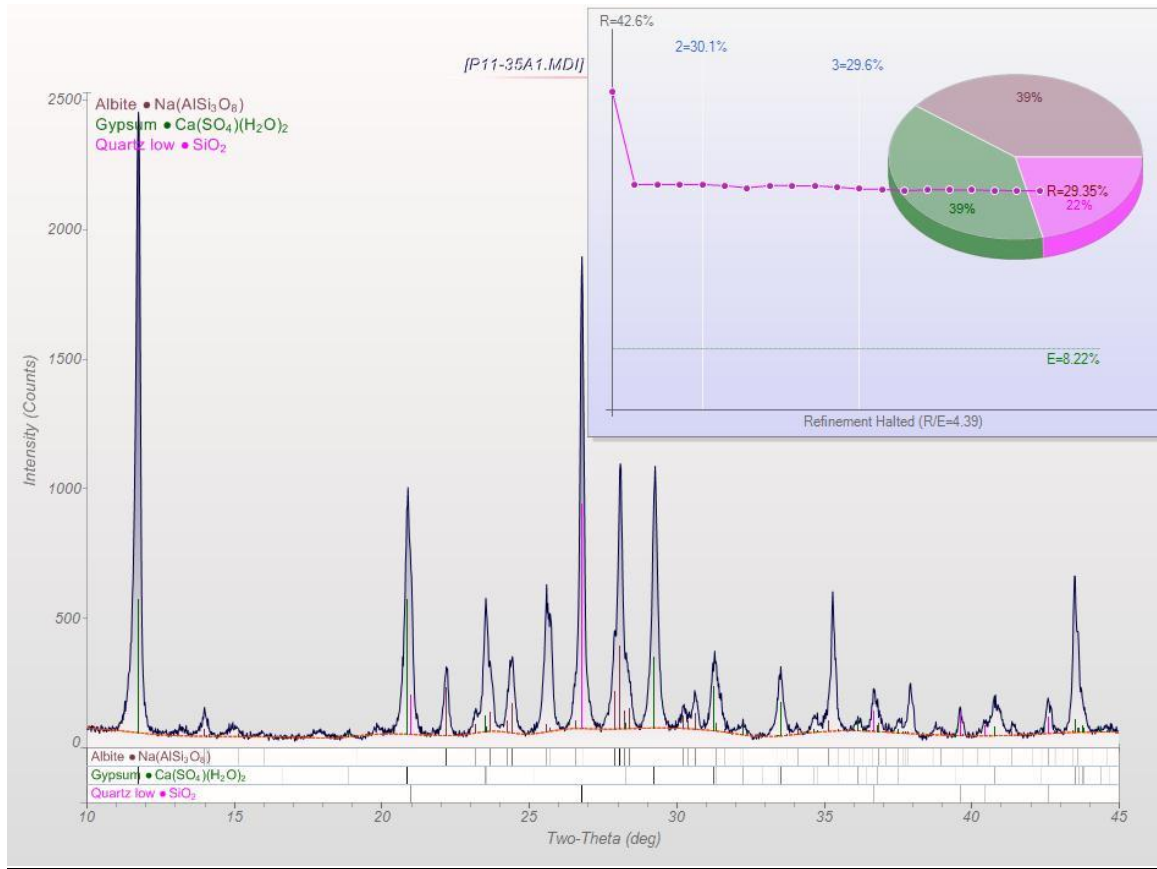


Figure A3. X-ray diffraction mineralogy of Sample P11-35A.

P11-31E: CBN

Sampling Site Information

The sample was taken from Cerro Ballena North with GPS coordinates of 14.306663⁰ S and 75.73250⁰ W. The sample originated from a unit that sits 3 meters above the white tuff that is considered the base of the section. The unit sits 10.6 meters below the T₂ marker bed and 15.7 meters below the T₃ marker bed that is considered the top of the section.

Outcrop Features

The bed is 0.2 meters thick. It is a coarse sandstone with many mollusk fossils and a Fe-derived orange color. A greater concentration of shells exists at the base. The bed has a sharp base and long-wavelength erosion at the base. A very fine silt diatomaceous mudstone drapes over the bed, and ripples with a wavelength at of ~25 centimeters appear at the surface of the drape. The coarse sandstone/drape is overlain by a gray siltstone with no visible sedimentary structures and medium sandstone lenses at the base. The coarse sandstone/drape overlays the dominant pink diatomaceous mudstone (PDM) facies of my sections. Near the top of the underlying PDM unit are thin discontinuous coarse sand lenses as well as trough cross-bedding.

Petrography

The sample contains 85% detrital material and 15% intergranular porosity. No cements are observed in thin section. The detrital components are as follows: volcanic rock fragments (45% of sample space), bone fragments (30%), clay pellets (10%), quartz (10%), and feldspar (15%).

Texture

The average grain size is estimated to be 609 microns (an average of grains with diameters of 792, 464, 828, 551, and 414 microns). The grains are moderately to well-sorted, sub-rounded to rounded, and have low to medium sphericity.

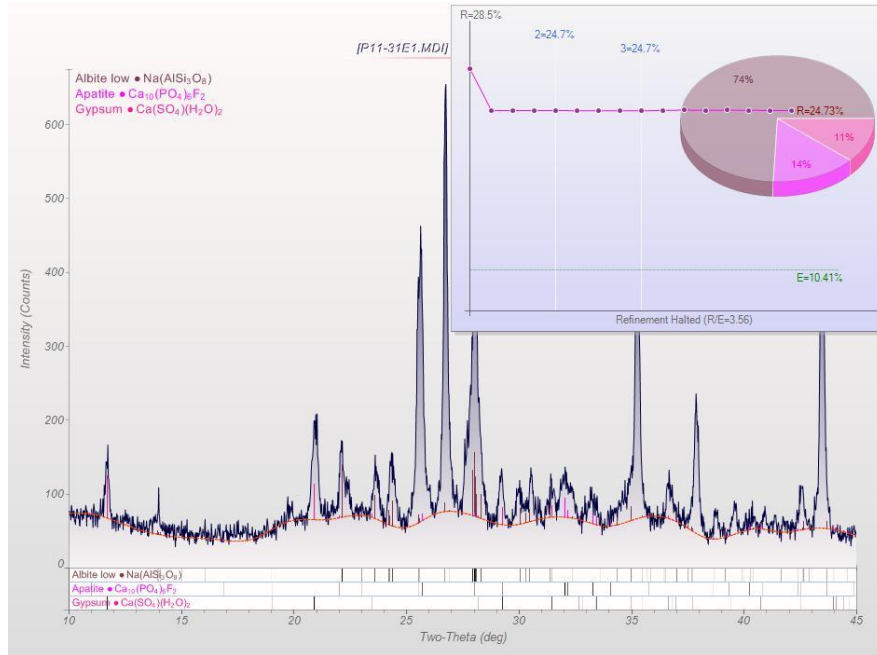


Figure A4. X-ray diffraction mineralogy for Sample P11-31E.

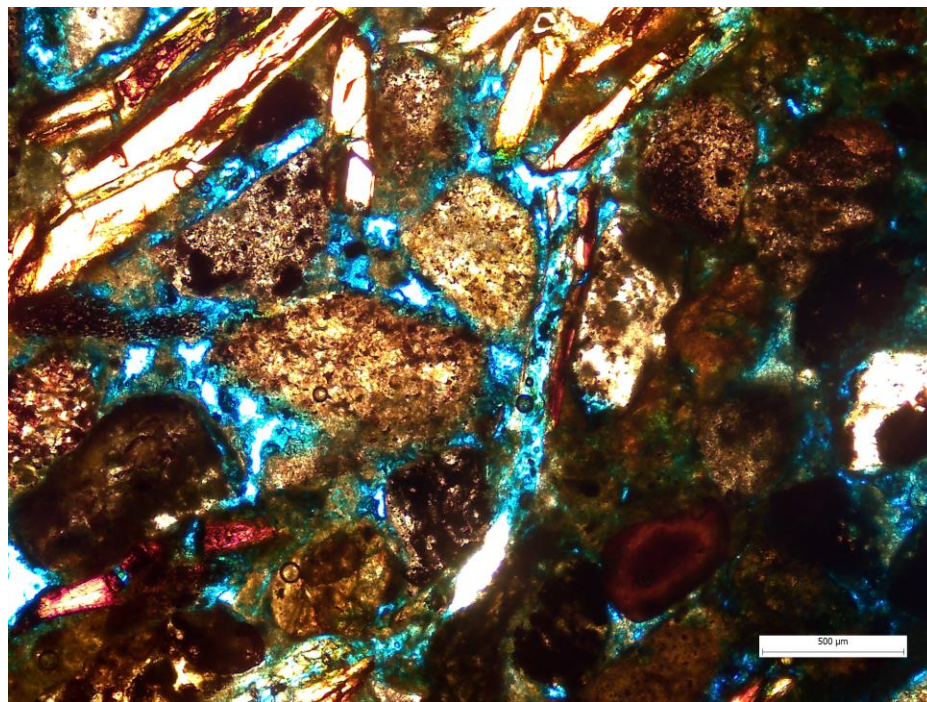


Figure A5. Overview of thin section for Sample P11-31E, showing volcanic rock fragments and bone fragments.

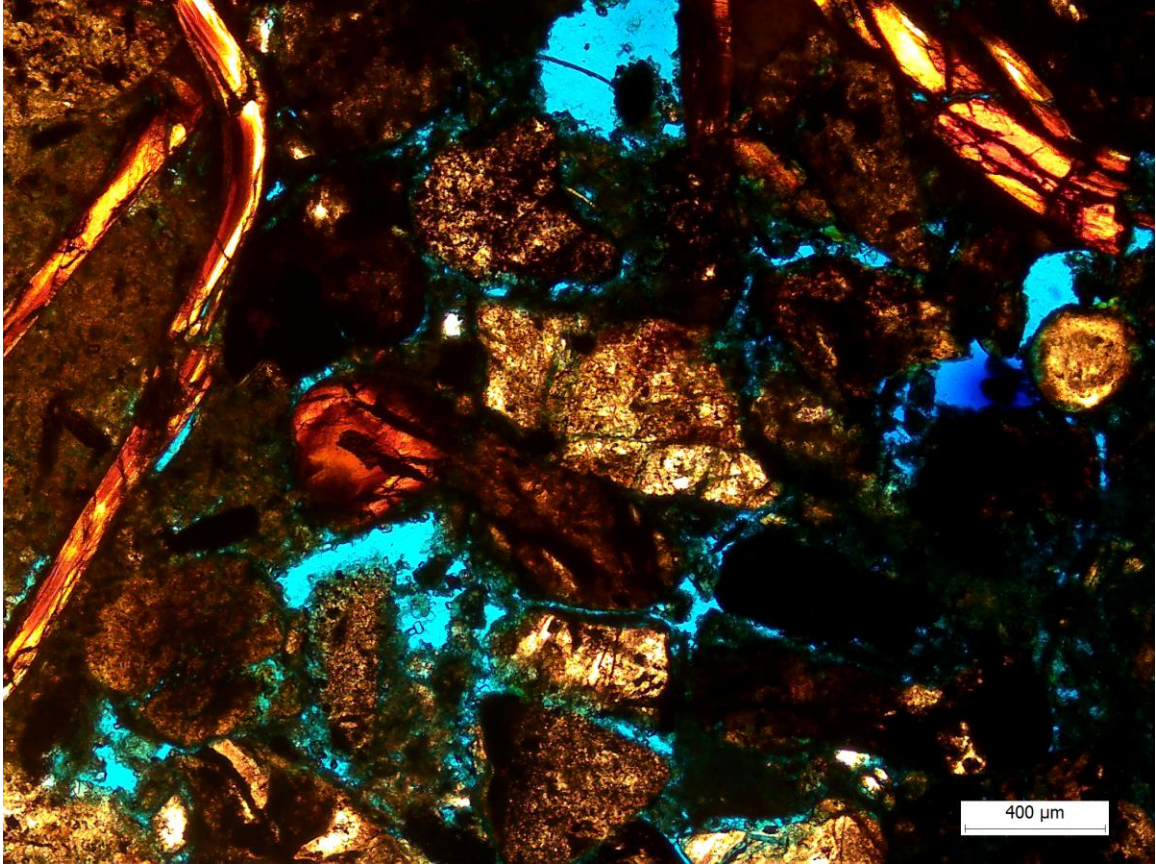


Figure A6. Thin section showing feldspar grains in the center of photo.

011-51B: CB

Sampling Site Information

The sample originates from Cerro Ballena, with GPS coordinates of 14.325437⁰ S and 75.72437⁰ W. It comes from a unit that sits 12.5 meters above the white tuff at base of section, 11 meters below the biotite-rich tuff considered the top of the section, and 5.2 meters below the dark gray T₂ tuff marker unit. The bed is 0.16 meters thick.

Outcrop Features

The sample derives from a coarse sandstone, which is the third unit in a series of four coarse sandstone beds in the Cerro Ballena outcrop within a 1.5 meter thick interval. It is bounded by an erosional surface above, and lies within diatomaceous siltstone (the most common lithology in the section) that contains articulated whale skeletons and abundant sedimentary structures such as ripples and cross-bedding.

Composition

The sample consists of 75% detrital material and 25% intergranular components, with the intergranular comprising 10% cement (gray-colored gypsum) and 15% porosity. The detrital components comprise approximately 95% volcanic rock fragments, 5% clay (replacing VRFs), 2% bone fragments, 1% mudstone, 1% sandstone fragments, 1% fossil fragments (barnacles), 1% plagioclase (within VRFs), and <1% quartz (also within VRFs).

Petrography

The thin section reveals porosity in the form of a well-defined ring around some grains. The majority of the grains are volcanic rock fragments. Some darker grains show signs of weathering and replacement by clay. Some volcanic rock fragments have quartz and feldspar grains embedded within them. Mudstone shows signs of being “squeezed” and deformed, and biotite shows indicators of expansion and weathering.

Texture

The average grain size is estimated to be 1.1 μm . The grains are moderately to well sorted, sub-rounded to rounded, and show moderate sphericity.

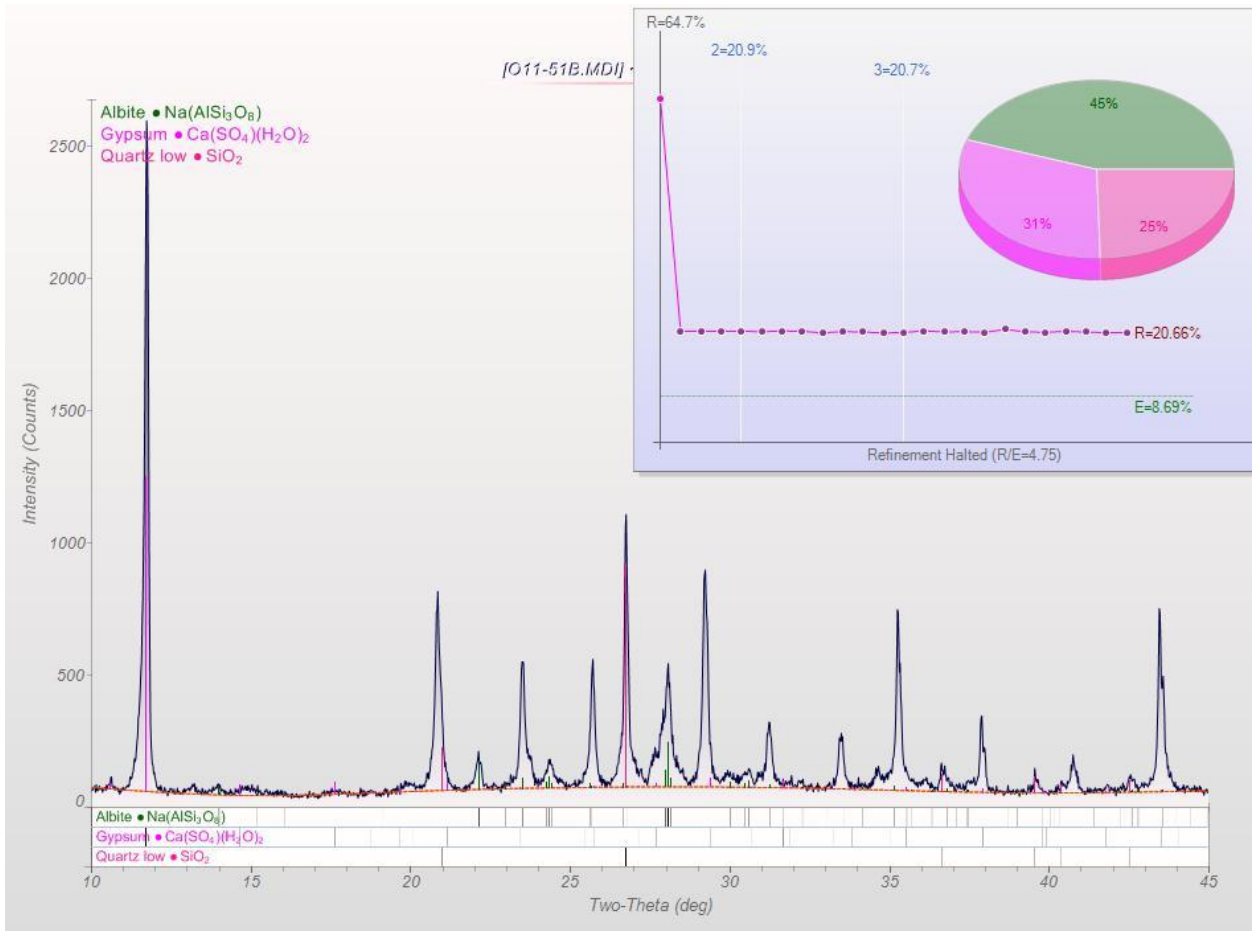


Figure A7. X-ray diffraction mineralogy of Sample O11-51B.

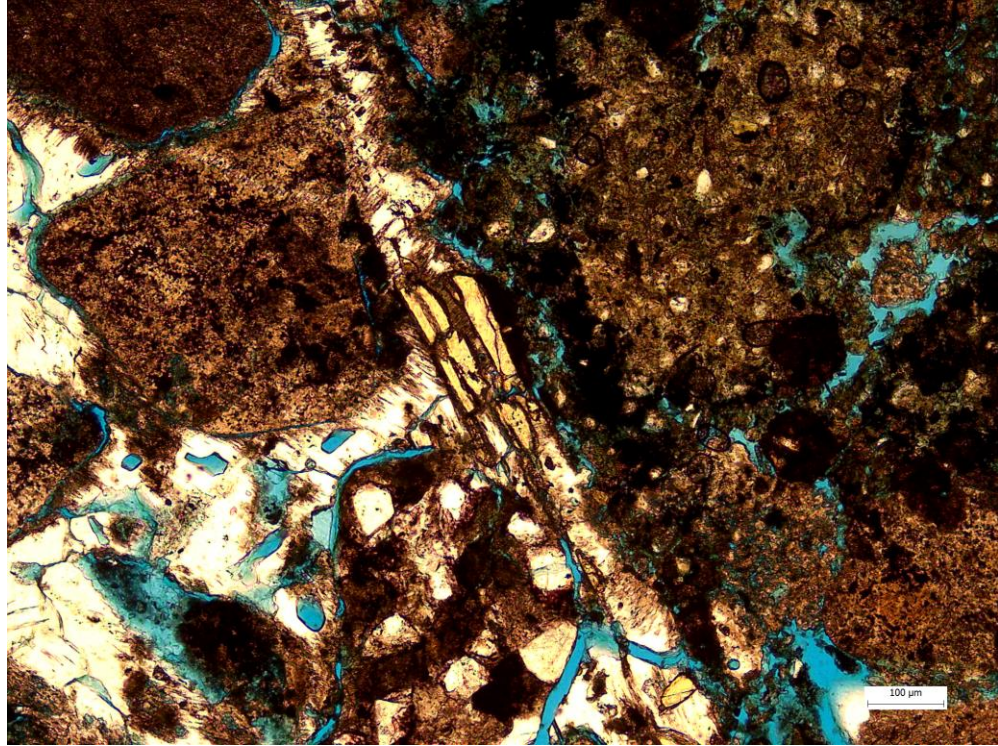


Figure A8. Barnacle fossil fragment (center of photo).

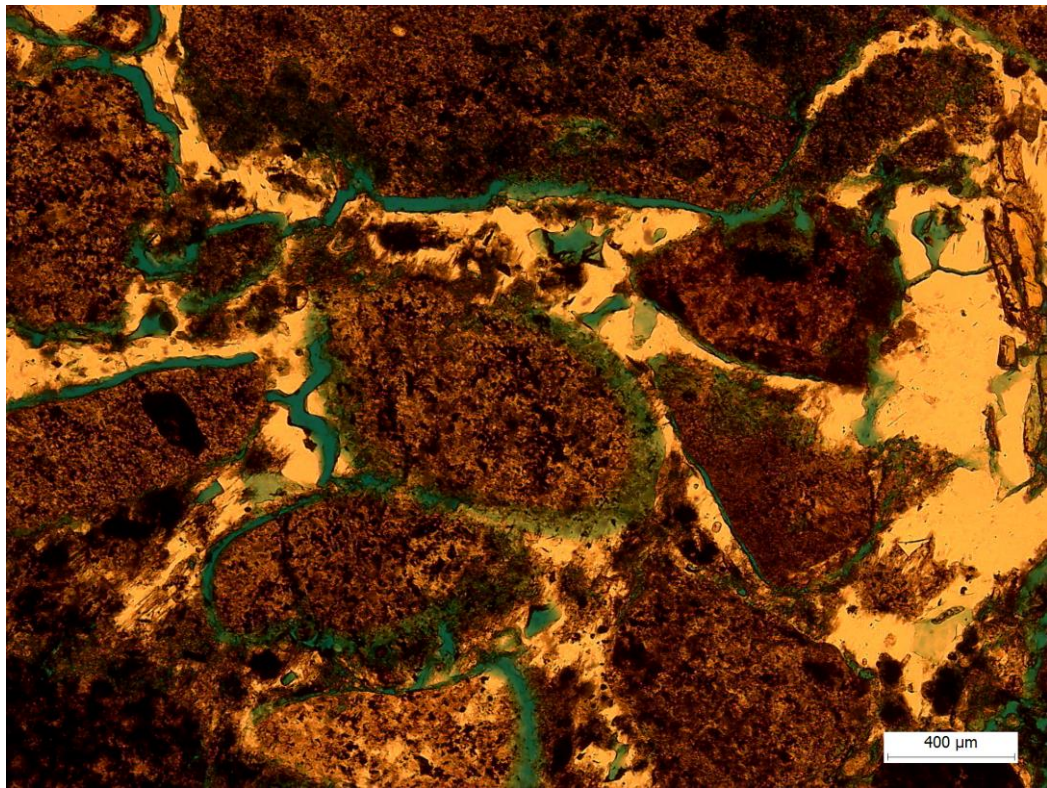


Figure A9. Thin section showing abundance of volcanic rock fragments.

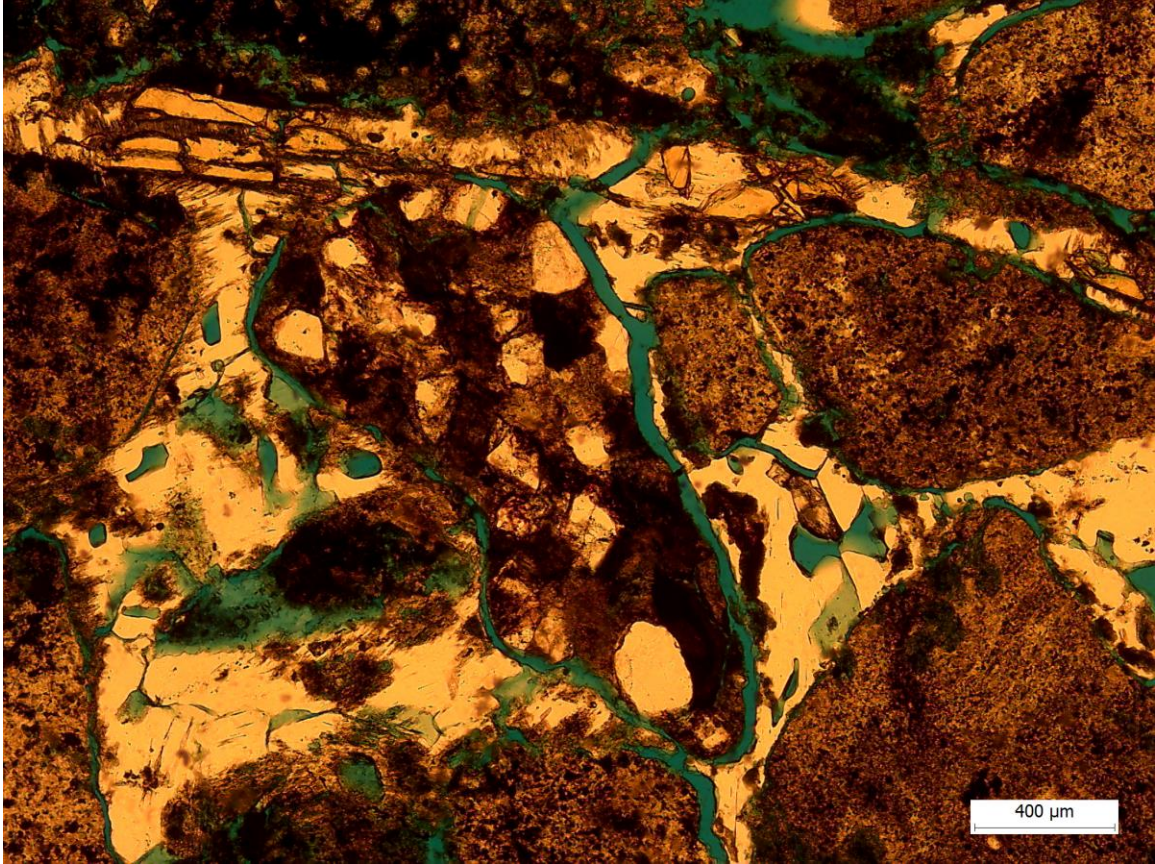


Figure A10. Thin section showing an example of sandstone rock fragment (center).

Facies Sldp: Planar-Laminated Diatomaceous Siltstone

011-33D: Cerro Hueco La Zorra

Sampling Site Information

This sample derives from Cerro Hueco La Zorra, with GPS coordinates 14.44631⁰ S, 75.68858⁰ W. It is found in a diatomaceous siltstone unit that is 31 meters above the white tuff at the base of the section. The unit sits about one meter below the T₂ marker bed and five meters below the T₃ unit at the top of the section.

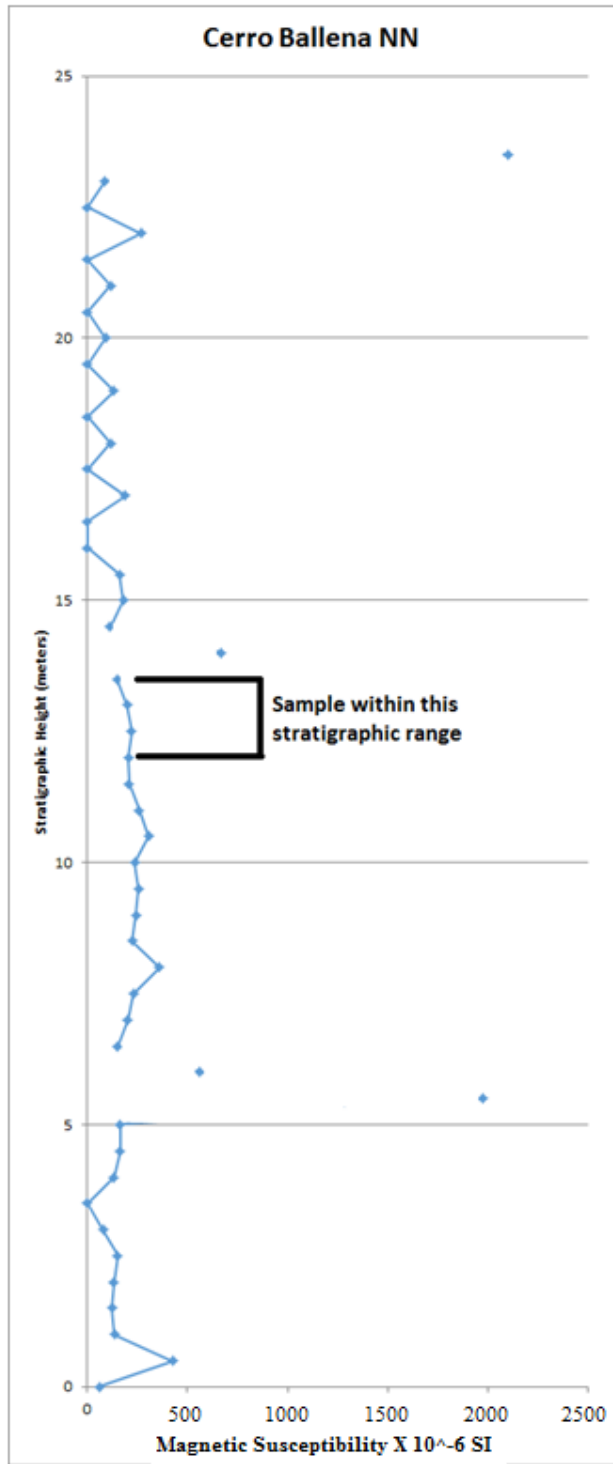


Figure A11. Magnetic susceptibility plot of Cerro Ballena, showing placement of Sample O11-52B 12- 13 meters from the base of the section.

Outcrop Features

The unit containing this sample is 7.7 meters thick. It consists of planar laminations and gutter casts. It is overlain by the ubiquitous dark gray tuff T₂ marker bed and underlain by a thin dark-colored tuff. Ledges of gypsum cement occur throughout the unit.

Petrography

In thin section, the microbedding has preferred orientation. The sample consists of 5-10% detrital material and 90-95% intergranular components. The intergranular components include 85-90% (percentage in relation to the whole sample) of diatom/clay matrix and 5-10% porosity (intergranular). The detrital components comprise feldspar (90%), quartz (7%), unidentified dark-colored grains (possibly pyrite or organic material) (2%), fish scales (1%), and bone fragments (1%).

Texture

The average grain size is approximately 98.2 microns (the average of grain diameters of 142, 177, 77, 43, and 52 microns). The grains are moderately sorted, sub-rounded to rounded, and have a low to moderate sphericity.

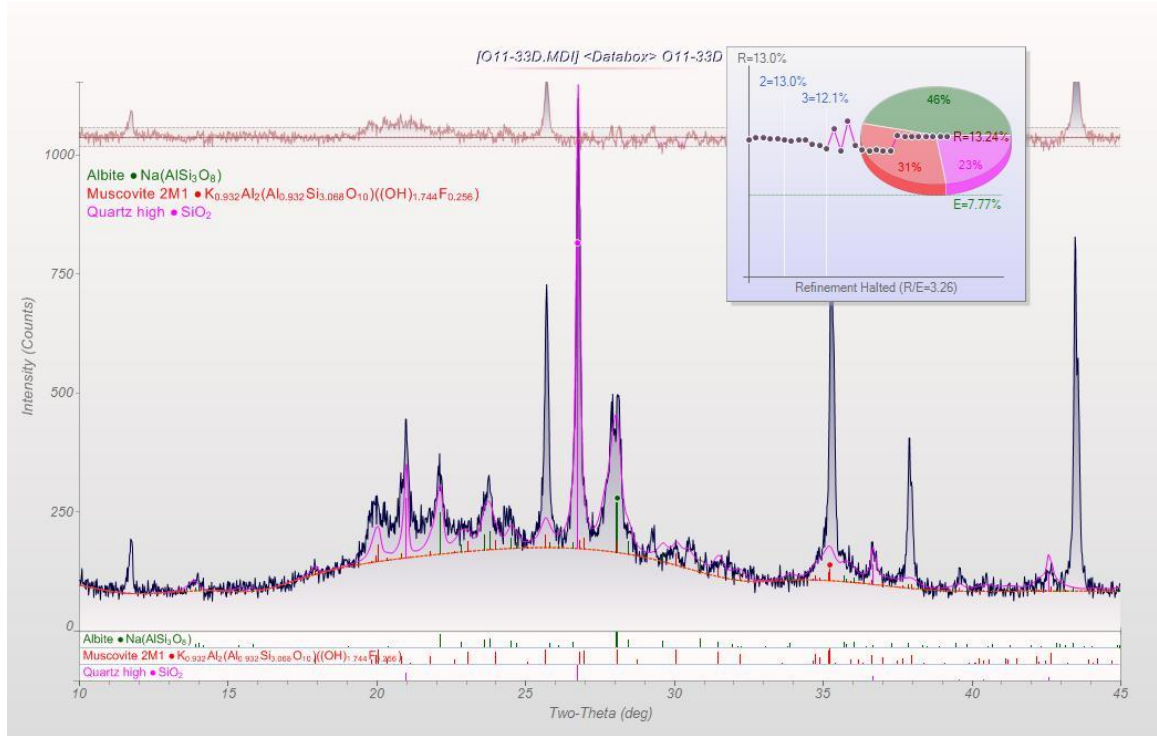


Figure A12. X-ray diffraction mineralogy of Sample O11-31D.

O11-29F: Cerro Hueco La Zorra

Sampling Site Information

This sample derives from Cerro Hueco La Zorra, with GPS coordinates of 14.44631⁰ S, 75.68858⁰ W. The unit containing this sample sits about 4.5 meters above the white tuff considered the base of the section. It occurs about 27 meters below the T₂ marker unit and 31 meters below the T₃ unit, which is considered the top of the section.

Outcrop Features

The unit is a pink-colored diatomaceous siltstone about 3.2 meters thick. Scouring and scour fills are visible within the bed. Planar laminations, channels and

channel fills, and truncation of channels also occur. The unit features wave ripple laminations, fish coprolites, and scales. It is overlain by a 0.25 m thick white-colored tuff, which may be equivalent to the 6.9 Ma-dated white tuff at the bottom of the other

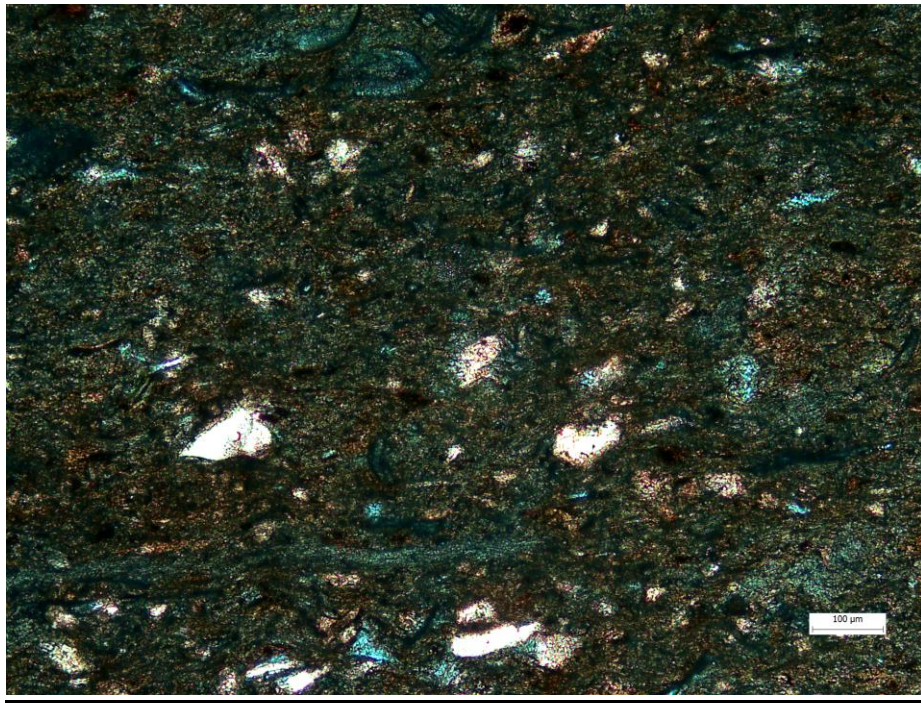


Figure A13. Thin section showing diatom (lines), the dominant mineral grains (feldspar), and diatom matrix.

five sections. (If so, then the white tuff placed at the base of *this* section is not the dated white tuff at the base of the other outcrops and considered the lowest stratigraphic unit of the studied interval. See Correlation section). The unit is underlain by a 0.30 m fine-grained, light-colored tuff, the top of which is planar laminated and the bottom of which is massive.

Petrography

General characteristics that stand out in thin section include occurrence of diatoms, glass shards, quartz, feldspar, mica (biotite), and clay; random orientation of structure and fabric; and the existence of pores that are oversized, perhaps due to dissolution.

Composition

The sample consists of 85% detrital material and 15% intergranular components, with at least 10% porosity (98% of which is microporosity and 2% of which is intergranular). The detrital components include 35% glass shards, 25% diatom fragments, 20% clay (marked by material imprinting, indicating a softer texture than VRFs would have), 15% plagioclase feldspar, 5% hexagonal quartz, and 1% mica. No VRFs appear to be present in the sample.

Texture

The average grain size is approximately 57 microns. The grains are poorly sorted and sub-angular to sub-rounded, and have low to moderate sphericity.

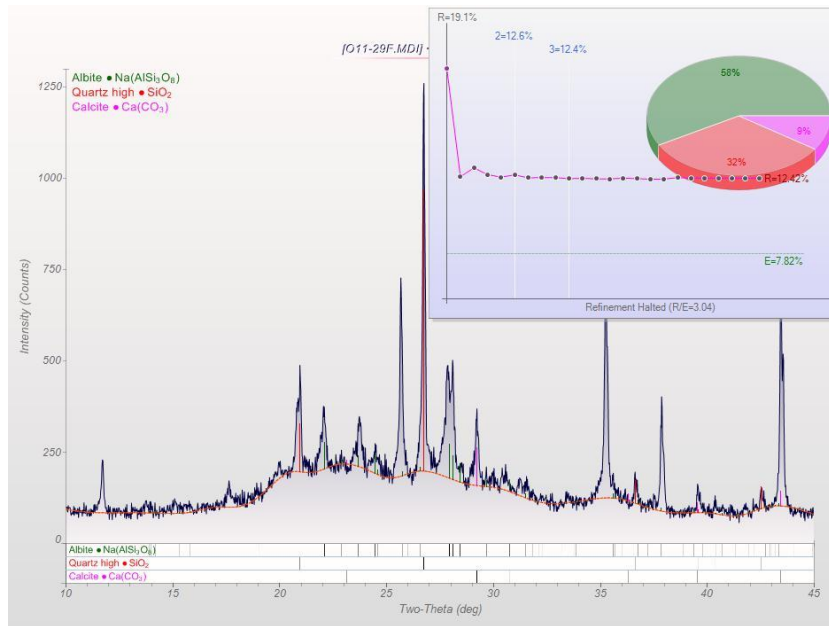


Figure A14. X-ray diffraction mineralogy of Sample O11-29F.

Facies Sldm: Massive Diatomaceous Siltstone

One sample from Cerro Ballena represents the massive diatomaceous siltstone facies.

O11-51C – Cerro Ballena

Sampling Site Information

This sample originates from Cerro Ballena, with GPS coordinates of 14.325437⁰ S and 75.72437⁰ W. The unit hosting the sample sits about 16 meters above the white tuff at the base of the section, 7.7 meters below the biotite-rich dark tuff, at the top of the section, and 1.7 meters below the dark gray T₂ tuff.

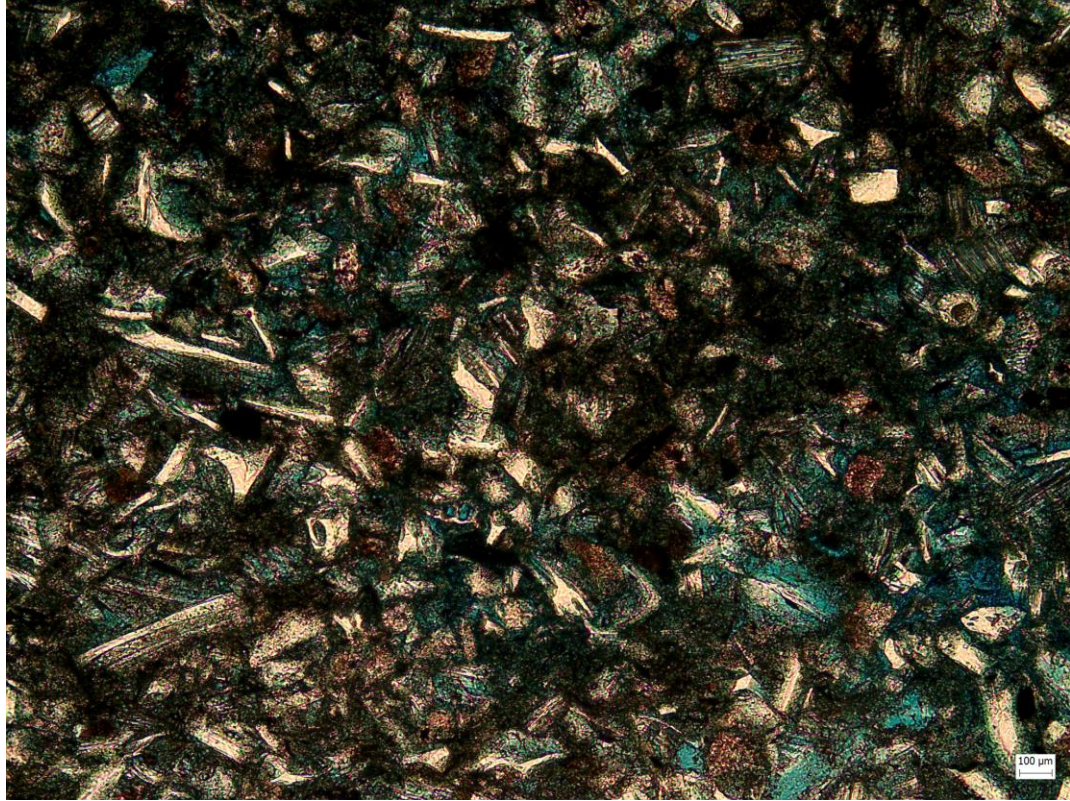


Figure A15. Thin section showing glass shards as well as distinct grains (feldspar)

Outcrop Features

The sample is mostly from a massive and fractured unit with minimal sedimentary structures. Some of the unit features sub-parallel parting.

Petrography

The sample consists of 92% detrital material and 8% intergranular components (5% pyrite, 2-3% clay). Microporosity is present throughout the glass fragments, as well as a practically negligible component of intergranular porosity. Detrital components include 67% diatom fragments, 40% feldspar, and 3% glass fragments (with the pore spaces in the same shapes as the glass fragments).

Texture

The average grain size is 78.8 microns (the average of grain size diameters 91, 31, 27, 124, and 121 microns). The grains are moderately well-sorted and subrounded to rounded overall (though few are angular or subangular).

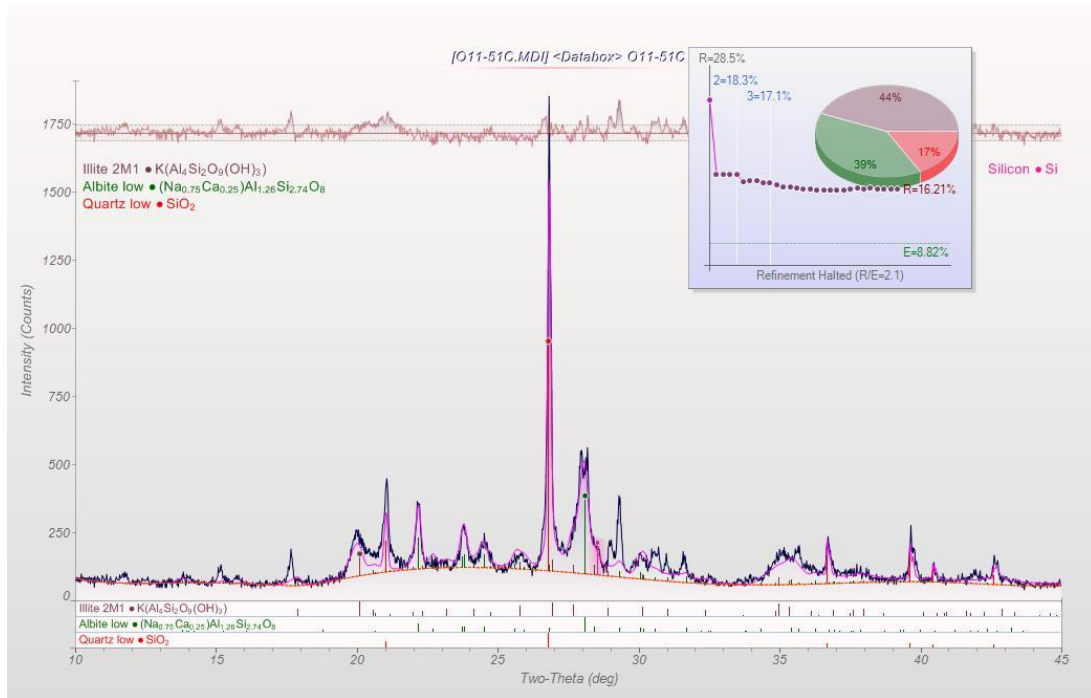


Figure A16. X-ray diffraction of Sample O11-51C.

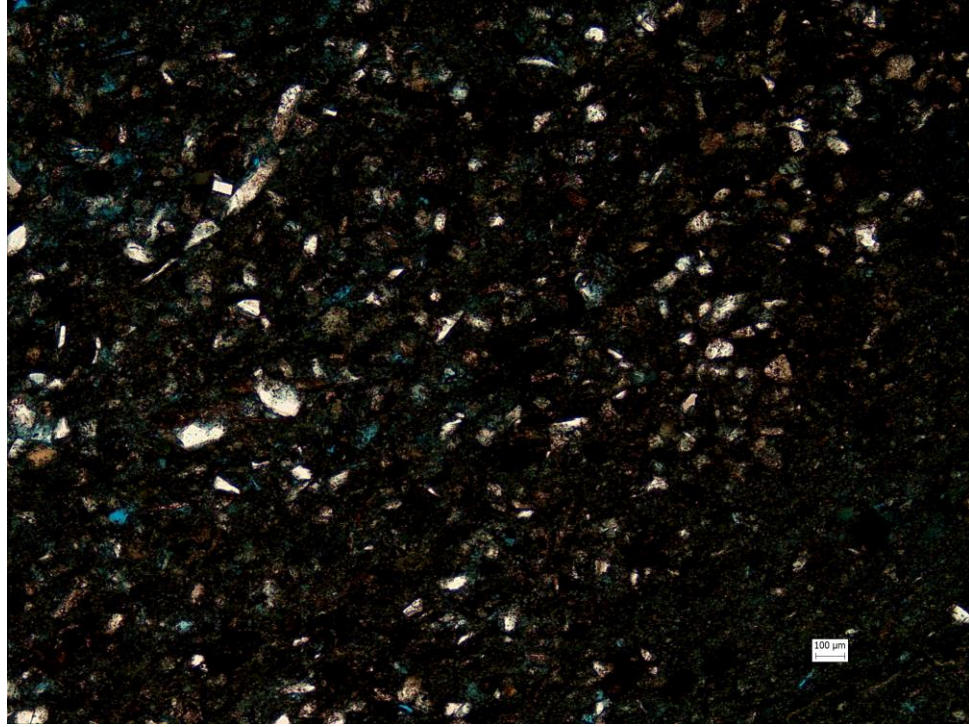


Figure A17. Thin section showing abundant feldspar grains and a few glass shards.

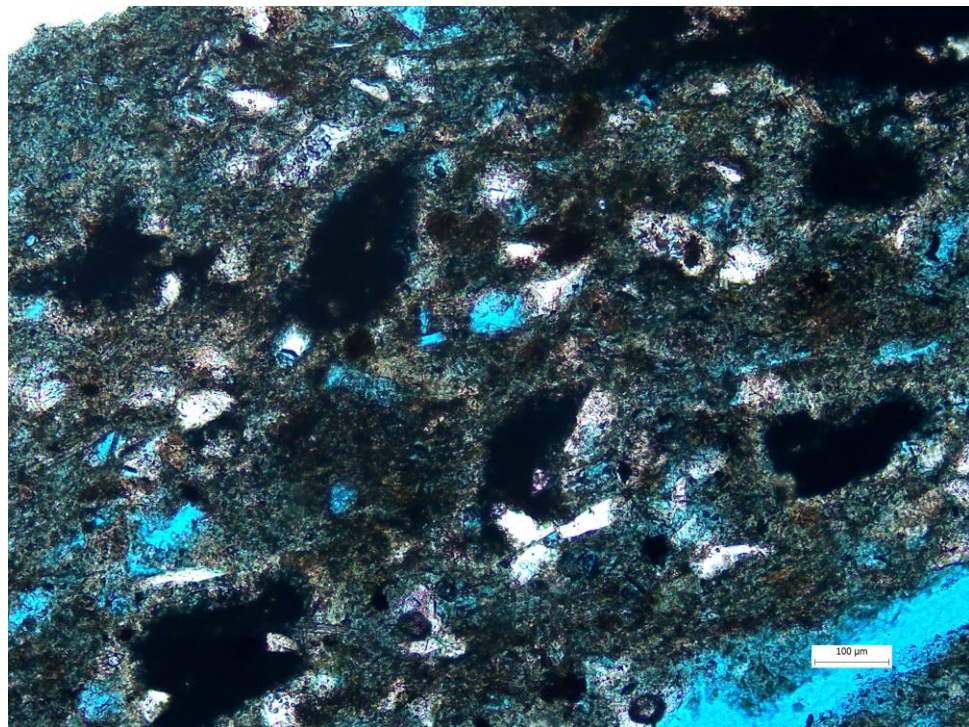


Figure A18. Thin section showing opaque minerals, possibly pyrite.

Facies Sld: Diatomaceous Siltstone

Cerro Blanco South: Possible Transition Zone from Shallow to Deep Water

This diatomaceous siltstone facies is represented by a sample in Cerro Blanco South located near the tuff complex (including the main white tuff) at the base. The sample was found in the outcrop that marks the transition from deeper (in the south) to shallower (in the north) water (see Discussion section).

P11-15B

Sampling Site Information

This sample originates from Cerro Blanco South, located at GPS coordinates 14.41546° S and 75.69006° W. The unit in which the sample was found sits 1.2 meters above the white tuff at the base of the section, 29.8 meters below the biotite-rich dark tuff considered the top of the section, and 26.8 meters below the T₂ marker bed.

Outcrop Features

The host unit is a silty, tuffaceous bed with visible biotite crystals. It overlays a 0.16 m thick platy silt that is planar-laminated. The silt bed has a lot of burrows, and contains some phosphate pebbles. The top of this bed contains burrowed, climbing wave ripples. Below the thin platy silt bed is a thicker silty bed that is planar laminated, undulating, and scour-filled, with soft-sediment deformation at the bottom.

Petrography

The sample consists of 18% detrital material and 82% intergranular components include 72% dolomite (possibly replaced diatomite as suggested by shape), 5% manganese (some oxidized and orange in color), and 5% porosity. The principal detrital components are 15% glass shards, 2% diatom fragments (presumably there was much more original diatomite material that was replaced by dolomite), and 1% feldspar.

Texture

The grains are well-sorted, well-rounded, and mostly spherical (some exceptions are subangular).

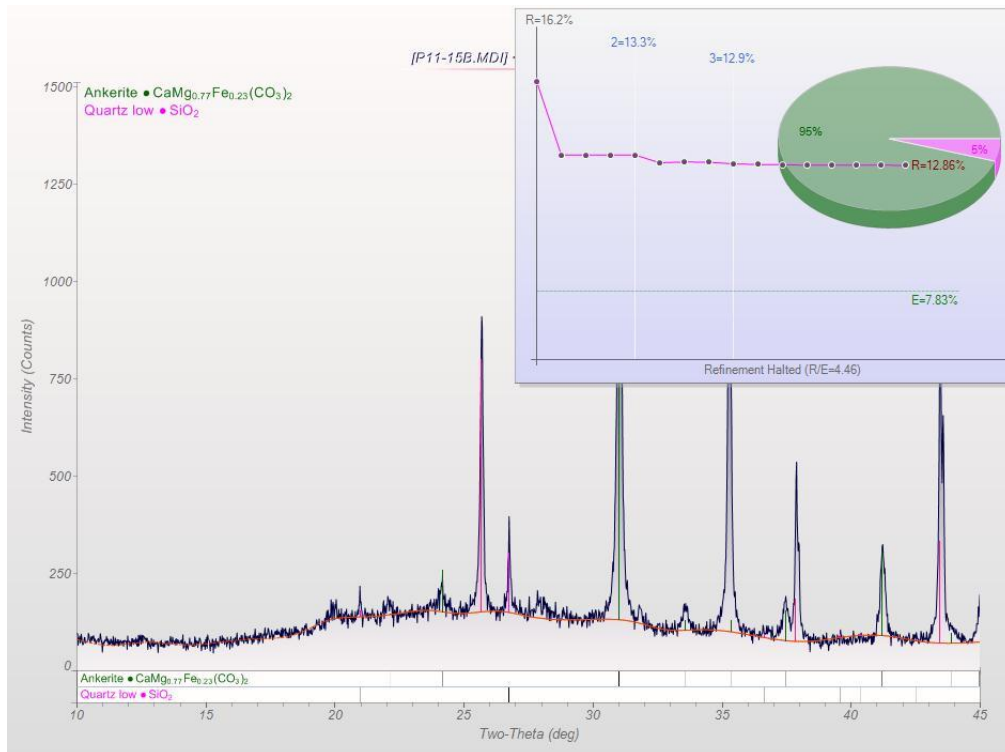


Figure A19. X-ray diffraction for Sample P11-15B.

Facies Sfs1: Fine Sand-Silt Mixture

The facies, which comprises a mixture of fine sand and silt, is represented by a sample in Cerro Ballena North.

P11-31D - CBN

Sampling Site Information

This sample originates from Cerro Ballena North, with GPS coordinates of 14.30663⁰ S, 75.73250⁰ W. The unit hosting the sample sits one meter above the white tuff at the base of the section, 17.7 meters below the biotite-rich dark tuff considered the top of the section, and 12.6 meters below the T₂ marker bed.

Outcrop Features

The host unit is a fine sand-silt planar-laminated bed draped over a coarse sandstone below. The coarse sandstone below contains brown pebbles and overlays a medium-gray silty tuff, the top 15cm of which is planar bedded with many burrows. The gray silty tuff also has wave ripple cross-laminations. The unit containing the sample is overlain by a thick wave-rippled and laminated very fine sand-silt tuffaceous gray bed (equivalent to the bed below it).

Petrography

The sample consists of 68% detrital material and 32% intergranular components (30% diatom and porosity, 2% clay). The detrital components consist of 43% volcanic

rock fragments, 25% glass shards, 3% shells, and 2% feldspar. The porosity is 95% microporosity and 5% intergranular.

Texture

The average grain size is 97.2 microns (the average of grain diameters 156, 60, 52, 76, and 142 microns). The grains are moderately to well-sorted and sub-rounded to rounded, and have moderate to high sphericity.

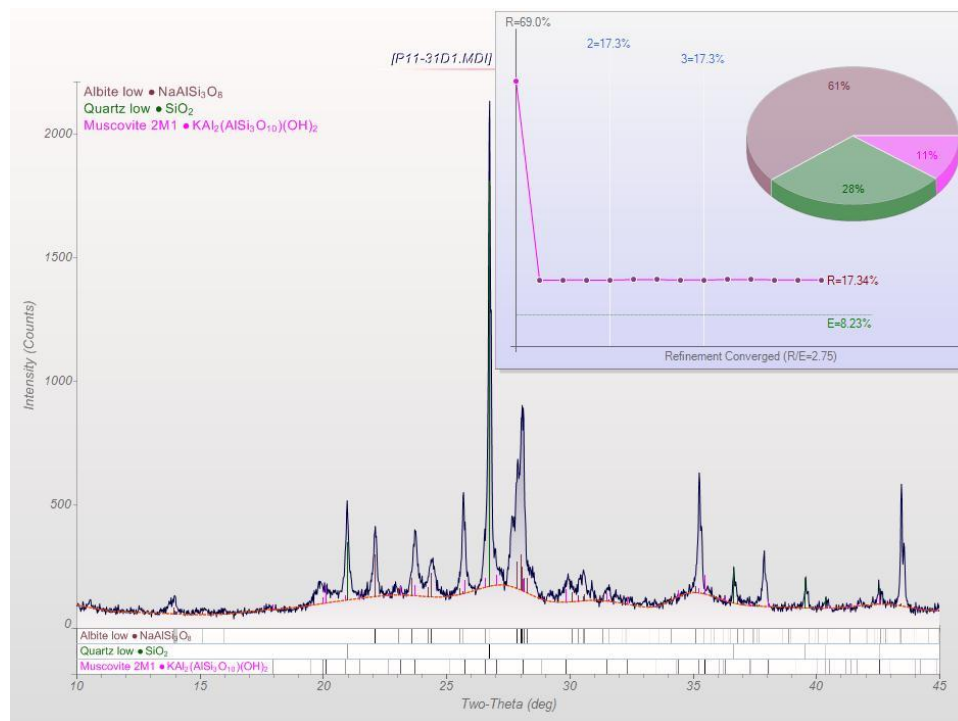


Figure A20. X-ray diffraction mineralogy for Sample P11-31D.

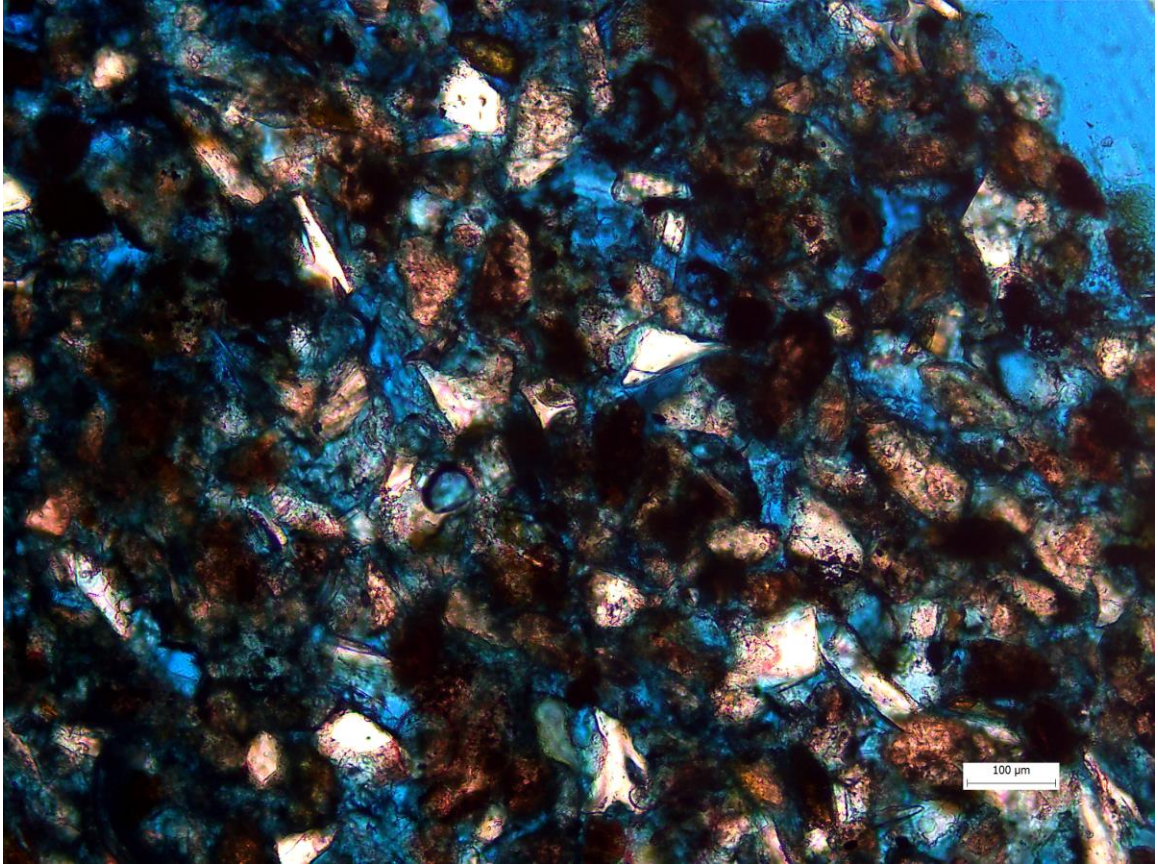


Figure A21. Thin section showing glass shards and volcanic rock fragments (dark brown grains), the dominant components of this rock.

Facies T: Tuff

011-53E – CYS

Sampling Site Information

The sample originates from a unit in Cerro La Yeseras, with GPS coordinates of 14.52874⁰ S and 75.57896⁰ W. The unit is a light-gray tuff 0.9 meters thick, sitting five meters above the white tuff at the base of the section. It rests 29.6 meters below the biotite-rich dark tuff at the top of the section and 25.1 meters below the T₂ marker bed, the mapped tuff unit used to correlate the outcrops.

Outcrop Features

The host unit is underlain by a 0.1 m thick claystone and overlain by a ~0.1 meter thick medium gray tuff. In the vicinity, just above the thick medium gray tuff, sits a thick diatomaceous tuffaceous bed that has scouring, pillow structures, and soft sediment deformation.

Petrography

The sample consists of 55% detrital material and 45% intergranular components (20% clay assumed to be dissolved from VRFs and re-precipitated, 15% cement mainly composed of anhydrite, and 10% porosity). Detrital components include 15% feldspar, 10% glass shards, 10% volcanic rock fragments, 5% quartz, 5% diatom fragments, 5% phosphate (pale green, rounded, elongated grains), 3% shell fragments (composed of calcium, appearing red-stained in thin section), and 2% bone fragments.

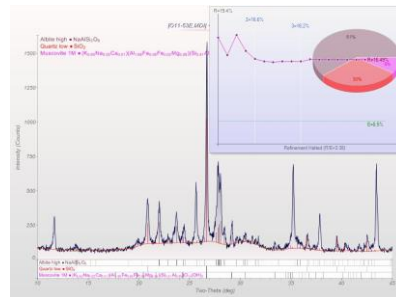


Figure A22. X-ray diffraction mineralogy of Sample O11-53E.

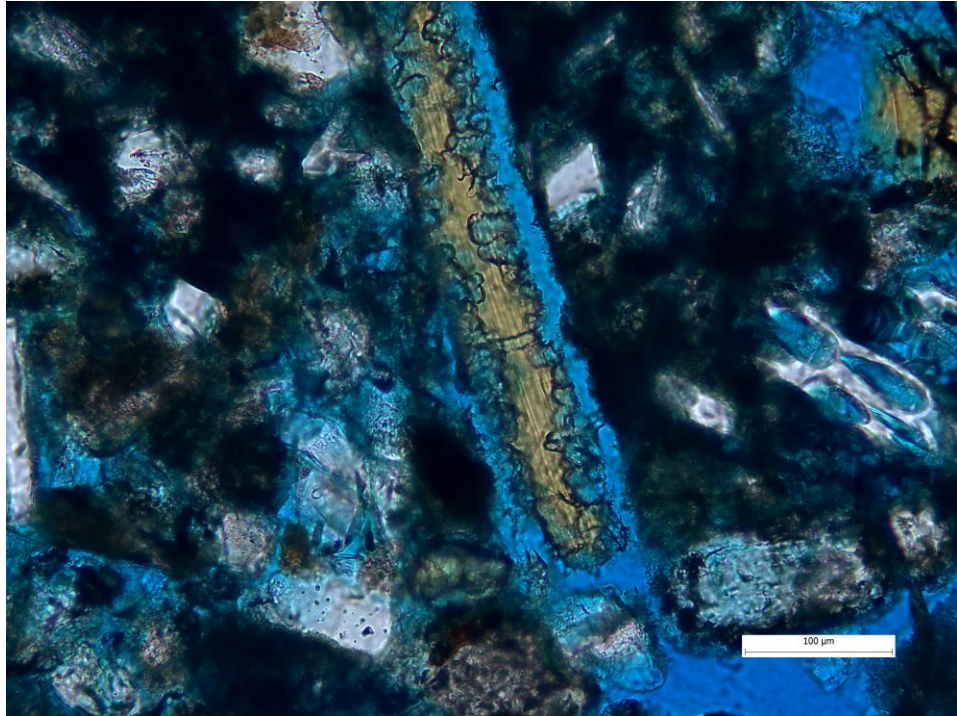


Figure A23. Thin section showing burrowing in phosphate grain fragment.

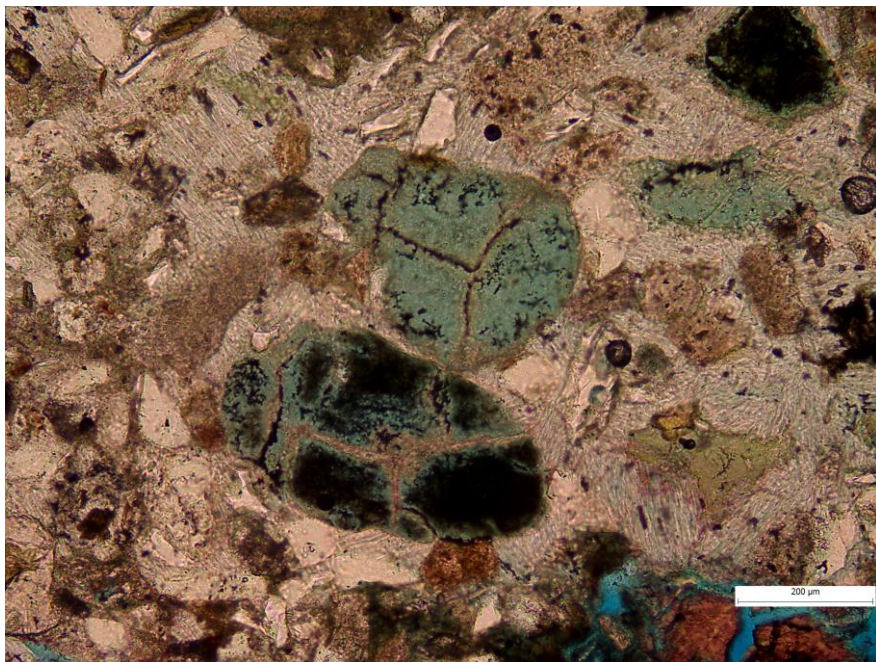


Figure A24. Thin section showing phosphate grains, which are present in only some Pisco Fm sediments.

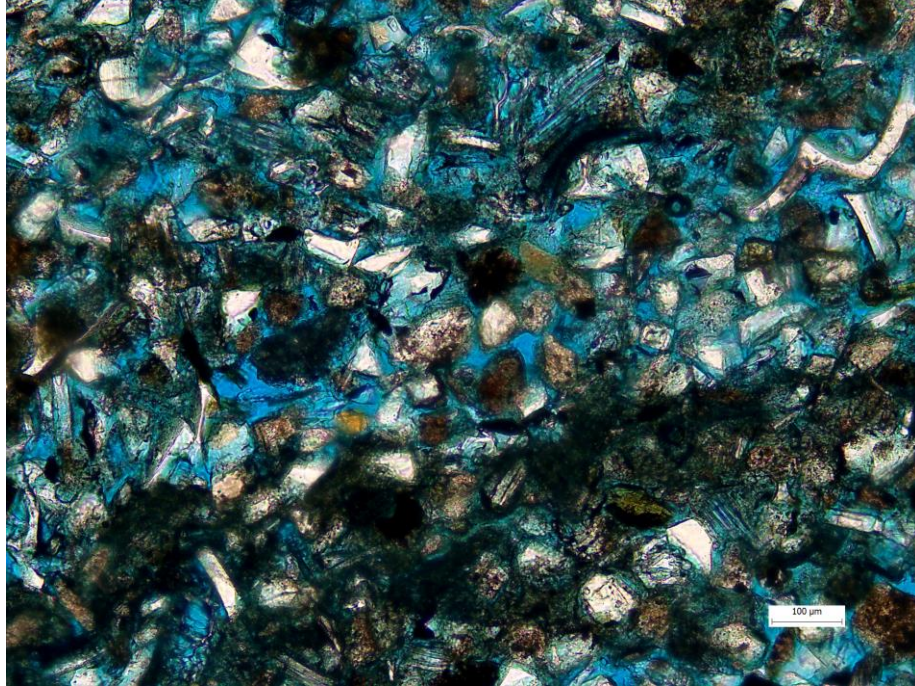


Figure A25. Thin section showing the many components of this rock, including quartz, feldspar, volcanic rock fragments, and bone fragments.

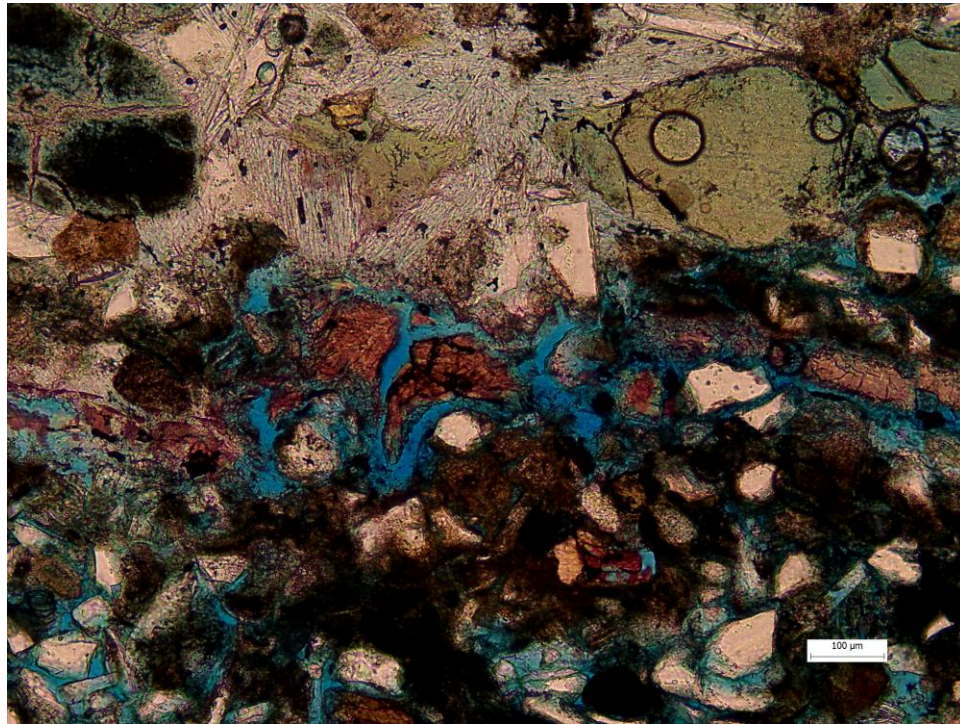


Figure A26. Thin section showing shell fragments (stained red due to calcium content).

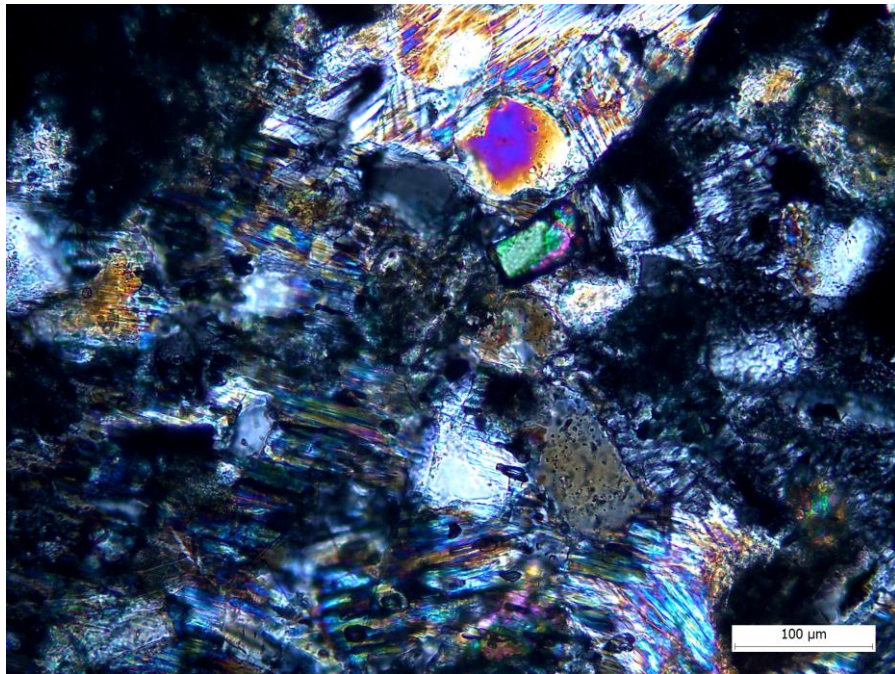


Figure A27. Thin section showing zircon grain (green) near the center of the photo (in cross-polarized light).

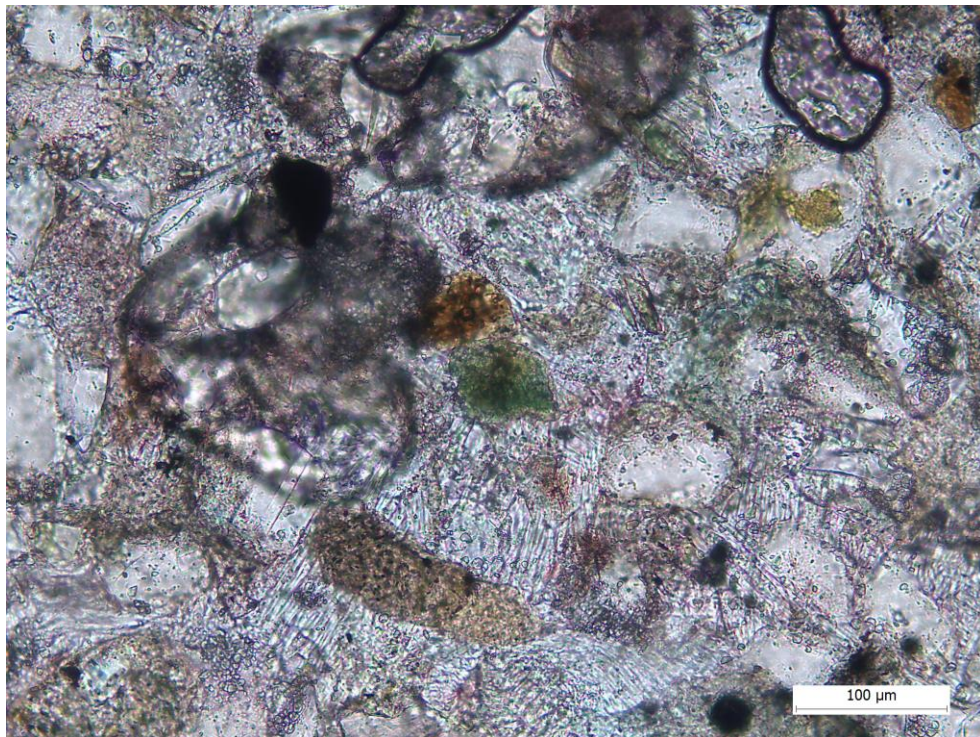


Figure A28. Glauconite mineral in the center of photo (greenish color).

Another sample collected from this facies is the biotite-rich white tuff that defines the base of the section and appears in all outcrops. The white tuff was dated by the $^{40}\text{Ar}/^{39}\text{Ar}$ and is sometimes mixed with silt. The average grain size is between 80 and 100 μm and the grains are well-sorted. The quartz and feldspar is angular and have low sphericity. The white tuff is composed of 85% detrital material and 15% intergranular porosity. Glass fragments make up eighty-seven percent of the detrital material (~74% of the entire rock) and feldspar and quartz make up 10% (8.5% of the entire rock). Light-brown biotite comprises 3% of the detrital material (~2.6% of the entire rock). No visible cements appear in thin section.

The tuff facies includes the important biotite-rich, $^{40}\text{Ar}/^{39}\text{Ar}$ -dated white tuff that defines the base of each section and appears in all six outcrops. This tuff has been used to correlate all six outcrops from the base. The representative sample for this was taken from Cerro Ballena.

A03-139ca Dated White Tuff

Composition

The white tuff consists of 85% detrital material and 15% porosity. The detrital components include glass (74% of total sample), feldspar (6%), quartz (2.5%), and biotite (2.5%) (light-brown in color). No cement is visible in thin section.

Texture

The average grain size is estimated to be 80 – 100 micrometers. The grains are well-sorted. The quartz and feldspar are angular and have low sphericity. The ash grains

have more aspect (i.e., possess greater elongation).

The facies also includes the mapped dark-gray, thick tuff used to correlate the sections, the T₂ unit. This dark gray tuff is a 0.15 - 0.25-meter-thick, continuous, prominent dark-colored gray tuff that appears in all six outcrops. It includes a substantial amount of gypsum cement that occurs on the top in outcrop. In some locations, such as Cerro Ballena South and Cerro Hueco La Zorra, climbing wave ripples are observed. Gutter casts and planar laminations also characterize this tuff.

The detrital material of this tuff includes brown-colored glass, volcanic glass fragments, and amphibole (which produces its distinctive dark gray color). The tuff also contains feldspar (~8%) and quartz (~4%). X-Ray diffraction analysis indicates the presence of plagioclase (anorthite). The cements are mostly composed of gypsum, with lesser amounts of anorthite.

The average grain size is approximately 43.8 μm. The grains are moderately sorted, have medium sphericity, and are subangular to sub-rounded. All of the porosity exists between grains. For photos, refer to Correlation section of the Discussion.

The thick, dark gray T₂ tuff unit that appears in all the outcrops (see Figure 2, Map of Study Area) is represented by Sample A11-16B from Cerro La Yeseras South.

11-16B Dark Gray Tuff from Cerro La Yeseras South

Sampling Site Information

This sample originates from the dark gray tuff (T₂ unit) in the Cerro La Yeseras South outcrop that I examined, with GPS coordinates 14.52895⁰ S and 75.57892⁰ W.

This unit is the primary time marker used to correlate all sections, and appears in the map (refer to Fig. 2).

The dark gray tuff bed (T₂ unit) containing this sample sits 30 meters above the ⁴⁰Ar/³⁹Ar-dated white-colored T₁ tuff unit that defines the base of the section and 4.3 meters below the biotite-rich dark tuff (T₃ unit) that defines the top of the section.

Outcrop Features

The unit is 0.15 meters thick here and up to 0.24 meters thick in some outcrops. It is a dark, gray-colored tuff overlain by gypsum cement at the top. In nearby outcrop Cerro Hueco La Zorra, the unit sits above very tuffaceous (white-colored) laminated silt that breaks in parallel or subparallel sheets. In some locations (e.g., Cerro Ballena South, Cerro Hueco La Zorra), climbing wave ripples are observed within the unit. Gutter casts and planar laminations also occur in the tuff.

Petrography

The dark gray tuff sample consists of weathered glass (brownish in color in thin section), volcanic glass fragments, dark-colored oxides (responsible for the distinctive dark gray color visible in outcrop), feldspar, and quartz. The porosity is 100% interparticle.

Clay likely fills the pore spaces, and darker brown isotropic grains are likely weathered glass. XRD analysis indicates that the cements are mostly gypsum, with some anhydrite. Plagioclase (anorthite) was also found. XRD also shows the glass as a distinct amorphous “hump.”

Scanning Electron Microscopic (SEM) analysis reveals the presence of gypsum (presumably the cement), feldspar (dominated by K, Si, and Al), light-gray, circular grains consisting of Fe, Ti, Ca, Si, and Al with Na and O (the composition of the melt), volcanic glass (dominated by Si and Al with minor amounts of Ca, K, Na, and Mg), dark-colored grains responsible for the dark gray color (dominated by Si, Al, and O, with lesser amounts of Fe, Ti, Ca, K, Na, and Mg), and amphibole.

Texture

The average grain size is 43.8 μm (the average of grain diameters 18, 8, 23, 54, and 116 μm). Grains are moderately sorted and mostly well-rounded, but some are subangular. The grains have medium sphericity.

Photos

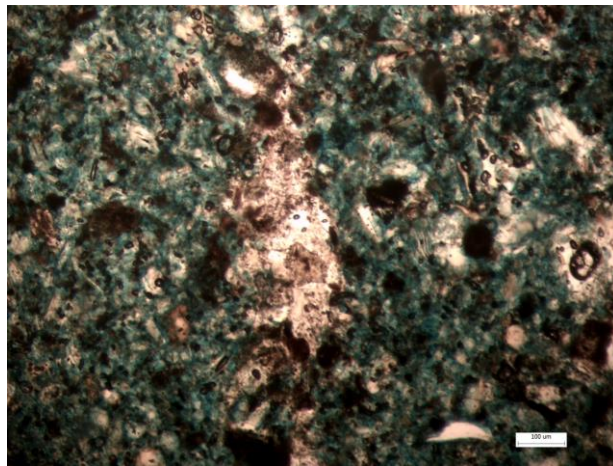


Figure A29. Thin section of the dark gray T₂ tuff unit in Cerro La Yeseras South, showing volcanic glass (dark, round brown grains) and hornblende or some type of amphibole (tiny abundant dark grains most likely responsible for dark gray color of the tuff).

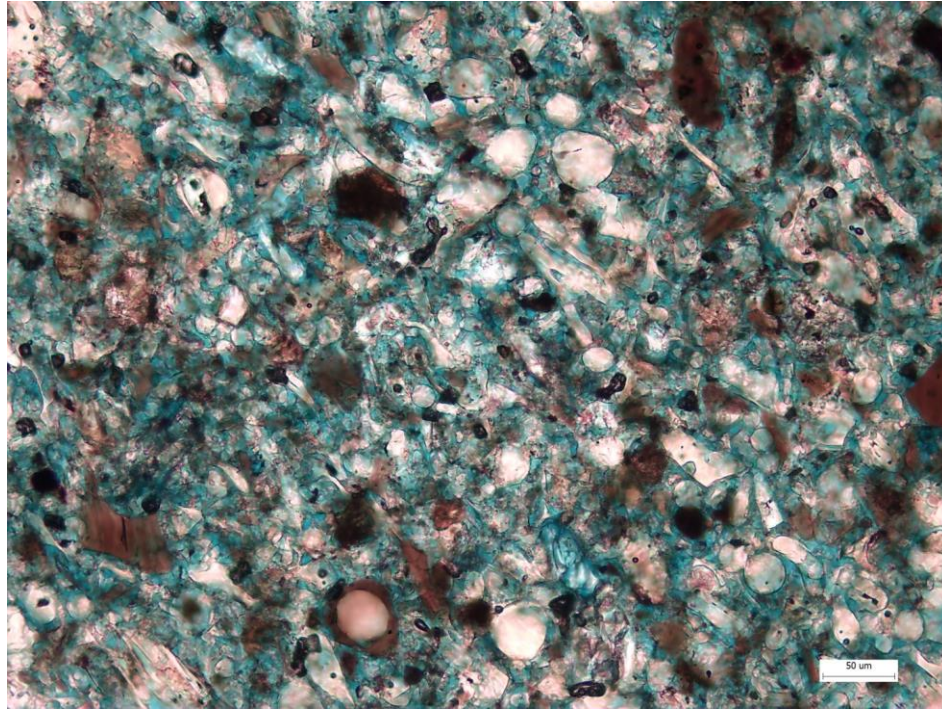


Figure A30. Another thin section of the dark gray tuff from the T₂ unit, showing the weathered (brown) glass as well as feldspar, quartz, and gypsum cement.

The facies also includes one of the primary time markers used to correlate all six outcrops: a dark gray, biotite-rich tuff (unit T₃) at the top of the section. It is separated between 3 and 6 meters above the thick, dark gray tuff (unit T₂), the other important upper time marker. It is a biotite-rich, dark gray-colored tuff associated with gypsum cement. See Figure A31 for thin section view of a representative biotite grain. The material is very brittle in outcrop. This unit can be identified by its position and large, abundant visible biotite crystals near the base.

The average grain size of this biotite-rich tuff is approximately 207 μm . The grains are moderately sorted and subangular to angular. All of the porosity is intergranular.

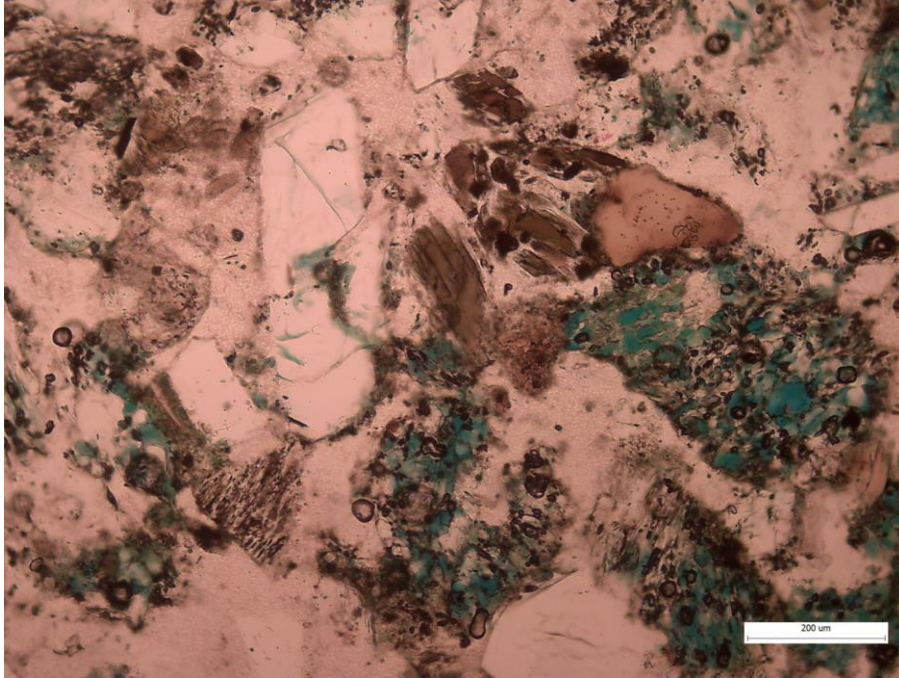


Figure A31. Thin section of the T₃ biotite-rich dark tuff. Notice the biotite grain (center, pleochroic), as well as feldspar (elongated, twinning, immediately to the left of the biotite) and quartz (above the feldspar). Cement between the grains is mostly gypsum, as indicated by x-ray diffraction analysis.

The biotite-rich dark tuff that sits at the top of each section (T₃) occurs in proximity to the time marker unit T₂, the dark gray tuff. It is represented by Sample A11-20B in Cerro Ballena.

A11-20B Biotite-rich Dark Tuff (Unit T₃)

Sampling Site Information

This tuff sample is found at Cerro Ballena, with GPS coordinates of 14.32544⁰ S and 75.72437⁰ W. This is the uppermost time marker used to correlate all six outcrops. It sits just above (6 meters in this outcrop, between 3 and 6 meters in the other outcrops) the thick, dark gray tuff T₂ that is also used as a time marker.

Texture

The average grain size is estimated to be 207 μm (the average of grain diameters 82, 105, 146, 273, and 427 μm). The grains are moderately sorted and subangular to angular. The porosity is 100% interparticle.

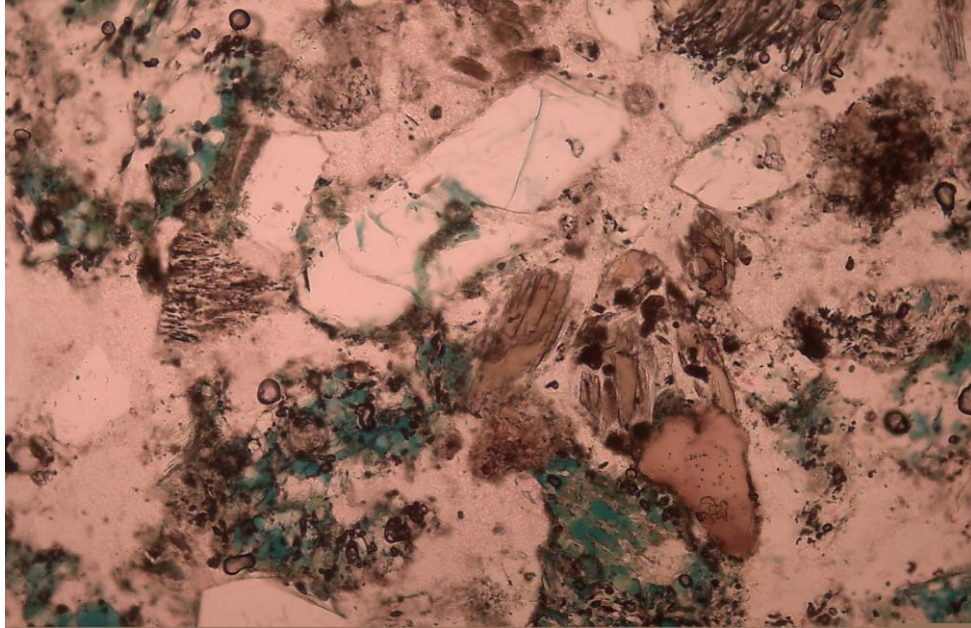
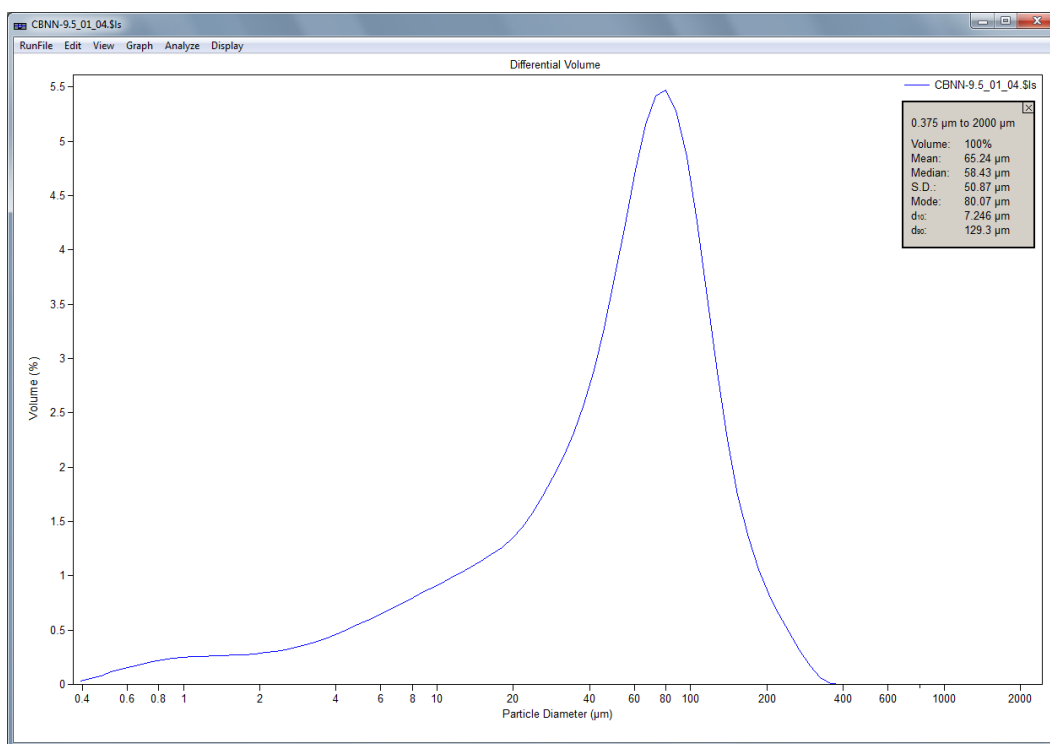
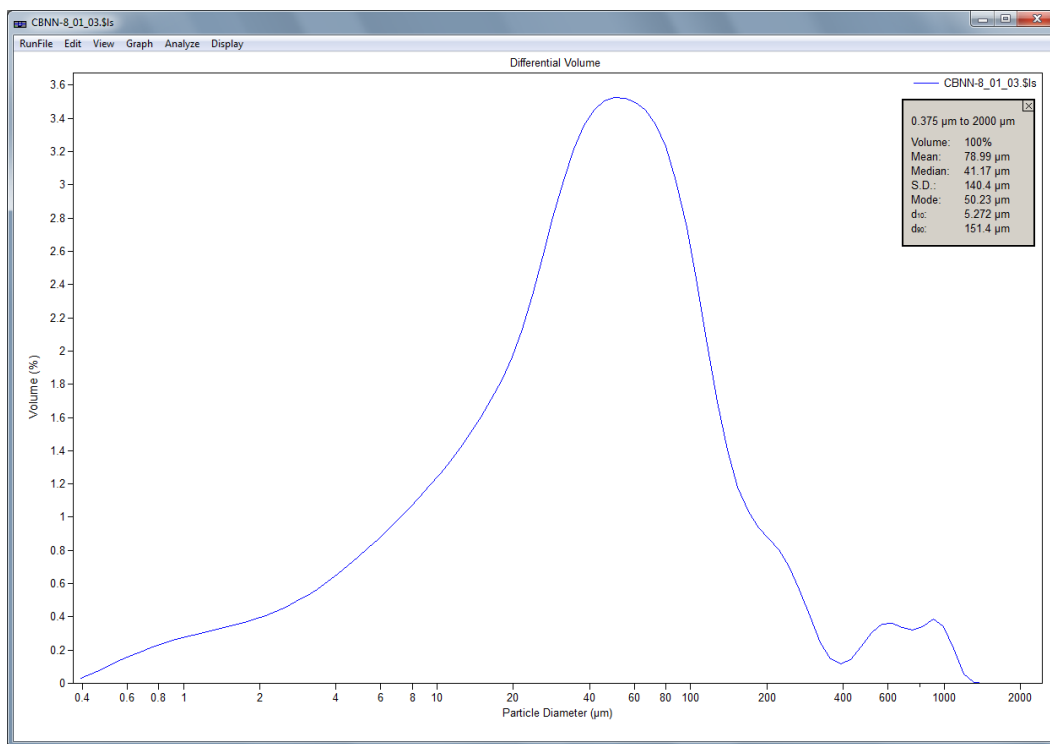


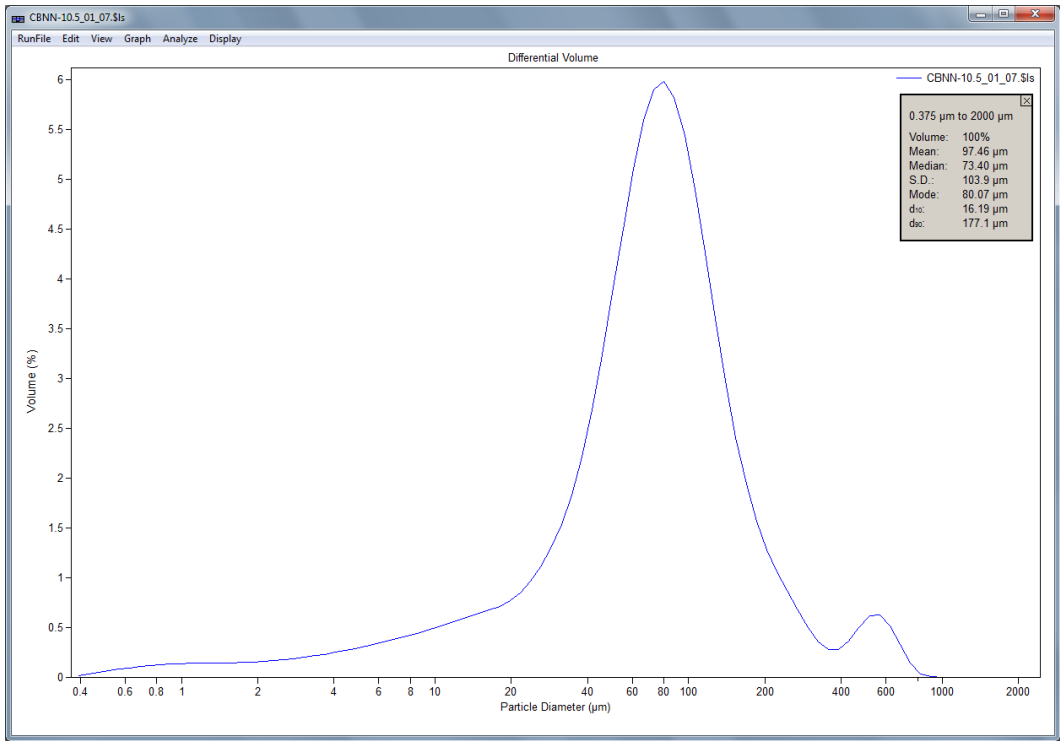
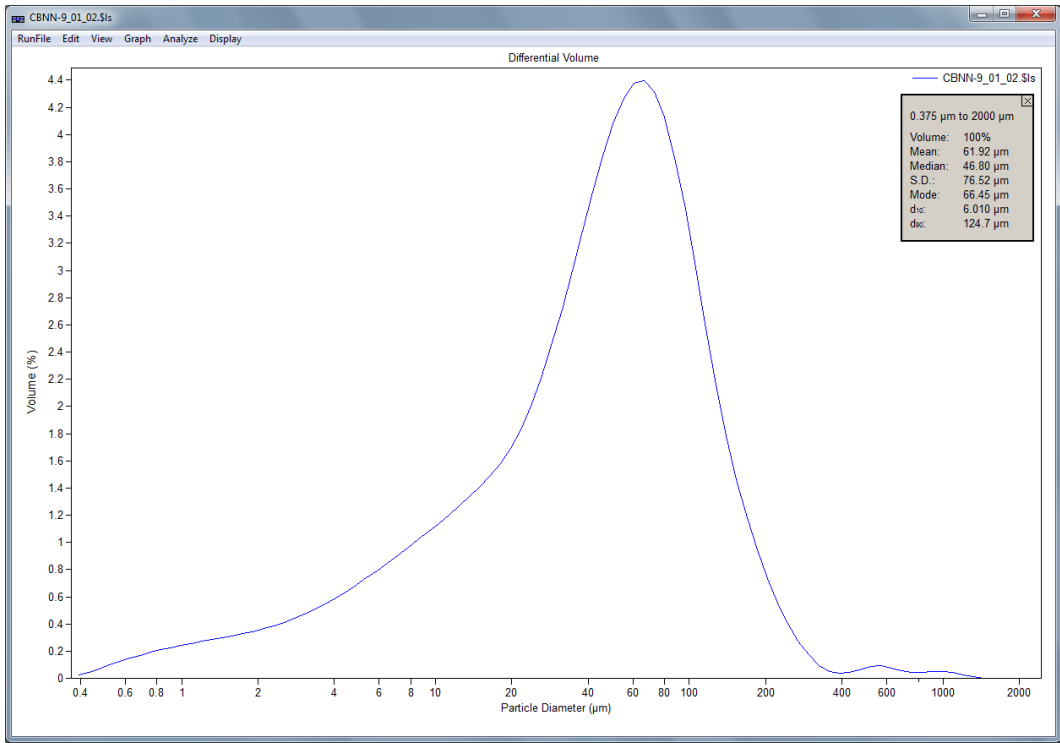
Figure A32. Thin section of same sample of tuff unit. When rotated on the stage of the microscope, the biotite grain in the center appears lighter in color due to its pleochroism.

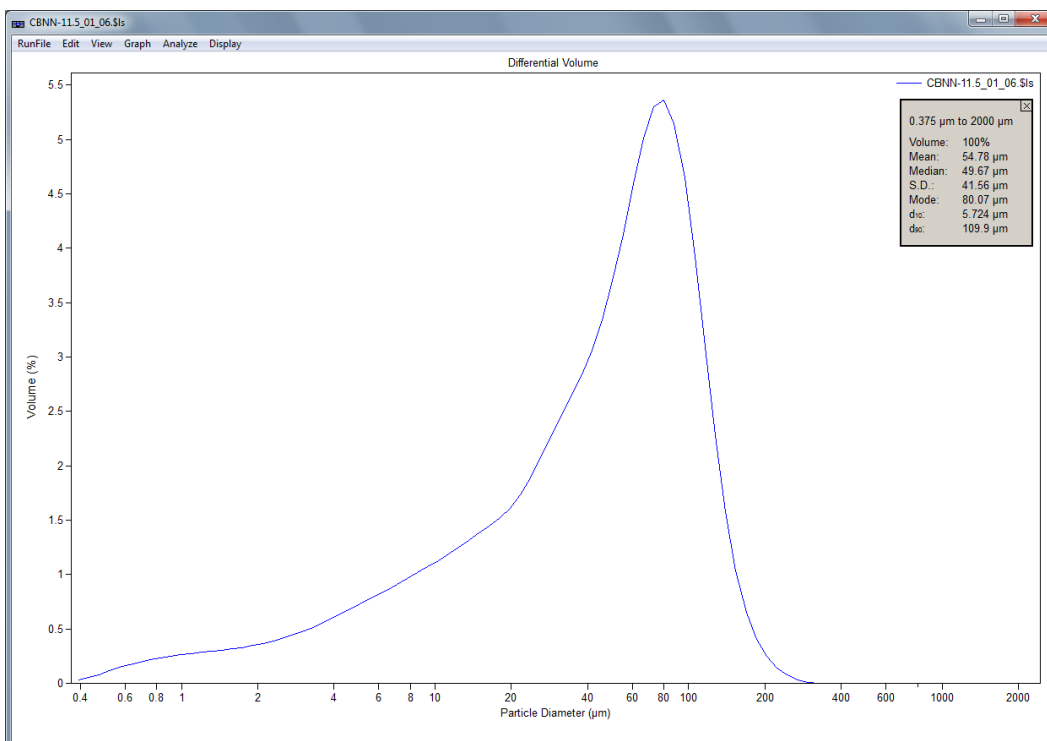
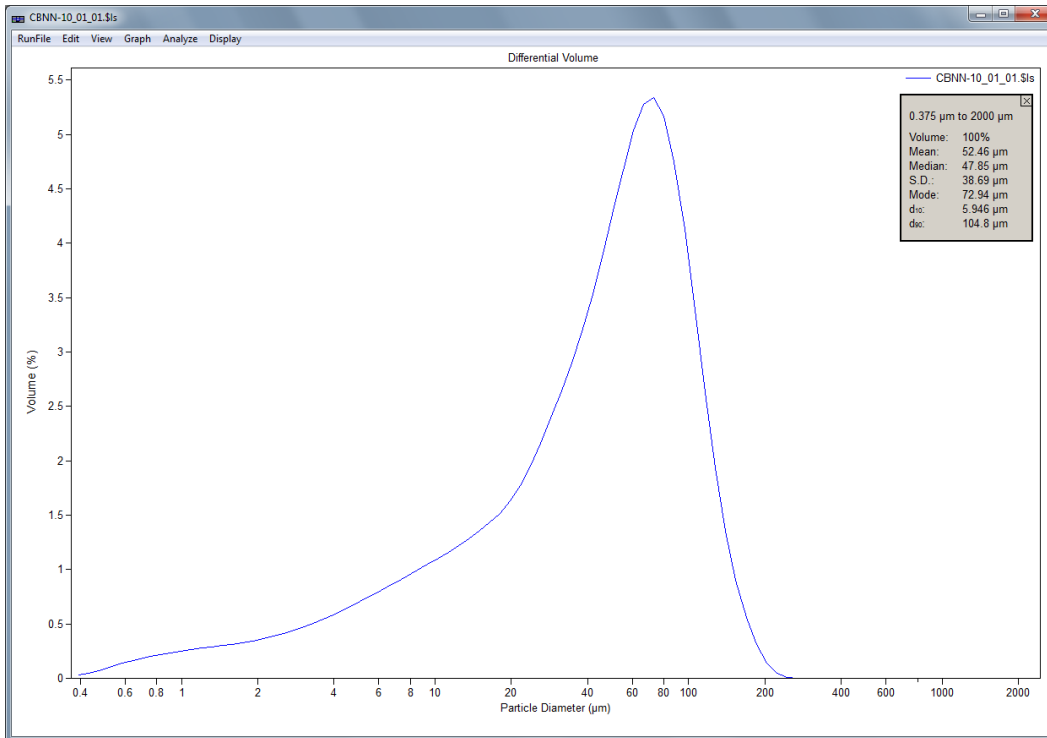
APPENDIX B

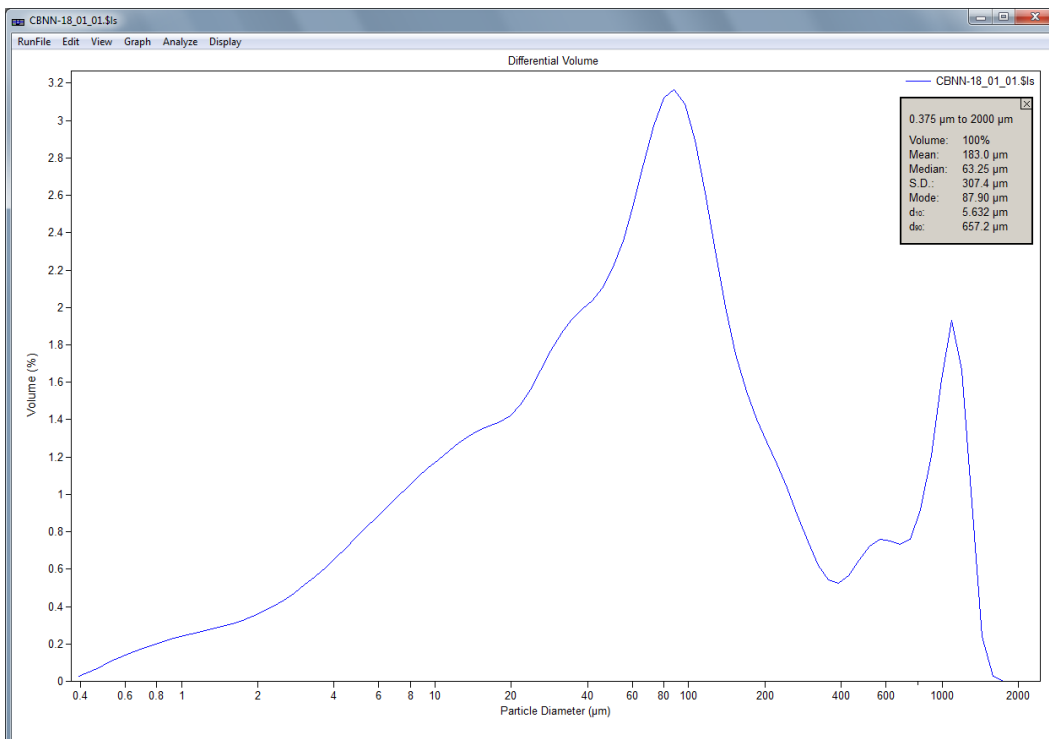
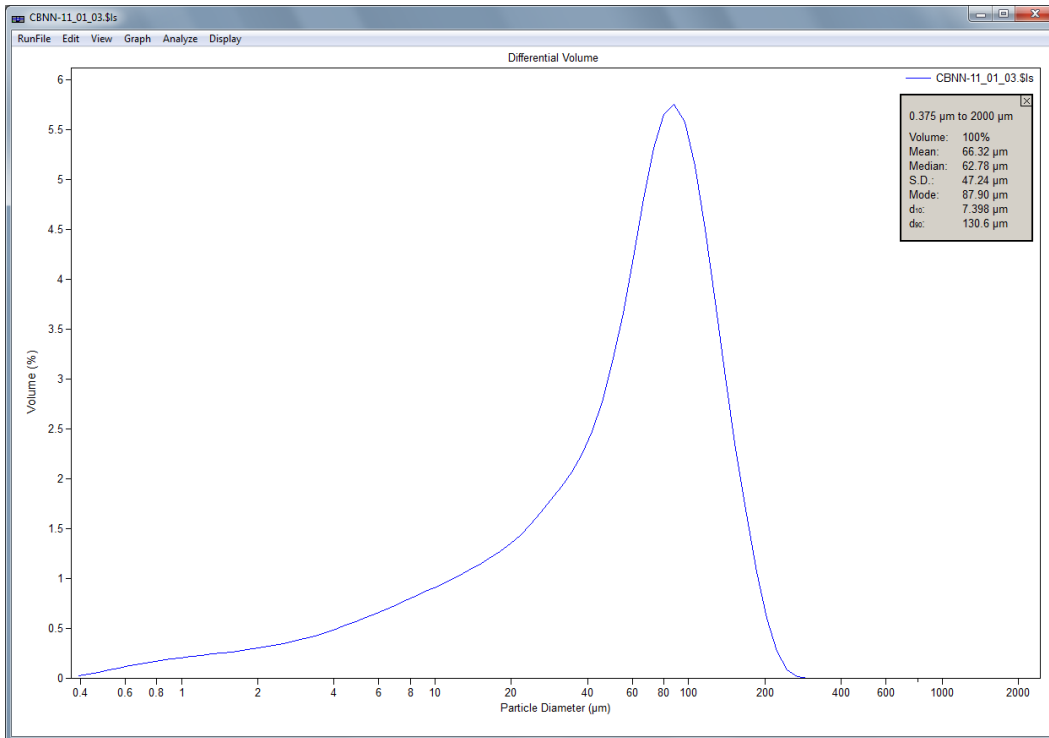
GRAIN SIZE DATA FROM LASER DIFFRACTION

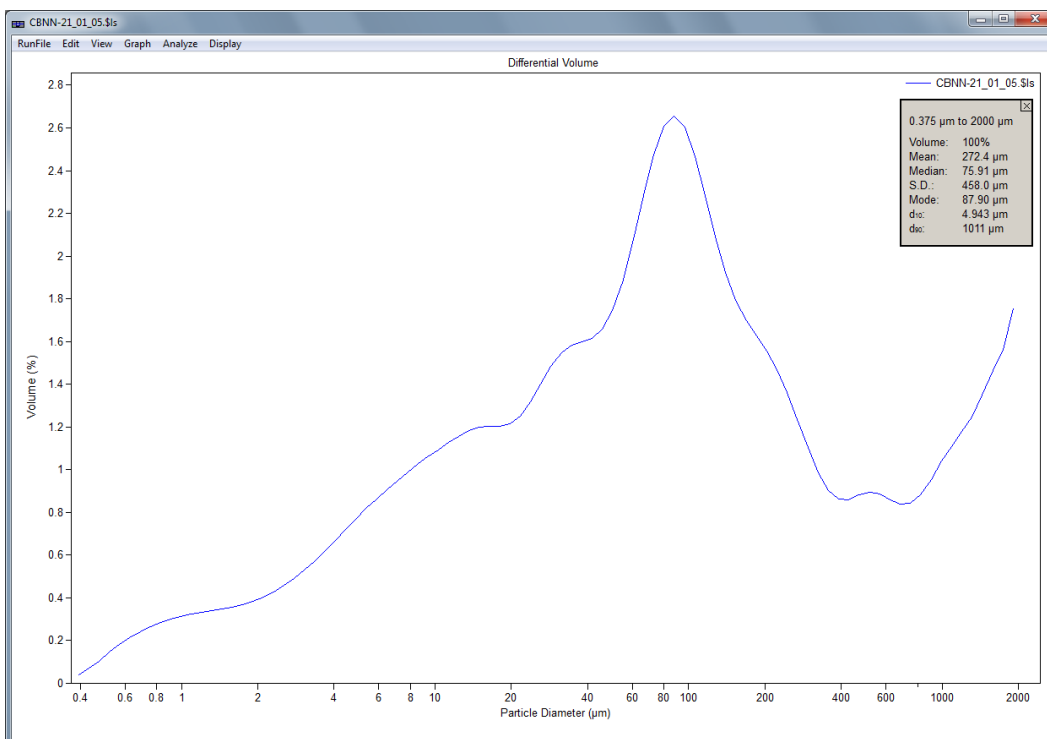
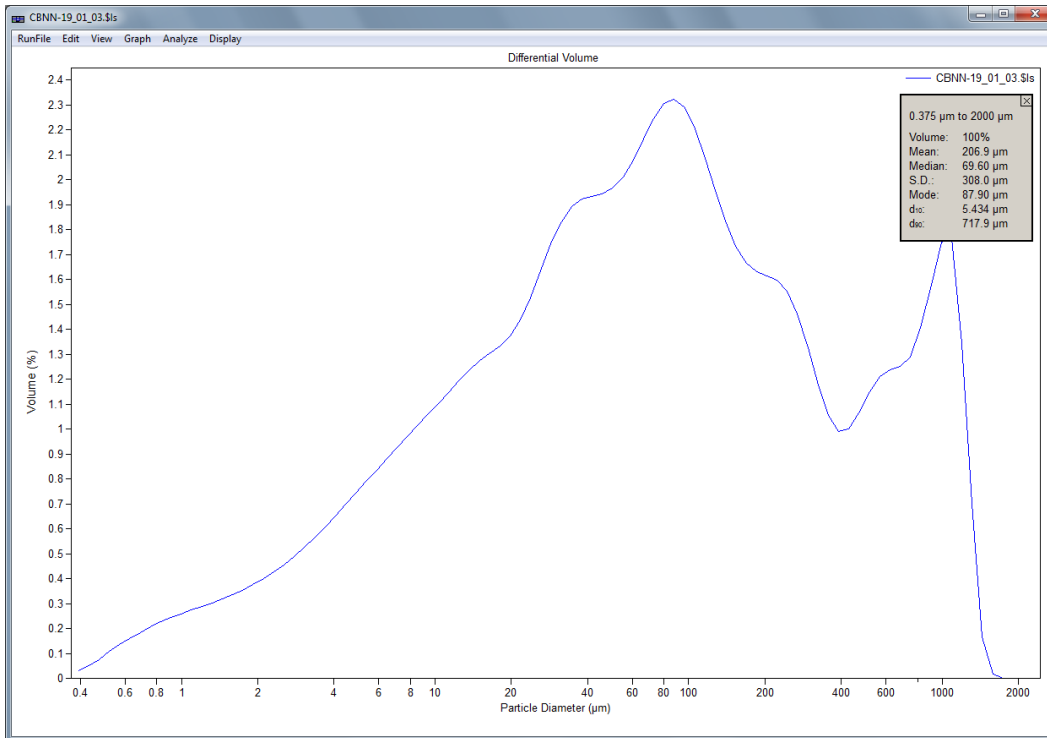
Cerro Ballena

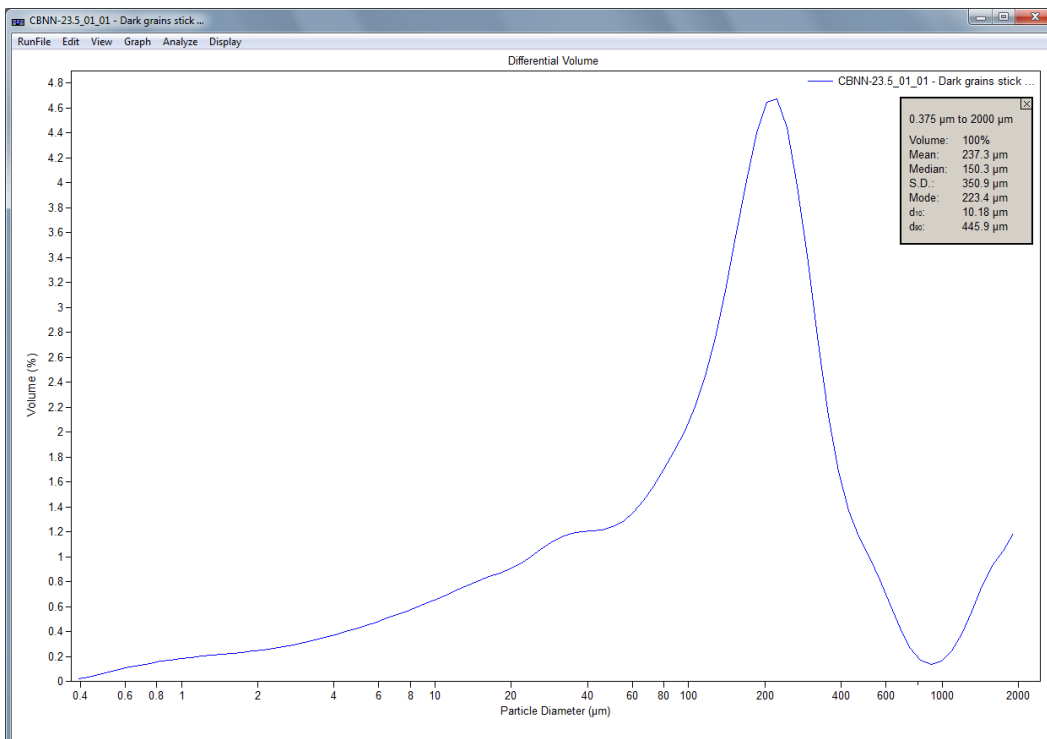
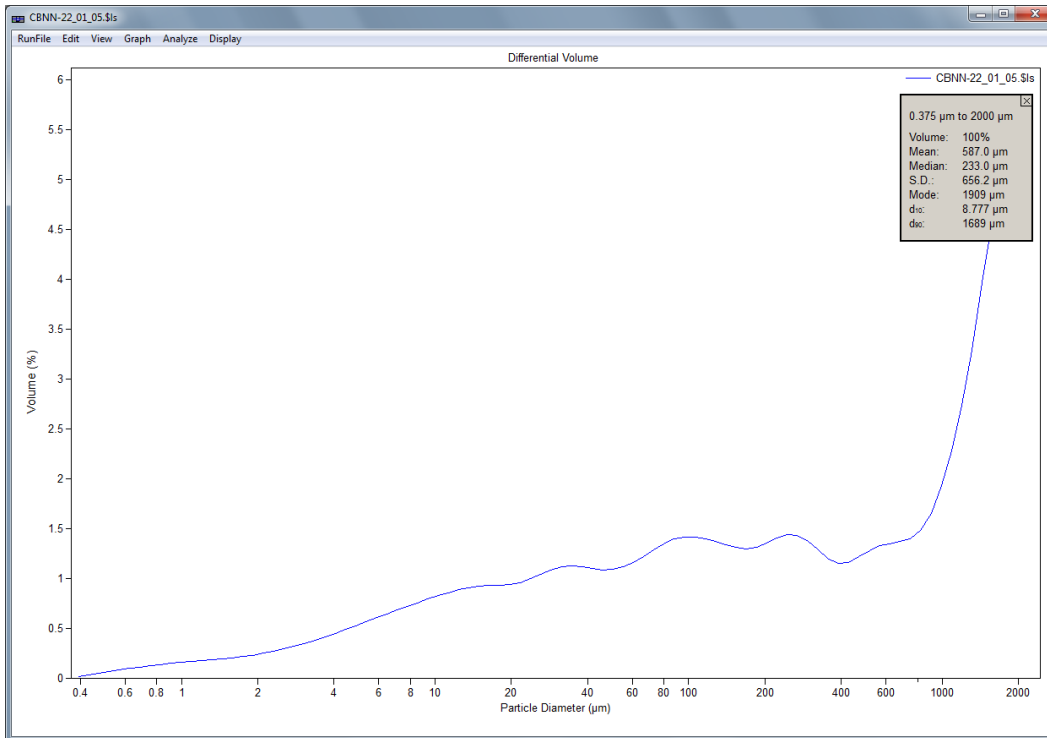


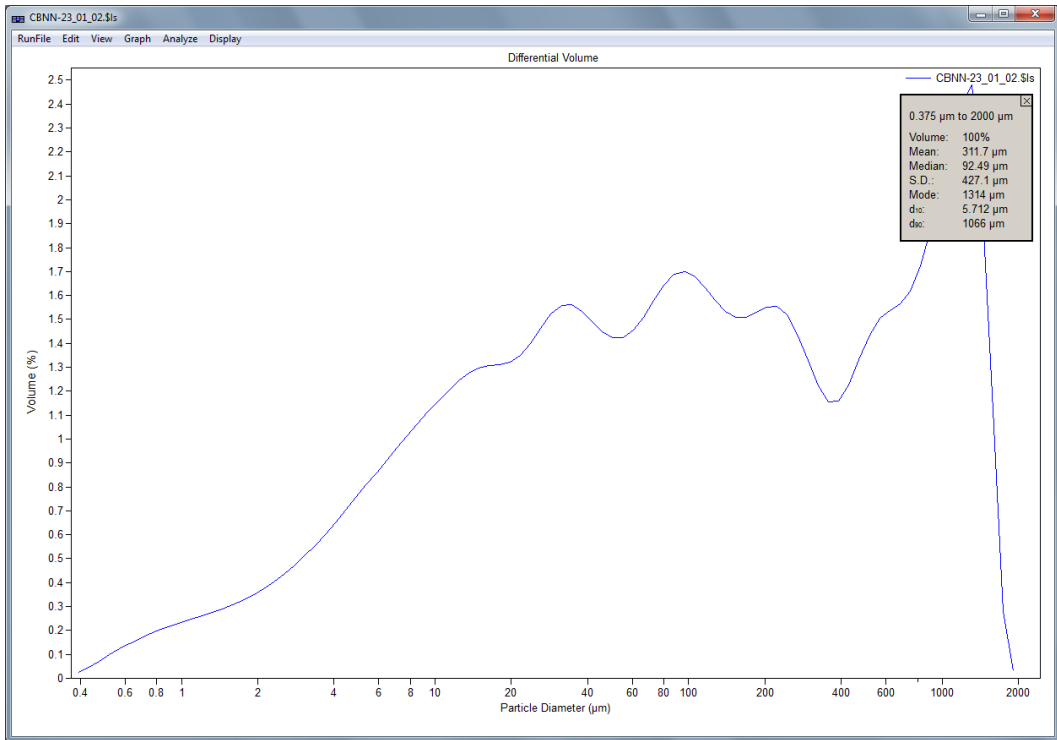












Cerro La Yeseras

